Theses and Dissertations

Spring 2010

Improving rotorcraft deceleration guidance for brownout landing

Gregory Mason Neiswander
University of Iowa

Recommended Citation

Neiswander, Gregory Mason. "Improving rotorcraft deceleration guidance for brownout landing." MS (Master of Science) thesis, University of Iowa, 2010.
http://ir.uiowa.edu/etd/561.

IMPROVING ROTORCRAFT DECELERATION GUIDANCE FOR BROWNOUT

LANDING

by

Gregory Mason Neiswander

A thesis submitted in partial fulfillment
of the requirements for the
Master of Science degree in Industrial Engineering
in the Graduate College of
The University of Iowa

May 2010

Thesis Supervisor: Associate Professor Thomas Schnell

Graduate College
The University of Iowa
Iowa City, Iowa

CERTIFICATE OF APPROVAL

_____

MASTER'S THESIS

_____

This is to certify that the Master's thesis of

Gregory Mason Neiswander

has been approved by the Examining Committee
for the thesis requirement for the Master of Science
degree in Industrial Engineering at the May 2010 graduation.

Thesis Committee: _____
                   Thomas Schnell, Thesis Supervisor

                   _____
                   Andrew Kusiak

                   _____
                   Peter O'Grady

                   _____
                   Kevin P. Jordan

TABLE OF CONTENTS

LIST OF TABLES

LIST OF FIGURES

LIST OF EQUATIONS

CHAPTER I. INTRODUCTION

<u>Problem Statement</u>

As a rotorcraft nears the ground, its rotor downwash can disturb loose terrain, obscuring the outside visual field and causing a dangerous situation known as a brownout (Figure 1). This problem is prevalent especially in dry, remote areas such as Afghanistan and Iraq. One pilot described it as "essentially flying a controlled crash into the ground with no outside reference."[1] Consequently, there has been a push for research to mitigate the effects of a degraded visual environment (DVE) on rotorcraft during low altitude maneuvering. Display symbology is one focus area of interest, as it is a relatively low cost and potential solution to spatial disorientation in DVE.

Providing the pilot with more intuitive and salient information increases pilot awareness of aircraft orientation and strengthens the decision making process for controlling the aircraft. However, in order for the display to be useful, the guidance algorithms must drive the symbology in a manner such that the pilot can safely track and maintain the guidance symbols throughout the approach.

The BOSS symbology is a set of rotorcraft symbology designed to provide the pilot with necessary information and guidance to safely land in DVE environments. It contains a set of algorithms used to drive various forms of guidance. These algorithms have been validated through simulation and flight, however the design is an iterative process with improvements being made after lessons learned following each study. From the last study, issues were brought forth regarding the longitudinal velocity algorithm. This algorithm sets up a deceleration profile and commands the forward speed of the aircraft throughout the approach.

The previous longitudinal velocity algorithm set up a deceleration profile that led the aircraft to be slow for long periods of time at the end of the approach. After flight testing with this algorithm, pilots recommended tailoring it to provide a quicker approach that required less time spent in brownout. Therefore an investigation of new algorithms or algorithm modifications was needed in order to reduce the amount of time spent in the approach and in the brownout DVE.

Additionally, the previous longitudinal velocity algorithm was constrained such that it only worked with certain descent profiles that had defined initial positions (IP). An IP is comprised of an initial altitude, initial distance from the landing point (LP), and initial airspeed. This algorithm behaved within the constraints of certain IPs, but became inconsistent if used with other IP conditions. Therefore envelope expansion of the longitudinal guidance algorithm was needed so it could fit a broader range of approaches and produce consistent guidance, increasing the overall applicability and robustness of the BOSS symbology.

Figure 1: EH-60 entering into brownout.

CHAPTER II. BACKGROUND

The following chapter details the background information and previous research conducted in regard to rotorcraft brownout. The brownout phenomenon is explained along with the causal factors to provide a strong understanding of its formation. An overview of spatial disorientation is provided as is its relationship to rotorcraft. Migitation techniques for brownout are thoroughly reviewed, with brief explanations within each research field. The BOSS symbology is detailed to provide an understanding of its design and development. Literature regarding rotorcraft approaches and differences between visual and non-visual approaches are discussed. Finally, different algorithms for rotorcraft deceleration are explained to provide the foundation of this experiment.

<u>The Brownout Hazard</u>

Imagine shooting an approach to an undefined landing area in the middle of the desert on a low illumination night based on GPS coordinates alone. Add to that sandstorms and talcum powder dust that begins to pick up at 50 feet and envelopes your cockpit and cabin at 20 feet above the ground. In fact, the best way to describe a true brownout approach is to ask you to close your eyes at 25 feet above the ground with near zero air speed and try to land. Now you have an idea of what a brownout landing is.

Capt J. Sherar, Brownout[2]

The issue of brownout has been a known problem for a long time; however, it has become a more prevalent research topic within the past decade because military helicopters have been crashing due to the harsh sand environments encountered in both Afghanistan and Iraq. Landing in brownout has been described as "far and away the most dangerous thing you can do as a helicopter pilot"[1], and it is costing the military

significant amounts of money, and more importantly lives. An article stated that DOD attributes over $100 million in total costs per year to brownout mishaps.[5] From an investigation of rotorcraft survivability[4], it was found that brownout was the leading cause of non-hostile fatalities during hover and low speed flight. Brownout was also the lead cause of combat non-hostile rotorcraft losses, and accounted for 65% of the combat non-hostile rotorcraft losses during hover and low speeds. It was reported that DOD attributes one third of all the helicopter mishaps in Operation Enduring Freedom to brownout.[5] Consequently, strengthening pilot awareness through improved flight displays for low speed maneuvering is a top priority from the DOD for preventing brownout mishaps.[4]
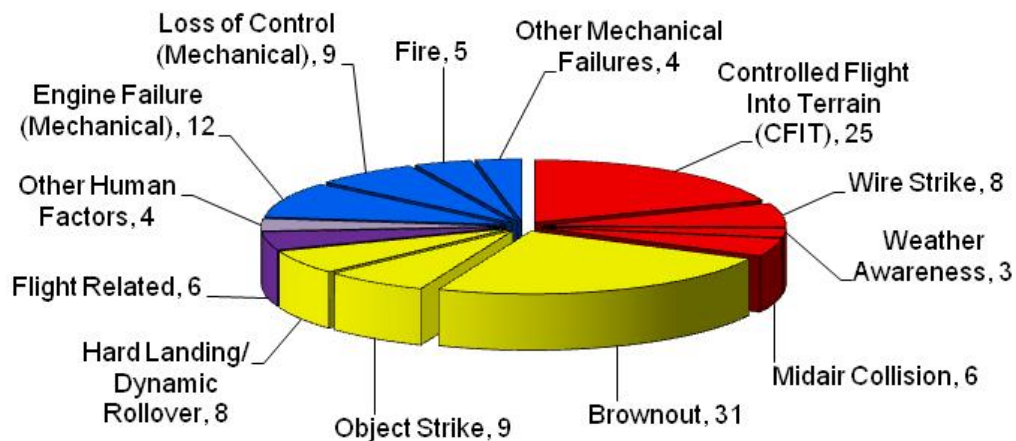
Figure 2: Breakdown of rotorcraft combat, non-hostile losses.

Note: Yellow shading represents human factors issues during hover and low speeds.

Source: Couch[4]

<u>Brownout Formation and Factors</u>

Ground Effect

Brownouts develop due to the inherent nature of the helicopter rotor system, which intakes air and accelerates it downward at a resultant vector depending on the angular deflection of the rotor blades. This accelerated air is known as the rotor downwash of the helicopter. During flight at high altitudes, the rotor downwash is easily dissipated into the surrounding air. But as the helicopter nears the ground, the downwash makes contact with the terrain surface, and creates a cushion of air in between the helicopter and the ground. This reduces the induced flow (air entering) into the rotor system[6] and is known as ground effect (Figure A1). The start of brownout is typically expected to begin when the aircraft enters in ground effect (IGE), which occurs at an altitude approximately equal to the diameter of the main rotor. However, brownout is also dependent on numerous other factors as discussed in the following paragraphs. Nonetheless, the H-60 has a rotor diameter of 53.66 feet[7] and therefore is expected to encounter brownout conditions around 50ft above ground level (AGL).

As the downwash impact velocity against the terrain increases, it starts to perturb loose sand, dust and debris. Once the downwash impacts the terrain with enough velocity, the loose objects become airborne and follow the trajectories of the rebounding downwash off the terrain. Depending on the amount of sand and debris present, this can create a mass of suspended particles in the air surrounding the aircraft, degrading the visual environment, and forming a brownout. The same phenomenon can also occur in snowy conditions with snow and is known as a whiteout.

Effective Translational Lift

Passing through effective translational lift (ETL) is another occurring rotorcraft aerodynamic principle that propagates the brownout. ETL occurs at higher speeds when the rotor system of the helicopter is more efficient. This is because a portion of the induced flow is parallel to the rotor system, requiring an increased angle of attack on the rotor blades, and thus providing more rotor thrust.[6] During this time, the rotor system intakes *clean air*, meaning no rotor downwash is in the induced flow. But as a helicopter slows, part of the rotor downwash (*dirty air*) from the front of the rotor system becomes re-ingested as induced flow into the back of the rotor system. This recirculation reduces the amount of clean air entering the system, which reduces the rotor thrust, making the aircraft less efficient. Passing below ETL thus requires an increase in collective pitch to maintain altitude.[6] When the aircraft is below ETL and IGE, the brownout cloud formed from the ground effect is exasperated by the low forward speeds, as the dust gets kicked up and then re-circulated through the rotor system.

Rotor Disk Loading

The rotor disk loading also is an important factor in the severity of brownout. Disk loading is the ratio of the helicopter thrust to the area of the rotor disk (pounds/inch).[6] Thus a single rotor helicopter in hover would have a thrust equal to the weight of the helicopter. Higher amounts of disk loading require faster rotor downwash velocities to maintain hover. Hence rotorcrafts with higher disk loadings are typically assumed to experience more severe brownout clouds because of the stronger downwash. In support of Sandblaster, a DARPA funded brownout initiative program, Cowherd[9] tested six airframes at the Yuma Proving Grounds (YPG) in Arizona. YPG uses tilled plots of sand to conduct brownout testing. The study aimed to investigate correlations

between airframe and brownout intensity. Table 1 shows the disk loading and the relative cloud intensity achieved. Results indicated that larger airframes with higher amounts of disk loadings were associated with higher cloud densities.

Table 1: Aircraft and associated disk loading and dust intensities.

Airframe	Disk Loading (lb/ft^2)	Cloud Intensity (relative)
UH-1	5	15
CH-46	6	25
HH-60	8	60
CH-53	10	100
V-22	20	100
MH-53	10	100

Source: Recreated from Cowherd[9]

Rotor Configuration

The number of rotors also plays a role in the amount of dust that is kicked up. Phillips and Brown[10] developed an Eulerian simulation for helicopter brownout to predict the formation of the dust cloud under different rotor configurations. By simulating simplified landing maneuvers for both single and tandem rotor platforms, it was predicted that the tandem experiences a higher severity of brownout, because the dust cloud formed closer to the tandem configuration and experienced a denser and more lasting dust cloud in comparison to the single rotor configuration (Figure A2). It is worth noting, however,

that these results disagree with the findings from Cowherd[9], as the CH-46 (a tandem rotor system) had a smaller disk loading since the weight is distributed between two rotors.

Blade Twist

In another study[11], Phillips and Brown again used the brownout model to examine the effects of tandem rotor configurations in brownout. A subset of the experiment studied the effect of blade twist on the size and shape of the brownout cloud. Blade twist refers to the amount of change in angle of attack the blade has across its length. Results suggested that, at least for tandem rotor configurations, rotor systems with more blade twist and equal amounts of disk loading experience less dense dust clouds than rotor systems with smaller amounts of blade twist.

Blade Tip Design

Other blade design elements such as the blade tip have been suggested to affect the formation of brownout as well. Pilots of the Agusta Westland EH-101 have claimed that its blade system developed by the British Experimental Rotorcraft Program (BERP) produce a "donut" of clear air around the aircraft.[1] Though specific causes for the phenomenon are not known, Agusta Westland attributes the phenomenon to advanced blade tip designs of the BERP blades.[12] However, Wadcock et al.[12] noted that a similar blade tip design is used for the Lynx helicopter, and does not experience the same "donut effect". Through CFD computational modeling, Wadcock et al. compared the UH-60 and the EH-101 to investigate reasons for the differing brownout performance. No conclusive evidence was found, but the authors hypothesized the airframe design of the EH-101 might be reason.

Surface Conditions

Additionally and undoubtedly, the environment is a pertinent factor of brownout. Surface composition is the leading environmental factor, as brownout occurs over loosely formed terrains like sand in desert environments. The severity of brownout however, can be dependant on the particle size distribution of the debris on the surface and the underlying surface texture.[13] The soil moisture is also a factor, as arid soil tends to have higher amounts of loose debris and dust that can easily be kicked up. The wind conditions dictate the severity of brownout, as it becomes more prevalent in low wind conditions when the brownout is able to remain more stagnant in the air. With moderate wind, the breeze helps to pull the dust cloud away from the aircraft, making it easier to maintain visibility during the approach and landing.

<u>Pilot Spatial Disorientation</u>

When the helicopter enters into low visibility conditions due to brownout, the pilot loses outside visual references needed to provide essential rate of closure information and altitude cueing to maneuver safely. Brownouts are particularly dangerous since they occur at low altitudes and at low speeds, when the aircraft is most instable and in close proximity to ground and obstacle hazards. As Key[14] reported from an investigation of Army pilot mishap data, rotorcraft can exhibit poor handling qualities during hover and low speed tasks, especially in DVE. Without any reliable outside visual reference cues, it is easy for the pilot to quickly develop spatial disorientation (SD), and subsequently make control inputs that lead to undesired or unintended velocities. These velocities expose the aircraft to an abundance of hazards including aircraft tipping or incursions with terrain and surrounding obstacles.

Sensory Stimuli

The human body primarily uses three sensory stimuli to derive situational awareness (SA) information: visual, vestibular, and proprioceptive. Visual cues are the most important for SA when the body or the surrounding environment is in motion. In dense fog or clouds, without any visual cues, even birds are incapable of maintaining enough SA to fly safely. That is because the visual field provides both critical monocular and binocular cueing to give speed, depth, and distance information.[15]

Vestibular information is provided via the semicircular canals and the otolith organs within the inner ear. The semicircular canals detect angular accelerations, while the otolith organs detect gravitational changes and linear accelerations.[16] These senses are involuntary and typically not consciously monitored or noticed.[17] But together these organs provide critical position and movement information. Furthermore, balance and coordination is strongly improved through the connection between the visual and vestibular information.

Proprioceptive information is provided through the body's somatosensory system and consists of sensory receptors covering the body that provide information for body position, movement, and force exertion. When coupled with vision, this system provides the needed feedback in order to perform precise or skilled movement.[17]

These three sources work together in unison to provide strong SA cueing to the brain for appropriate decision making. However, if any of them provide contradictory information to the others, the brain receives sensory mismatches, which then lead to confusion. This confusion between stimuli can propagate illusions in which the brain misinterprets information and makes false judgments, which then induces SD.[15]

Types of SD

SD can be classified into three general categories, all of which can be incurred during a brownout. Type I is unrecognized SD, meaning the pilot does not become aware of any hazardous SD situation. This can be particularly dangerous because the pilot does not become aware of any corrective actions needed, and thus can provoke controlled flight into terrain (CFIT) situations. Type II is recognized SD, meaning that the pilot realizes something is wrong, but cannot specifically define the problem. The realization of some error allows the pilot to take some sort of corrective action, but this can be dangerous because the pilot can unintentionally input incorrect control. Type III is incapacitating SD, meaning that the pilot is aware of an incorrect situation and is able to define the situation, but has simply too high of workload or stress to be able to take any action to remedy the situation.[18]

SD in Rotorcraft

In 2002, Mattews et al.[19] conducted a survey study to examine SD within the pilot community of the United States Air Force (USAF). Over one hundred USAF rotary wing pilots responded and it was found that the top four SD incidents for rotorcraft were undetected drift, misleading altitude cues, brownout/whiteout, and the "leans". In 2003, Holmes et al.[20] surveyed the UK military pilot community regarding SD and over 300 rotary wing pilots responded. In agreement with Mattews et al., it was found that the top four rotorcraft SD incidents in the UK pilots were the "leans", loss of horizon due to atmospheric conditions, undetected drift, and misleading altitude cues. All of these four SD incidents can occur during a brownout landing.

The "leans" is a term coined to describe an SD illusion in which the pilot feels as if the aircraft is banked when in actuality the aircraft is straight and level. This illusion

can be caused by poor visibility and gravitoinertial forces.[21] In a decelerating approach, the rotorcraft goes through lots of minor pitch and roll changes to maintain correct track towards the LP. During this time, the pilot can become accustomed to gravitoinertial forces at a certain angle and lose sense of *straight and level*. Especially, in a degraded visual environment, it can be difficult to visually determine the aircraft bank angles due to the loss of the horizon reference. Additionally the gravitoinertial forces can be misleading because of the confounding deceleration forces the pilot feels as aircraft slows and descends towards the LP.

When brownout envelops the cockpit windows, it not only obscures the outside visual scene, but also gives false motion cues because of the dust particles in the rotor downwash. This is a type of vection, which is an optical illusion that can be seen at low altitudes when the downwash creates misleading optical flows around the helicopter.[21] These trigger false senses of motion primarily from peripheral vision.[18] At hover, these flows within the dust can create a sense of climbing because of the downward motion of the dust in the downwash. This gives misleading altitude cueing and vertical rate cueing to the pilot. As the downwash impacts the ground, the flows can give a sense of moving backwards because the downwash moves radially away from the helicopter. Both these illusions can trick the pilot into correcting for something that does not need correcting, which can then lead to unintended drift velocities.

Replacing Lost Spatial Information

As discussed previously, the hazard of brownout stems from the loss of reliable visual information to the pilot during a critical phase of flight. SD is formed due to the vestibular and proprioceptive systems' heavy reliance on the visual stimuli for sensory validation. Anderson et al.[3] notes that regardless of the environmental condition, in order

to successfully maneuver and make a safe landing the pilot must be: (1) aware of the current aircraft state at all times, (2) understand the navigation needed to reach the LP, (3) assess the suitability of the LP, and (4) detect any obstacle hazards surrounding the LP. Without the ability to maintain visual contact of the LP, all of these requirements have the potential to be compromised. Therefore, it is imperative to replace the lost information back to the pilot through alternative means. There are three primary methods to provide this information back to the pilot: display symbology, sensors, and multi-sensory cueing.

Display Symbology

Display symbology is an essential component for increasing pilot SA in DVE. Through the use of intuitive symbols, critical information can be presented and interpreted adeptly by the pilot to make appropriate decisions for safe control of the aircraft. This section reviews literature on different concepts of symbology and the capabilities they provide.

There are different methods to visually present aircraft information to the pilot. Conventionally, this information has been displayed through the use of round dials situated on the panels in front of the pilot. Dials require the pilot to derive aircraft state from a culminating assessment of individual inspection of each dial. Advances in display technology have allowed for pertinent flight information to be displayed on CRT or LCD panel-mounted displays (PMDs), creating centralized sources of information, with potential reductions in the required visual scan pattern.

Symbology can be designed to provide information from different perspectives. The three primary formats are egocentric, and exocentric (perspective), and 2-D plan view (Figure A3). Egocentric symbology is depicted from the pilot perspective. Exocentric symbology is displayed from a perspective that is a tethered distance and

angle behind the aircraft. Plan-view refers to a format in which symbology is displayed from a vantage point directly above the aircraft. Wickens and Prevett[22] studied the effects of the three types of display formats. It was noted that the transition from an egocentric viewpoint, to an exocentric viewpoint, to a 2D-plan view correlates with a decreasing amount of ecological relation the pilot has with the display format. Hence, there is an amount of naturalness associated with an egocentric perspective. The egocentric display provided significantly better tracking for both the vertical and lateral axes. However, it provided less global spatial awareness concerning obstacles and environment surrounding the aircraft in comparison to the 2D plan view and exocentric view. In another article, Wickens[23] also noted that while 2-D provides greater precision in locating spatial surroundings, it also demands more attentional and cognitive loads. This indicates that there is no single solution in terms of display perspective to provide high levels of both global spatial awareness and tracking performance. However, rotorcraft displays have typically used the egocentric format for flight navigation and maneuvering, and plan-view format for hover and landing tasks. The following subsections detail symbology relevant to this study found for both display formats.

Rotorcraft Egocentric Display Symbology

If used in a PMD configuration, egocentric formatted symbology is typically paired with imagery also in a forward-looking viewpoint. The imagery can be generated either from an on-board aircraft sensor or synthetic terrain from a pre-stored database. This pairing allows for *conformal* (scene-linked) symbology within the PMD, which creates the illusion that the symbology is referenced the actual outside visual scene. McCann and Foyle[24] found that scene-linked symbology allows for concurrent processing between the imagery information and symbology information.

The flight path marker (FPM), also referred to as a flight path vector, is one of the most common conformal symbology pieces in an egocentric display (Figure 3). This symbol is typically depicted as a circle with some form of winglets around it. It is used as a predictor for the true direction of travel of the aircraft. In other words, whatever is in the center of the circle, the aircraft will eventually either fly-to or impact, which is why it has also been nicknamed the "smoking-hole indicator". The FPM is commonly found in fixed-wing aircraft, but has great utility in rotorcraft, since rotorcraft can easily fly velocities off-angle from the pure longitudinal direction. Visually, the pilot can generally determine the true direction of travel by monitoring the spatial flow of the environment. However, this symbol enhances the pilot ability for precision flight, especially in poor visibility conditions or environments with poor environmental cueing (i.e. sparse, un-textured desert floor). Sachs et al.[25] noted that the FPM improves performance and lowers workload because it allows the pilot to use pursuit/preview control since it is a predictor of future state.
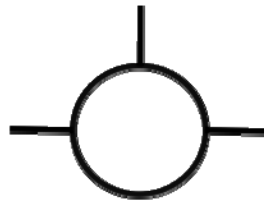
Figure 3: General symbol for a flight path marker (FPM).

To guide the FPM, there have been various "fly-to" cues used in the past. One of the most common is through the use of highway-in-the-sky (HITS) symbology, which provides a virtual pathway to guide the aircraft.[26] This has received considerable amounts of attention from both the fixed-wing and rotorcraft research communities, with application utility for general aviation (GA), commercial travel, and military operations.

One of its most prevalent benefits is its ability to enable the pilot to fly complex approaches with low amounts of tracking error[27] and better flight path awareness[28, 29]. However, for simple straight-in approaches, HITS can potentially be over cluttering. This was seen in a rotorcraft study by Keller et al.[30], which examined various display types for a straight-in approach to brownout landing. Two of the displays were identical except one additionally included HITS. Comparison between the two revealed that the HITS provided no significant benefit for the landing task, and additionally was associated with higher workloads and lower situational awareness ratings. For non-complex maneuvers, such as the final descent in a landing approach, using a simple indicator to show the location of the LP can be sufficient to guide the pilot. This type of guidance was used in the prototyped Comanche symbology[31] for waypoint navigation. Waypoint makers were used so that the pilot could place the FPM over the marker, and thus eventually arrive at the waypoint.
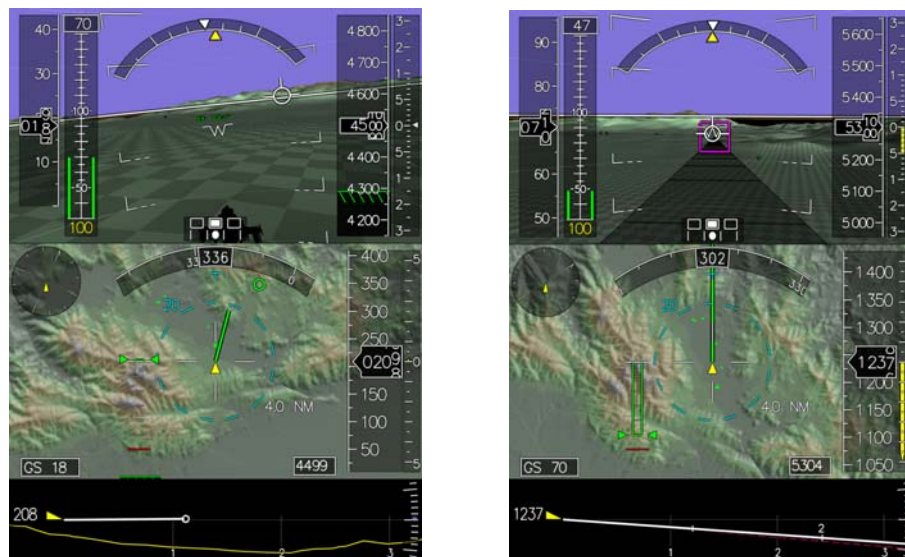
Figure 4: Synthetic vision displays with/without HITS.

Source: Keller et al.[30]

Error tapes are used to inform the pilot of the difference between current state and some desired state. They are useful as a feedback tool because they are minimalistic in design and use qualitative reasoning rather than quantitative. This alerts the pilot that correction is needed and provides a relative estimate of the error, without over informing the pilot of unnecessary details. An effective way to present the error is off a wing of the FPM. This format allows the pilot to maintain attention on the FPM and concurrently track any error for a given metric. Figure 5 shows FPM error tapes from a HUD symbology set that NASA Ames developed for the AV-8 V/STOL (Vertical/Short Take-Off and Landing) aircraft[32].
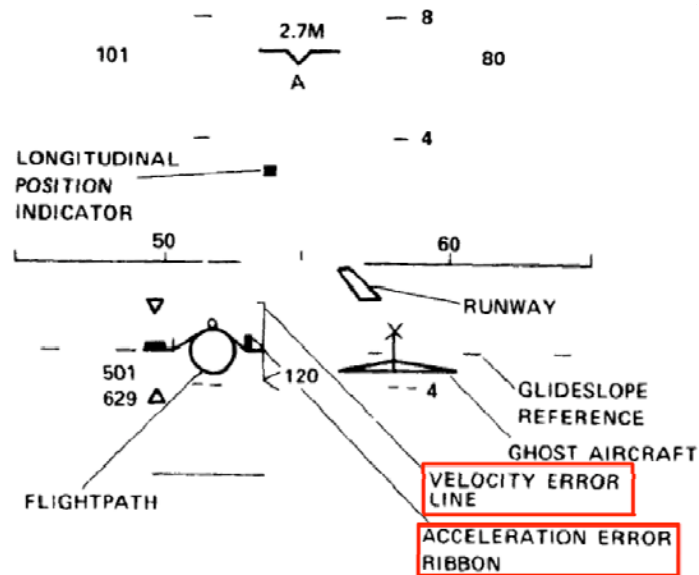
Figure 5: NASA HUD approach symbology for V/STOL aircraft.

Note: Error tapes boxed in red.

Source: Modified from Merrick et al.[32]

Rotorcraft Plan-View Display Symbology

The plan-view format as noted before is used primarily during landing and hover maneuvers for rotorcraft. The center of this display can be thought of as the center of the aircraft from a top down view. The symbology can be overlaid onto a top-down terrain view (such as a DTED moving map or synthetic terrain generated from a forward sensor), which can help in obstacle detection and avoidance. The following paragraphs detail the symbology relevant to this study that can be found on plan-view display formats.

A velocity vector is depicted as a line that grows from the center of the screen (the aircraft) in the direction that the aircraft is heading and in magnitude relative to the vector formed from the longitudinal and lateral velocity of the aircraft. An acceleration ball is a predictor of the velocity vector, as there can be a significant lag between change in cyclic control and the resulting aircraft velocity change. The acceleration ball almost directly correlates to the movement of the cyclic control. Together these provide strong velocity cues to the pilot for both magnitude and direction. To establish hover, the pilot simply holds the acceleration ball in the center of the display, and the aircraft comes to a hover.

A rising ground symbol (RGS) can be used to provide added awareness of height above the ground. This symbol represents the height of the terrain, so as the aircraft descends to the ground, the symbol moves up towards the center of the screen (indicating the aircraft is nearing terrain). Note that this symbol is *not* in plan-view format, but rather egocentric format. This is in disagreement with the overall display format, though it has received positive pilot review for providing saliency in height above terrain.[30,34] Figure 6 shows the hover page for the NASA V/STOL HUD symbology[32] which included a "landing deck" symbol to provide height information above the LP.
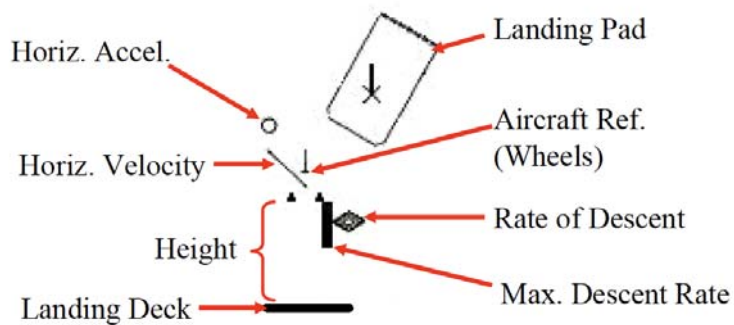
Figure 6: NASA HUD hover symbology.
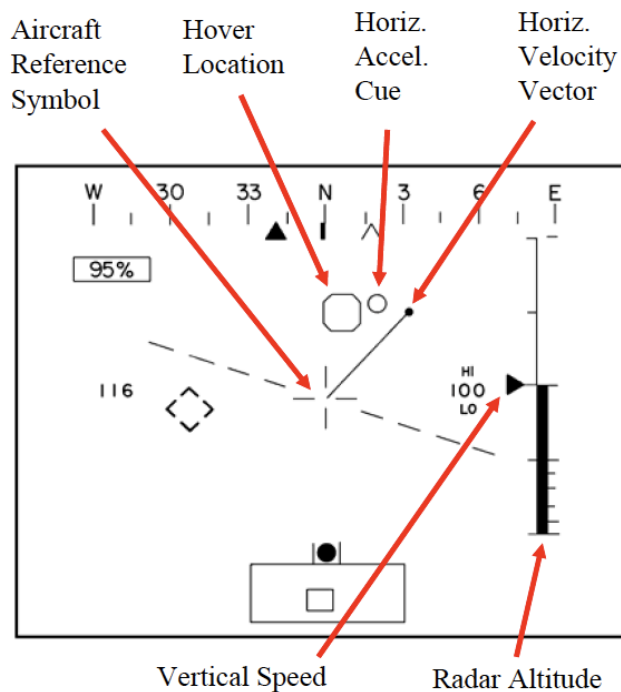
Figure 7: AH-64 hover page symbology.

The inclusion of the velocity vector/acceleration ball and rising ground symbol can help to mitigate pilot induced oscillation (PIO) during unusual attitude (UA) in brownout. McNerney[33] analyzed UA recovery data from a study at the NASA Vertical Motion Simulator.[34] The study compared BOSS symbology which has the velocity vector, acceleration ball, and rising ground symbol, against a standard HMD display that does not have any acceleration cue nor a ground symbol. The analysis found that the standard HMD symbology was associated with the slowest time to stabilize and the lowest amount of stability.

A LP marker (LPM) represents the true coordinates of the center of the LP. This has also been used as a hover hold marker, as seen in the AH-64 symbology[35] (Figure 7). For holding a hover above a certain location, the pilot would keep the acceleration ball inside the hover location symbol. This would ensure the pilot maintains a hover directly over the intended location. For landing approaches, it is useful to provide spatial reference for the location of the LP. As the aircraft nears the LP, the LPM moves towards the center of the screen. Eventually once the aircraft reaches the LP, the LPM arrives in the center of the screen, indicating that the aircraft is at the LP.

Sensor Imagery

Sensors are a way of providing real world imagery to the pilot in a heads down format. Through interpretation of this imagery, the pilot can derive information to satisfy the four listed requirements for making a successful landing. However, heads down sensor imagery is limited its field-of-view (FOV) and therefore is unable to provide strong peripheral cues like the out-the-window (OTW) view. So it can be difficult to detect minute translational rates. Though when paired with symbology, sensor views can immensely help with navigation, LP selection, and hazard detection.

Passive sensors detect the naturally occurring energy in the environment. These include sensors such as CCD (charge-coupled device) cameras and FLIR (forward-looking infrared). CCD cameras provide a supplemental OTW view and night-vision capability (depending on the spectral range), although they cannot see through atmospheric conditions and dust. FLIR detects thermal energy, and therefore can operate in all light conditions and can even penetrate through fog and minimal amounts of dust (Figure A4). However the image becomes obscured once in moderate to heavy dust environments.

Active sensors, unlike passive, actually emit some form of radiation towards the viewing area, which is reflected back and measured by the sensor. Millimeter wave (mmW) radar is an active sensor that operates at an extremely high frequency, which enables it to penetrate through atmospheric (fog, clouds, haze) conditions as well as dust. It collects three-dimensional coordinate data of the area ahead of the aircraft. Therefore this technology can be used to build a dynamic three-dimensional terrain map based on the surveyed terrain data. The Sandblaster program used a mmW radar coupled with a pre-stored DTED database (Figure A5).[5] This provided the pilot with a synthetic world that dynamically updated with sampled terrain data to reveal any potential hazards or obstacles throughout the approach and brownout.

LADAR (laser detection and ranging) is another type of active sensor. It is a laser on a gimbaled mount that scans the forward-looking area of the aircraft. LADAR is able to provide dense high-resolution three-dimensional data, which is depicted to the pilot as a dense dot cloud of terrain samples. It is accurate enough to reliably detect obstacle hazards as small as sixteen inches high and hanging wires.[36] Though it cannot penetrate through dust, the terrain can be surveyed prior to brownout and stored. That way, even in brownout, the pilot can use the three-dimensional synthetic world created from sampling. The AFDD and AFRL teamed up in a program called 3D-LZ in which BOSS symbology was coupled with a high performance scanning LADAR (Figure A6).[36]

Tactile and Aural Cueing

Research has been done to investigate the utility of cueing methods through alternative sensory stimuli. Aural cueing is one example, which uses pilot sense of hearing to interpret informational cues. Haas[37] used three-dimensional auditory cueing to warn helicopter pilots of four different mechanical emergencies. It was found that the inclusion of the auditory cueing significantly reduced the response time. Schnell et al.[38] conducted a fixed-wing study to test a spatial orientation enhancement system (SOES). The system included auditory (verbal) cueing to inform the pilot of unsafe aircraft orientation and unsafe speeds. The study found that the verbal cueing worked to alert the pilot of an evolving unusual attitude and aided in quick recovery for maneuvers with long evolutions along one flight parameter (i.e. pitch, or bank). However, not all 3-D audio is beneficial. Albery[39] and Schnell found that three-dimensional audio, when replicating wind noises, increased workload during extreme pitch angles.

Tactile cueing takes advantage of proprioceptive stimuli and uses tactors, which vibrate against the skin to convey information. The pilot typically wears some sort of vest or suit with strategically placed tactors. As the pilot flies, obstacle hazard or aircraft state information is delivered to the pilot through the vibrations. By determining the locale of the occurring vibrations the pilot can then determine a course of action to reduce the vibrations. As an example, if the aircraft oriented itself into an unsafe left-roll attitude, the tactors would fire on the left of the vest, indicating to roll right (away from the tactors). Jansen et al.[40] examined the utility of a tactile belt for helicopter flight in DVE conditions. Results showed that the inclusion of the tactile sensors increased the accuracy, allowed for better control, and reduced the amount of time to complete the maneuver. Albery[39] discussed results from a fixed-wing simulation test of the SOES, which also included a tactile vest. The vest aided in reducing aileron reversals when recoveries from extreme banks, and also aided in recovery from extreme pitch angles.

Additional Brownout Mitigation Initiatives

Beyond the human factors research to provide essential information to the pilot through sensory cueing, there has also been substantial research for brownout mitigation spanning a broad range of scientific fields. This section briefly discusses some of these other notable research initiatives. They include modeling the problem, predicting its onset, modifying the environment, augmenting the aircraft, and training the pilot.

Better Understanding of Root Cause

As mentioned in earlier discussion of brownout, there are numerous factors that account for the formation of brownout, and clearly there is still much to be discovered between these relationships of aircraft and environment. Therefore there has been research in modeling brownout and the parameters that feed into brownout (as discussed in the brownout section). However, one of the more notable current initiatives is a project headed up by Leishman and the University of Maryland.[41] Leishman is working on an expansive project for the US Air Force called the Multidisciplinary University Research Initiative (MURI) on Brownout. It is a five-year project (starting in August 2008) to develop a predictive tool to assess hazards of brownout dependant on an extensive list of factors.[5] These factors include those discussed in the brownout section (disk loading, number of rotors, blade twist, blade tip design, fuselage shape, surface type and surface condition) as well as other factors like blade loading, placement of rotors, and number of blades. The hope is that through modeling, a better understanding of the importance of these factors and their associated interactions will be gained. With this understanding, future design implications and procedural methods for rotorcraft can be determined.

Predicting Brownout

Rabaja[13] studied the polarimetric signatures of soils in order to determine if relationships existed such that susceptible areas to brownout could be remotely predicted via polarimetric radar. An algorithm was developed to analyze the soil moisture content, the particle size distribution, and the surface texture of polarimetric radar terrain data. Figure A7 depicts the grey-scale polarimetric image (scaled) and the same image colored using the algorithm to detect brownout conditions (red indicating susceptible brownout areas). This study showed promising results for the detection of brownout through use of the algorithm on the radar data.

Modifying the Environment

Another solution to mitigate brownout dust is dust abatement through the use of dust palliatives. These compounds can be applied to the LP surface by ground crew prior to landings. They coat the surface with a residue to help reduce the amount of dust kicked up by the helicopter during landing. Additionally, because the amount of dust is reduced, they also help reduce the amount of wear and tear that a helicopter experiences in dust environments.[42] These can be a relatively quick and effective way to solve the problem. The draw back though is that the LP must have dust abatement equipment available and must have been prepared ahead of time. Equipment includes a large water source to dilute the palliative compound, and a large distributor vehicle to spread the palliative.[42] This reduces the usefulness for tactical considerations, as many times an LP cannot be prepared ahead of time. Tingle et al.[43] studied the effectiveness of a number palliative compounds and tested three types of palliative distributor vehicles. It was found that some palliatives worked reasonably well to create a firm surface crust on the top of the LP. However, the study noted that the all three palliative distributor vehicles had

drawbacks. Two were found to have poor mobility in the loose sand, while a third did not agitate the palliative product properly.

Another option for dust abatement is to carry the palliative onboard the aircraft so that it can be dropped onto an LP prior to landing. Luttman[42] discusses this option in a contemporary issues paper. The CH-53E is a candidate aircraft to perform the task using a large bucket attached via sling load. This would be entirely feasible because of its large payload capabilities; however, the aircraft once loaded with a heavy sling load would become limited in its maneuvering and airspeed capabilities, which reduces its usefulness under tactical considerations. Rather than slung load, the palliative could be carried via tip tanks on the aircraft's auxiliary wings and dispersed using a release valve. This would maintain the aircraft agility and maneuverability, but may require tedious maneuvering over the LP to cover the area. Furthermore perceptual considerations would need to be taken, as the dispersion of palliatives via aircraft could be perceived as chemical munitions. So overall, environmental palliatives are useful in routinely traveled and occupied locations, but are not (yet) feasible for isolated, tactical environments.

Augmenting Aircraft Flight Controls

Augmentation is another option for enhanced aircraft stabilization to reduce pilot workload in brownout environments. Flight controls can be augmented to provide different levels of control commands. A standard, un-augmented aircraft is typically a rate command system in which a control deflection commands a rate. However, in an aircraft with control augmentation, cyclic deflection can be programmed to command an attitude or even a velocity. These augmented states can reduce the amount of controlling required during an approach and lessen the workload for the pilot. As Lebacqz[44] found during an IMC (instrument meteorological conditions) decelerating rotorcraft approach

study, attitude command augmentation was needed in order to have satisfactory handling quality ratings.

Full-authority flight control augmentation (fly-by-wire) removes the dependency of mechanical linkages between the flight controls and the control surfaces, and replaces them with computer-controlled servos. The UH-60M Upgrade aircraft included fly-by-wire control, allowing for various advanced flight regimes.[45] The Sandblaster program developed its brownout solution around this platform to take advantage of the advanced control capability.[5] The fly-by-wire system enabled the pilot to simply set up the approach and press a button, and then the aircraft automatically flew the approach, decelerated, and established a hover above the LP. The pilot could then press another button to drop the aircraft down to touchdown (TD) at the LP. This high fidelity augmentation greatly reduces the hazards of brownout, as it provides, in a sense, an "autopilot" to fly the approach and hover without the need for outside visual reference.

The BOSS symbology has purposely *not* been integrated with more advanced flight augmentation (yet), and instead has been tested using rate-command systems. This is intentional in order to show the true potential of the symbology, by enabling the more basic rate-command systems to safely land in brownout environments. Also the majority of rotorcraft in the military are rate-command systems.

Training for SD

Until new technologies come to replace current aircraft systems, the best option for mitigating brownout hazards is to enforce effective training for SD. Braithwaite[46] examined different methods for teaching SD to determine effectiveness. The most critical training recommendation from the study was to "make training more experienced-based", meaning training is greatly enhanced through the inclusion of hands-on simulation and in-flight demonstrations. Johnson et al.[47] developed a set of SD

simulation scenarios to use for Army aviators. The scenarios were modeled after actual SD incidents, to provide a high degree of realism within the environment and associated tasks. In one scenario, the student pilot was set at a 50 ft hover, and then given a standard task to change the radio frequency. During that time the instructor pilot set the aircraft into an unnoticeable rearward drift and decent. The pilot was then handed the controls 15 ft above the ground and asked stabilize the aircraft (if possible). These types of scenarios are beneficial to experience in a simulator because they mimic the real-world situations without the hazard. The scenarios from the study were met with a high level of acceptance as a training method from the subject pilots, and have since progressed into an actual training tool for the US Army.

Another option to provide a realistic brownout scenario in simulation is to develop an accurate brownout model, as done by Wachspress et al.[48] Using physics-based modeling, a high fidelity brownout model was developed capable of calculating the wake flow of the rotor wash in real time and applying it to a particle transport model. The model provided realistic cloud formation specific to the aircraft model, the environment surface, and the flight conditions. By using an accurate brownout model, simulation training can accurately mimic real world conditions and hence train mitigation techniques to a higher level of accuracy.

BOSS Symbology

The BOSS symbology is a tailored set of rotorcraft symbology with guidance to allow for safe landings in brownout. It was developed to meet the specific demand of presenting critical flight information to safely provide all necessary spatial cues and rate information so that the pilot can safely land the aircraft while under zero visibility conditions.   The symbology is presented in two display formats: a vertical situational

display (VSD) and a horizontal situational display (HSD) (Figure 8). The VSD is an egocentric view format, and its symbology is overlaid onto a forward-looking sensor view. The HSD is a plan-view format, and can be overlaid onto a top-down terrain view, although was not for this study. The VSD is used for the majority of the approach while the HSD is used at lower speeds when the aircraft is close to the ground and to the LP. In order for the aircraft to land safely at the LP, the pilot must concurrently manage three profiles: vertical (altitude) profile, lateral (cross-track) profile, and longitudinal (speed) profile. The following sections explain the control process for both the VSD and HSD displays to manage these profiles.
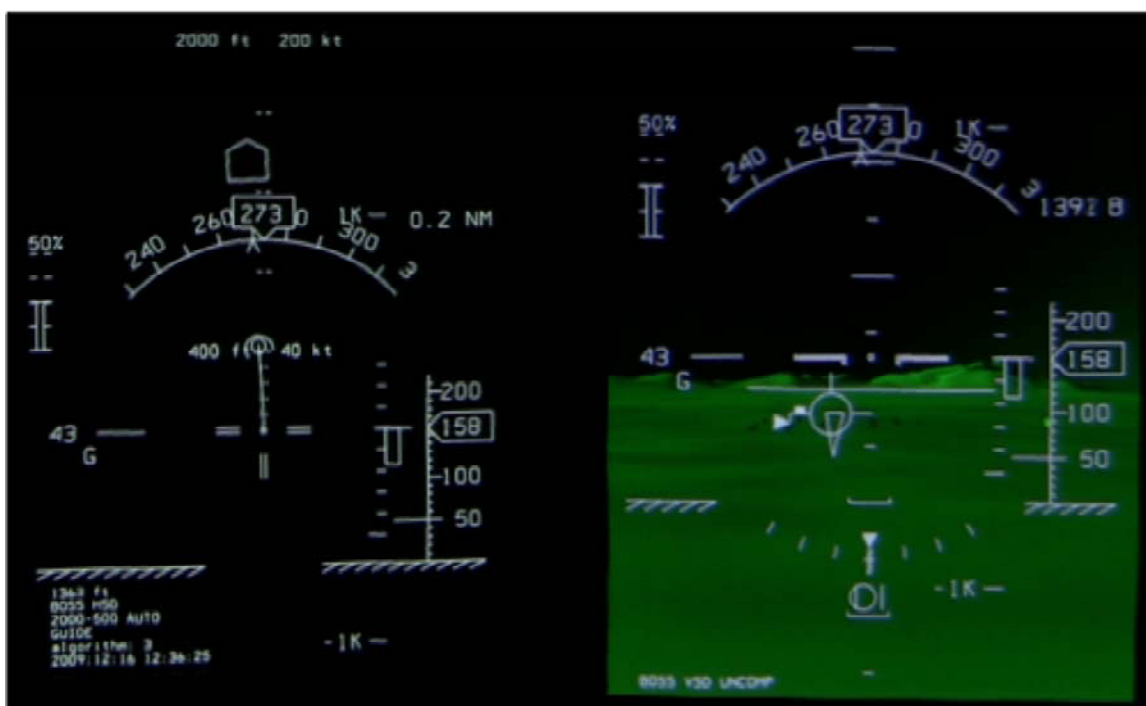
Figure 8: BOSS symbology.

Note: VSD on right, HSD on left.

Vertical Situation Display

The VSD is configured to enable the pilot to fly a heads-down visual approach using the symbology coupled with the under-laid sensor image (Figure B1). Conformal symbology includes the pitch ladder, FPM, and LPM. The LPM is an inverted triangle that is vertically projected from the center of the LP. If the pilot places the FPM over the bottom of the LPM, the aircraft will align itself onto the correct vertical profile and lateral profile to eventually arrive at the LP. Speed error is presented as a tape off the left wing of the FPM. This error refers to the speed difference between the aircraft's current groundspeed and the commanded groundspeed at any point along the approach. In order to manage the longitudinal profile, the pilot monitors the error tape, and makes subsequent pitch changes in order to bleed off any error that appears. By continuously minimizing this error tape, the aircraft stays on the correct longitudinal profile. This design of the VSD provides all necessary information at a small, single area of the display. By maintaining focus on the FPM, LPM, and speed error tape, the pilot can simultaneously manage all three profiles without need for a constant broad scan pattern.

At low speeds, the FPM becomes overly sensitive, making it instable and unusable. Therefore at 30 knots (kts) the FPM becomes dashed, indicating it will turn off soon, and then it turns off at 20kts. Therefore, sometime in between 30kts and 20kts, the pilot transitions from the VSD to the HSD. The HSD symbology is then flown for the rest of the maneuver until TD.

Horizontal Situation Display

The HSD is presented top-down format (Figure B2). The RGS however is presented in an egocentric format, as discussed in the Rotorcraft Plan-View Display Symbology section. The RGS is coupled with the radar altitude and vertical speed (V/S)

tape to provide quick assessment of terrain height with strong peripheral saliency so that terrain hazards can be detected in the peripheral vision. This allows the pilot to focus most of the attention on other symbology, with fewer required cross checks to the radar altitude. While on the HSD, the pilot manages the vertical profile by using the RGS and V/S tape.

The plan-view symbology includes the heading tape, velocity vector, acceleration ball, speed hook, and a LPM. The speed hook is a piece of symbology used to represent the speed that the aircraft should be at, and is designed such that the acceleration ball fits snugly into it. By placing the "ball in the cup" the aircraft follows the correct deceleration profile. During the approach, the speed hook moves towards the center of the screen indicating required deceleration. If the aircraft flies off course, the speed hook will swing radially to indicate required lateral correction. Therefore the speed hook concurrently manages both the longitudinal and the lateral profiles of the approach.

The LPM is depicted as a homeplate, with its center being the center of the desired LP. It is position referenced, so as the aircraft proceeds to the LP, the LPM moves towards the center of the screen, indicating the aircraft is nearing the LP. Once the aircraft is closer to the LPM than the speed hook, the pilot controls the acceleration ball into the LPM. This decelerates the aircraft the final five knots to arrive at the center of the LP with little or no forward groundspeed.

The HSD scales down three times during an approach. It starts at 2000ft/200kts to the top of the screen, then scales to 1000ft/100kts, and lastly down to 500ft/50kts. At a scaling change the velocity vector, acceleration ball, speed hook, and LPM all "jump" to a new position. The drawback of this is that it requires the pilot to refocus attention on the new position. But the benefit is that it allows for greater sensitivity in the symbology. So when landing, the pilot can better detect small unwanted velocities and also have better positional accuracy. At the finest scaling, the size of the LPM is roughly 50 feet in diameter.

Rotorcraft Landing Approaches

The following sections detail literature for the formulation of speed guidance and for approaches. Pilot behaviors for controlling aircraft in visual and non-visual conditions are explained and the differences between them are described as well. And current recommended approach profiles are provided for landing in DVE environments as mandated by the US Army for the H-60 Blackhawk.

Control Behavior during a Visual Approach

Garren et al.[49] stated that during visual approaches, pilots do not typically constrain themselves to following a specific velocity profile but rather modulate deceleration during the approach to achieve safe landing at the point of touchdown. This agrees with general tau theory, which postulates that pilots modulate speed based off the visual flow field experienced during the approach and attempt to maintain a constant ratio of speed and altitude for a constant tau-ratio. Padfield et al.[50] noted that under tau theory, the information regarding the speed and deceleration of the approach are not critically important in order to fly a precise landing or deceleration to a hover.

Moen et al.[51] conducted a study to analyze the characteristic shapes of the various rate profiles flown during helicopter visual approaches to hover. All approaches were flown between 6.5 degrees and 12.5 degree glideslopes. Four types of helicopters were used for the flight test, and included one light observation aircraft, one light utility aircraft, and two medium transport aircraft. Over 230 visual approaches were flown
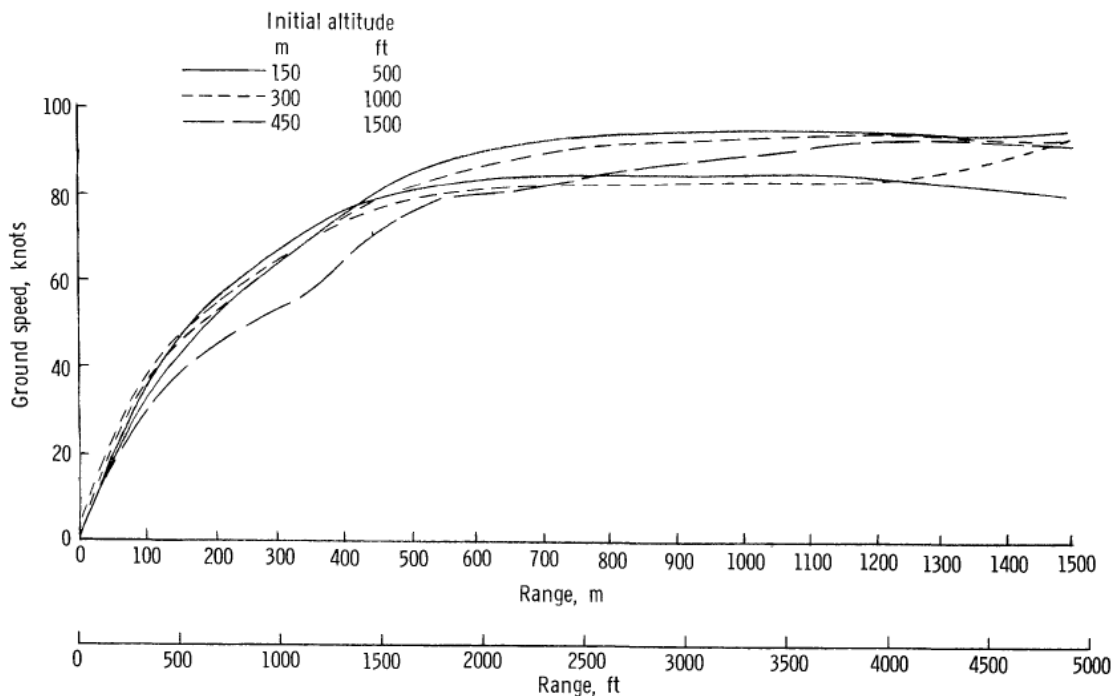
Figure 9: Typical visual deceleration profiles

Source: Modified from Moen et al.[51]

using military and NASA research test pilots. Figure 9 shows the typical deceleration profiles for an 80 knots visual approach.

Results of the visual approaches showed that pilots exhibited a behavior of increasing deceleration with decreasing range. During the visual approach the max longitudinal deceleration value ranged between 0.14g and 0.24g and occurred roughly 60 meters from the LP. The deceleration of course is highly correlated to the pitch of the aircraft, which was found to reach max nominal pitch values between 7 degrees to 11.5 degrees. Nominal pitch refers to the pitch attained above or below the trim pitch value of the aircraft. Trim pitch is dependant on the airspeed, as helicopters have different trim pitch values at different speeds. Lastly, it was found that the pitch-controlling

(longitudinal cyclic) increased significantly during the last 120 meters of the approach. These all indicate an aggressive flare maneuver at the end of an approach, in which the pilot bleeds off excessive airspeed by pitching the aircraft up and decelerating the aircraft. Kelly et al.[52] conducted a study to examine the benefits of using an augmented vertical velocity system to decouple the vertical and longitudinal control axes of the helicopter. During VMC approaches, it was found that pilots do not like visual approaches without a flare maneuver at the end.

Control Behavior during a Non-Visual Approach

Expectedly, there are noticeable differences between the way pilots fly approaches in visual meteorological conditions (VMC) and IMC. In general, pilots are much more confident with aggressive flight maneuvers during VMC than IMC. Garren et al.[49] studied a display and control concept for IMC landing approaches using a CH-46C research helicopter. Over 100 decelerating approaches to a hover were performed with an 80% success percentage. Results showed that pilots were reluctant to pitch up more than 12 degrees during the approach. Although it was noted that part of the reasoning for only pitching 12 degrees was because of lack of pilot confidence in the research system. Additionally pilots were also generally unsuccessful with 0.08g deceleration profiles because of the hesitancy to pitch higher than 12 degrees nose up. Deceleration rates up to 0.08g profile could be performed in zero or light wind conditions. However, it was noted that the deceleration was limited due to the hesitancy to pitch higher than 12 degrees. For the aircraft tested, the trim pitch attitude for hover was roughly 8 degrees, leaving a nominal pitch of only 4 degrees for deceleration. It was also discussed that the display layout of necessary situation information sources was rather spread out, which lead to inadequate cross check capabilities. The study thus recommended integrating guidance information and SA information. Figure 10 shows a
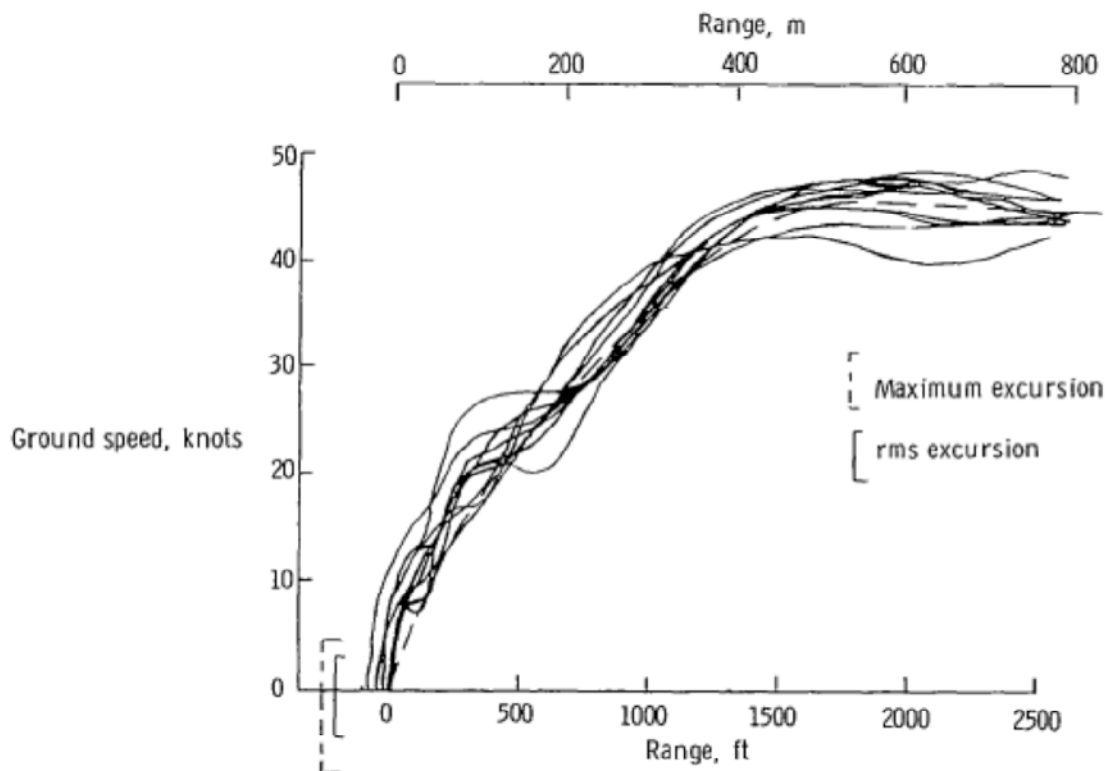
Figure 10: Non-visual deceleration profiles

Source: Modified from Garren et al.[49]

sample of the deceleration profiles flown by a pilot from the study. In comparison to Figure 9, it can be seen that much higher levels of groundspeed are upheld for longer periods of time under the VMC conditions.

Kelly et al.[53] studied the problems associated with steep decelerating approaches for helicopters in IMC conditions. The experiment tested a variety of variables including glide slope angle, deceleration profile, flight director-control laws, and control response characteristics. Results showed no significant differences between the approach performance using glideslope angles up to 25 degrees, and that vertical rates exceeding 1000ft/min were unacceptable for an approach. It was also reported that touchdown

vertical velocity of 90ft/min worked well, in that it was gentle but provided positive indication of touchdown. As with the previous study, pilot comments also recommended display integration of both guidance and SA information to aid in workload reduction.

In another study, Kelly et al.[52] graphically depicted the pilot workload experienced during an IMC deceleration approach (Figure 11). From examination of the figure, it can be seen that workload increases at the start of the deceleration task and maximizes during the low speed deceleration transition to hover. This is also where workload has the potential for greatest amount of variance and can reach unacceptable levels.
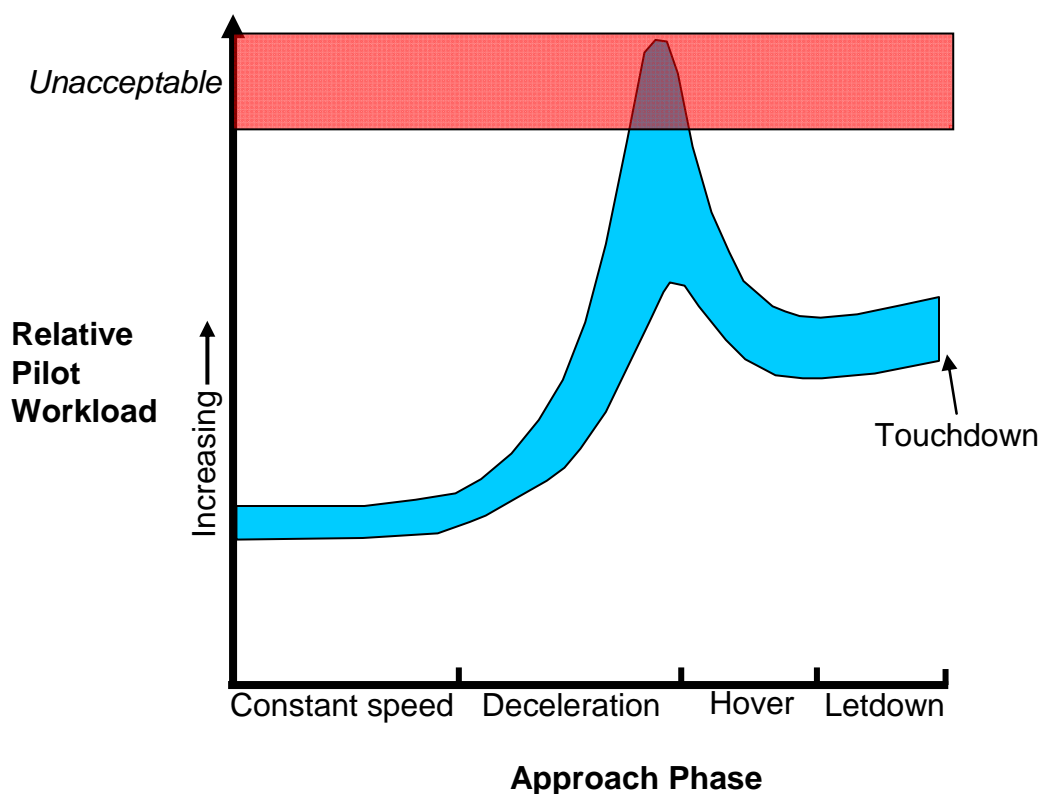
Figure 11: Workload by phase of flight during an approach from

Source: Recreated from Kelly et al.[52]

Operating Procedure for DVE Landing

There are predefined strategies used for degraded visual landings. The H-60 Aircrew Training Manual[54] details three different approach strategies for landing in snow, sand, or dust environments. The first is an approach to hover out of ground effect (OGE) with a vertical descent to the LP. The second is an approach for a landing with forward airspeed. And the third is an approach for landing with zero forward airspeed.

Termination to a point OGE. This approach requires OGE power and may be used for most snow landings and some sand/dust landings. Make the approach to a hover OGE over the intended landing location. Slowly lower the collective and allow the aircraft to descend. The rate of descent will be determined by the rate in which the snow/sand/dust is blown from the intended landing point. Remain above the snow/sand/dust cloud until it dissipates and visual references can be seen for touchdown. After ground contact, slowly lower the collective to the full down position and neutralize the flight controls.

Termination to the surface with forward speed. This termination may be made to an improved landing surface or suitable area with minimal ground references. Once the appropriate approach angle is intercepted, adjust the collective as necessary to establish and maintain the angle. As the apparent rate of closure appears to increase, progressively reduce the rate of descent and closure to arrive at the touchdown area slightly above effective translational lift. At this point, maintain the minimum rate of closure that ensures that the snow/sand/dust cloud remains behind the pilot's station. Apply slight aft cyclic just prior to touchdown to prevent burying the wheels or toes of the skis. When the wheels or heels of the skis contact the snow/ground, slowly lower the collective and allow the aircraft to settle. Lower the collective as necessary, neutralize the flight controls, and apply brakes as necessary to stop forward movement.

Termination to the surface with no forward speed. This termination should be made to landing areas where slopes, obstacles, or unfamiliar terrain precludes a landing with forward speed. It is not recommended when new or powder snow or fine dust is present because whiteout/brownout conditions will occur. The termination is made directly to a reference point on the ground with no forward speed. The angle should be slightly steeper than a normal approach and the approach speed faster than a normal approach. After ground contact, slowly lower the collective to the full down position, neutralize the flight controls, and apply brakes as necessary to ensure no forward movement.

H-60 Aircrew Training Manual[54]

These approaches are what are currently being used for brownout landings. However, even these are not free from hazards. From an interview with military helicopter pilots, McCauley[55] reported that while hovering in brownout at 10ft above the ground, neither the instruments nor the motion cues are adequate to maintain hover for more than just seconds. Thus, the OGE hover approach could be dangerous if the pilot does not descend to the ground quickly without hanging in the brownout for too long.

The approach for landing with forward speed is typically what is flown for brownout conditions. But it requires long, flat landing zones (LZs) so the helicopter can land with the forward airspeed. It also requires a fast approach followed by substantial amounts of deceleration at the end (in brownout) which can be hazardous. Additionally, it is not well known whether it is suitable for approaches when flying in formation with other rotorcraft.[3]

<u>Longitudinal Deceleration Guidance Algorithms</u>

The following sections discuss deceleration algorithms for the longitudinal speed guidance. A brief discussion on the balance of an algorithm is provided, followed by details of algorithms from literature. These include an exponential deceleration, constant deceleration, piece-wise constant deceleration, hybrid deceleration, and constant-attitude deceleration, and the manual deceleration.

Algorithm Balance

The algorithm driving the guidance needs to provide a safe balance between its aggression and time performance (Figure 12). An algorithm can be designed to minimize the amount of time required to complete a maneuver, but at the cost of requiring higher levels of aggression near the ground. Likewise an algorithm can be designed to minimize the aggression of the maneuver, but then leads the aircraft to be slow for extended periods of time. So within the algorithm, it is necessary to find an acceptable balance that allows for reasonable amounts of aggression with minimal amounts of time. This balance in the design of the algorithm commands the rates at which the guidance cues move on the display.

The information is conveyed to the pilot through the moving guidance symbology via the display interface. At that point, the pilot must interpret the symbology and determine the correct respective control inputs to follow the guidance. This requires the pilot to figuratively balance the stability of the aircraft to the incurred tracking error from following the symbology. It is therefore necessary to use an algorithm that facilitates this balance, and provides guidance that enables the pilot to track the symbology with minimal tracking error and concurrently provides acceptable aircraft stability throughout the maneuver.
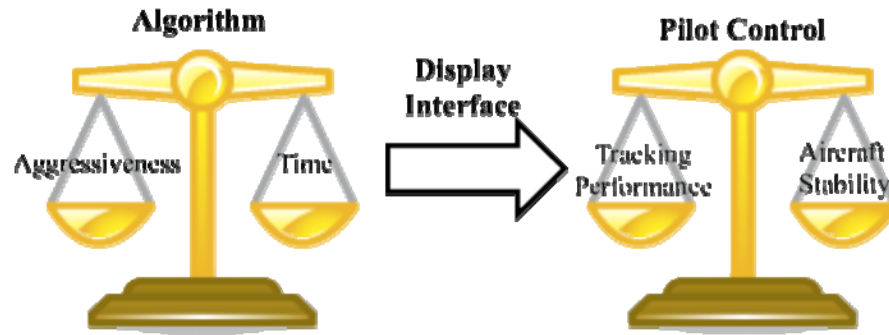
Figure 12: Balances of control within the system.

Exponential Deceleration

The Exponential Deceleration algorithm slows the aircraft at an exponential rate with respect to time as seen in the deceleration profile in Figure 13. This algorithm has also been called the "linear" algorithm, as it decelerates at a rate proportional to the distance the aircraft is away from the LP. A basic form of the equation can be seen in Equation C1.

This algorithm leads the pilot to perform a larger initial deceleration and then successively less amounts of deceleration as the aircraft nears the LP. Previous literature[49,53] as well as earlier BOSS studies[56,57,34,30,58] which implemented this algorithm have all come to the same conclusion regarding its performance: it causes the approach to take too long and invoke too slow of speeds near the LP. As Phatak[61] comments about this algorithm, it is an easy algorithm to implement, but it is "totally unacceptable" because of the long times spent at low speeds. This slow approach thus causes the aircraft to spend an extended period of time below effective translational lift (ETL) at low altitudes, which propagates brownout. Below ETL is also when the aircraft exhibits
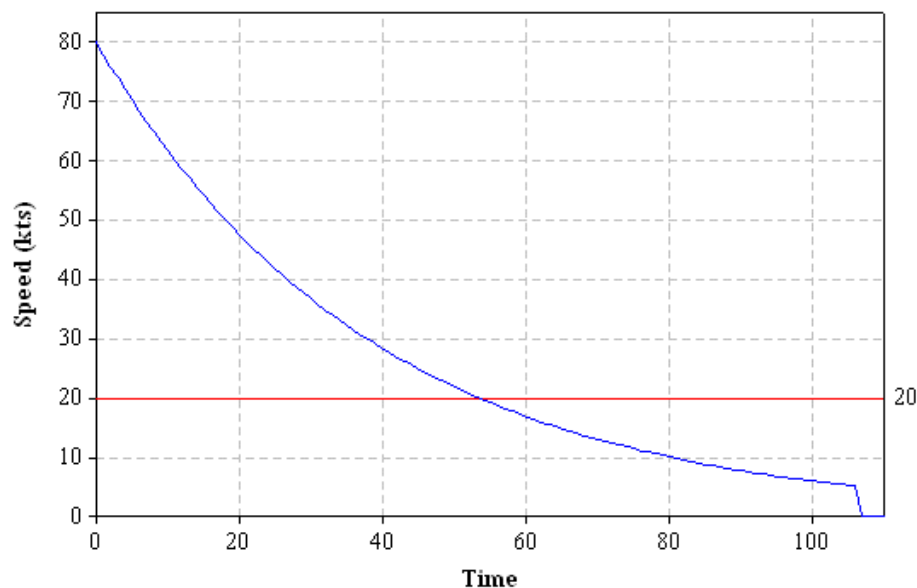
Figure 13: Exponential deceleration, velocity profile

Note: Red line – approx. ETL.

poorer handling qualities[14]. So this algorithm is not desired because of the tendency to prolong the amount of time spent in brownout with slow forward speed.

Constant Deceleration Algorithm

The Constant Deceleration algorithm uses a constant value for deceleration throughout the entirety of time in the approach as seen in Figure 14. In comparison to the Exponential Deceleration, it is a much more aggressive approach as it maintains higher speeds for longer periods of time. Thus it vastly reduces the excessive amounts of time in the approach and time below ETL. A form of the algorithm can be seen in Equation C2.
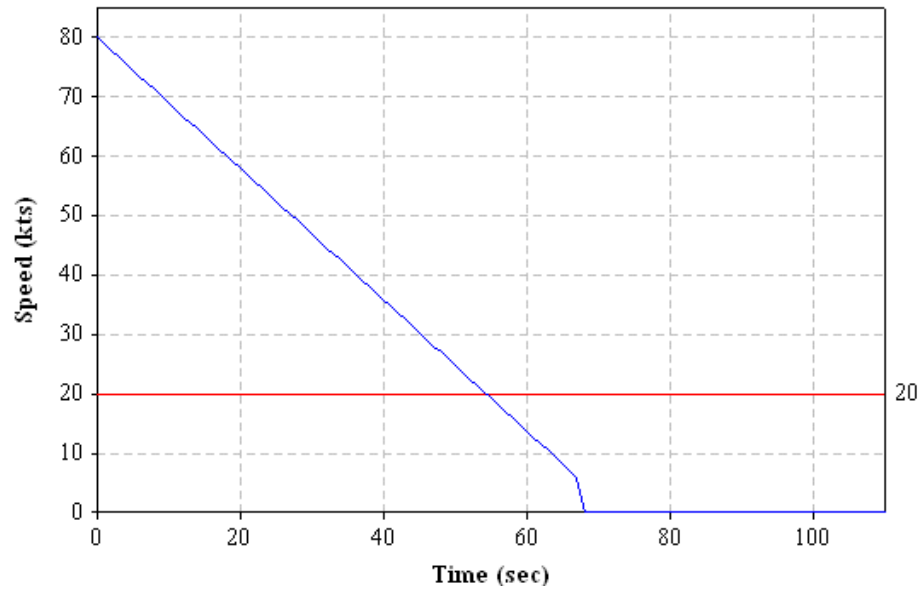
Figure 14: Constant deceleration, velocity profile.

Note: Red line – approx. ETL.
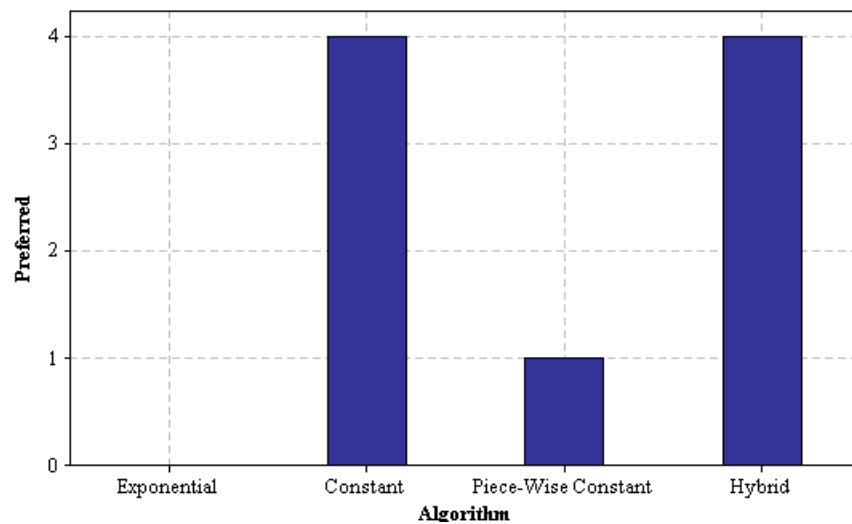
Figure 15: AFRL informal algorithm preference results.

Source: Recreated from McKinley et al.[58]

The AFRL started an initiative to investigate potential improvements to the BOSS symbology guidance equations.[58,59,60] New algorithms including the Constant Deceleration were tested during an informal study to improve its previous algorithm (Exponential Deceleration). Pilots from the study[58] commented that the Constant Deceleration felt much more similar to the way they visually fly. And from a preference rating, it was found that the Constant Deceleration tied for the most preferred algorithm (Figure 15). However, as mentioned in the previous section, pilots are less hesitant to fly aggressively while under DVE conditions. Thus while the Constant Deceleration is a definite improvement from the Exponential Deceleration, it has the potential to be too aggressive near the LP. As both Phatak[61] and Lebacqz[62] noted, this profile causes increasingly high pitch attitudes near the LP to maintain the constant deceleration. However, selecting a lower constant value for the deceleration can mitigate this effect.

Piecewise Constant Deceleration

To try to mitigate the potential over-aggressiveness of the Constant Deceleration, the AFRL developed a mixed constant deceleration algorithm (Piecewise Constant Deceleration) to slow the deceleration at close proximity to the LP (Figure 16).[60] Two different constant deceleration profiles were used, and the algorithm switched between them at a predetermined transition point (D_t = 1000ft) and transition velocity (V_t = 30kts). A form of the algorithm can be viewed in Equation C3.[60]

The initial deceleration was slightly more aggressive than the secondary deceleration. This algorithm provided a reasonably good descent profile. However the transition between the two deceleration rates caused a noticeable discontinuity in guidance at the switchover point (notice the rate change in Figure 16). This change in rate forced the pilots to push forward on the cyclic to arrest the deceleration and fit the new rate command. Pilots felt the transition between the two was not desirable and thus
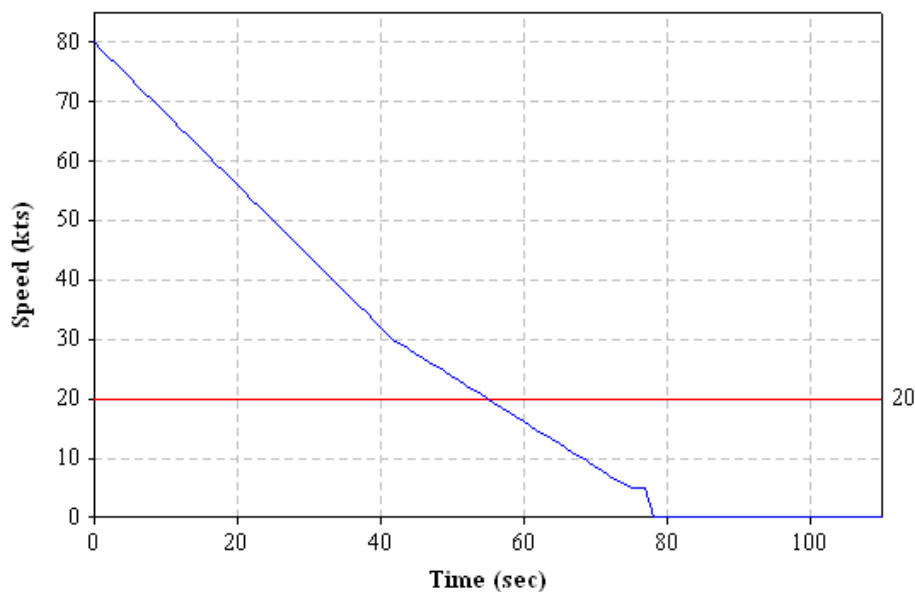
Figure 16: Piecewise constant, velocity profile.

Note: Red line – approx. ETL.

during the informal evaluation, the Piecewise Constant Deceleration was not overly preferred, as seen in Figure 15.

Hybrid

Another way to mitigate the aggressiveness of the Constant Deceleration is to include an Exponential Deceleration at the end of the profile (Figure 17)[49,53]. This provides the Constant Deceleration in the beginning to maintain higher amounts of airspeed, and then transitions to the Exponential Deceleration, which sets the aircraft up with sufficient airspeed to bleed off at the tail end of the approach. The exponential profile in the end also creates a smooth transition to lower the nose of the aircraft from a high pitch angle to a lower pitch angle. This prepares the aircraft up for a safer landing

and reduces the likelihood of developing aft velocity. Because of the Constant Deceleration in the beginning, it also maintains higher amounts of speeds, and thus reduces the amount of time in brownout in comparison to the pure Exponential Deceleration. Kelly et al[53] found this to be a vast improvement over the Exponential Deceleration.

The AFRL tested the Hybrid algorithm with the same D_t and V_t parameters as the Piecewise Constant Deceleration. A form of the algorithm can be seen in Equation C4. Pilots preferred this profile and the constant deceleration profile equally (Figure 15).[60] Through recommendation from experimental pilots (XPs), the Hybrid algorithm was eventually chosen to replace the Exponential Deceleration algorithm for the BOSS symbology.
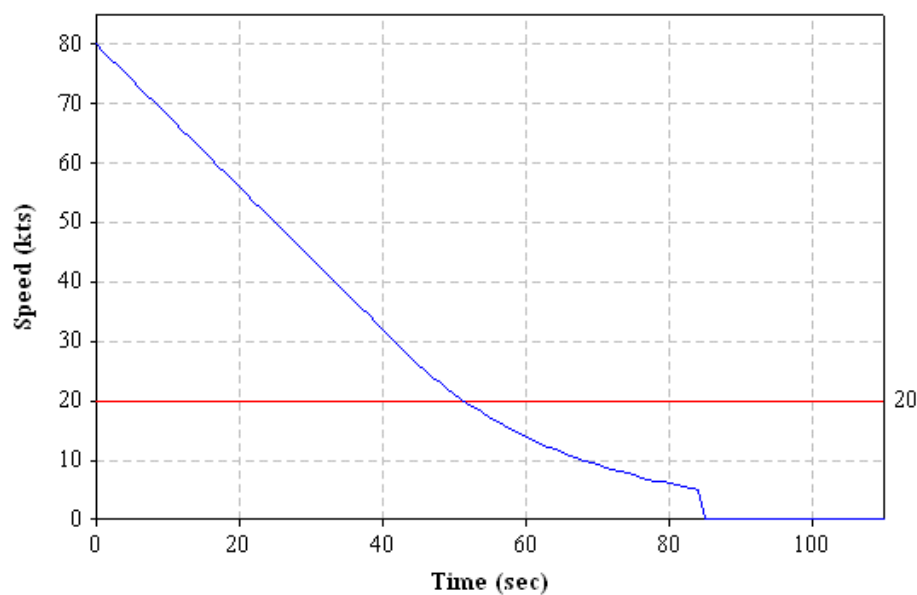
Figure 17: Hybrid deceleration, velocity profile.

Note: Red line – approx. ETL.

The Hybrid algorithm has been subsequently tested in BOSS simulation[56] and also tested in real brownout, as it was used during flight tests at the YPG.[36,66] It was during these flight tests in actual brownout conditions that pilots commented on the large amount of time spent at low speeds (in brownout) nearing the LP. Thus it was recommended to adapt the Hybrid to reduce the amount of time spent in brownout.

Constant Attitude

Another algorithm used to reduce the amount of controlling required during an approach is the Constant Attitude algorithm. This algorithm enables the pilot to hold a set attitude through the entire approach. This algorithm commands higher deceleration levels at the beginning of the approach, and lesser amounts of deceleration towards the end. Phatak[61] showed this works because the helicopter typically has a trim pitch profile that increases with decreasing airspeed as seen in Figure A8. The Constant Attitude algorithm when paired with an attitude-command augmented aircraft can make the approach much easier, because in this situation, the cyclic stick position commands an attitude. Thus the pilot can hold a stick position, which commands a certain attitude, for the entire approach.

Kelly et al.[53] found that this algorithm enabled easier transitions to hover than the Constant Deceleration. Moen[63] tested a type of Constant Attitude algorithm and found that during simulation trials the deceleration profile for 100kts initial airspeed was the most gentle and easiest profile to perform. Though during flight tests, pilots commented that this deceleration profile was too slow and resulted in a near hover far from the LP. Niessen[64] also used a Constant Attitude deceleration profile while comparing different display and control augmentations. In one instance the pilot was so focused on managing the deceleration profile, the aircraft unintentionally climbed 600ft in altitude. From the study, it was recommended that some form of flight director be included for decelerating

approaches to hover. Lebacqz[44] tested the Constant Deceleration, the Constant Attitude and an algorithm created to mimic visual flight deceleration (increasing deceleration with decreasing range), though no significant differences were found between them. However, in another report, Lebacqz[62] recommended the Constant Attitude algorithm for aircraft with attitude-augmented systems due to the less amount of controlling required.

Manual Deceleration Model

Heffley[65] developed a model for decelerating a helicopter from high speed to a hover using the rules of visual perception and a crossover model of the human operator. The model was formed using the hypothesis the pilot manages velocity proportionally to the perceived range. This agrees with the discussion above regarding pilot behavior during the visual approach. The model was validated against flight data and shown to respond close to that of pilots flying a VMC approach. This profile thus requires increasingly larger amounts of deceleration as the aircraft nears the LP (Figure A9). The author suggested this algorithm be used to drive an autopilot, as it flies like the pilot normally would under VMC operation. This algorithm would not be ideal for brownout applications however, as it requires substantially more deceleration aggressiveness near the ground than even the Constant Deceleration.

CHAPTER III. EXPERIMENTAL OBJECTIVES

1. Develop a mathematical model to compute the deceleration profiles for the longitudinal velocity using different algorithms.

2. Investigate new algorithms to reduce the amount of time spent in the approach and at low speeds.

3. Tailor new algorithms to have robust capability for guidance from various initial altitudes, distances, and airspeeds.

4. Down-select a set of algorithms to be used for a formal evaluation.

5. Evaluate algorithms in formal piloted simulation experiment with rotorcraft pilots.

6. Analyze results of study to quantify potential benefits of new algorithms.

7. Extend results to provide a recommendation for the future deceleration algorithm of the BOSS symbology.

CHAPTER IV. MATHEMATICAL MODEL DEVELOPMENT

In order to study the effects of the algorithms on the flight profiles, a mathematical model was developed to simulate the deceleration. The model was created using Simulink in Matlab. Simulink provided a graphical environment for model-based design, allowing for the design, simulation, and evaluation of the speed guidance algorithms. It was the desirable modeling platform, as it facilitated rapid testing of various algorithms and provided comprehensive graphical results for quick interpretation.

Simulink Model

A simple model was developed in Simulink to predict how an algorithm would behave during an approach. The system therefore only included the initial conditions, the algorithm, and the display (Figure 18). The actual Simulink model can be viewed in Figure D2. In this system, the initial and current flight conditions were fed into the algorithm, which then computed the appropriate speed guidance value (in kts). Since the model was developed to examine the behavior of the guidance, the calculated guidance value was fed back to the beginning of the system to create a closed loop system. The speed guidance was also fed into the display module where it was converted into pixel movement for the display. Both the algorithm module and the display module were programmed using embedded Matlab functions. All relevant flight parameters were sent out of the system for analysis and interpretation.
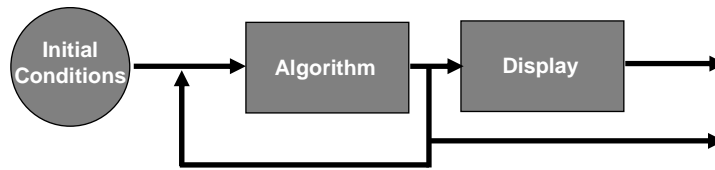
Figure 18: Simple model system.

GUI Interface

To easily manipulate the Simulink model, a GUI interface was programmed using the Matlab GUI layout editor (Figure D1). The model and interface together provided a useful application from which the algorithms could be inspected and analyzed to direct further development.

Within the GUI, the desired algorithm could be selected via a set of radio buttons. All parameters relevant to the algorithms could be quickly set and adjusted using slider bars and text fields. These parameters included the initial velocity of the aircraft, the initial distance from the LP, the transition point distance from the LP, the transition velocity, and the velocity bias. To facilitate determining distances from the LP, a converter was programmed to convert feet to nautical miles. Once the algorithm was selected and the parameters set, the speed profile could then be plotted. The graph options allowed for various colors and line styles to be used for the plots. Additionally a hold button allowed for multiple plots to be plotted on the graphs, so that easy comparison between algorithms or parameters could be made.

The default output for the graphs provided three plots to evaluate the speed profile: velocity vs. time, velocity vs. distance, and acceleration vs. distance. However, the third graph had the capability to also show the acceleration vs. time, the screen position vs. distance, and the screen position vs. time. The screen position plots showed the rate at which the symbology would move across the screen. A summary section was

also included in the bottom left of the GUI to show all the current parameters selected. It also calculated the amount of time the profile would take, the time spent below 20kts, and the maximum deceleration value (in g's). Use of the Simulink model and GUI interface allowed for quick and effective evaluation of the algorithm.

CHAPTER V. ALGORITHM DEVELOPMENT

This chapter details the work completed with regard to new algorithm development. The first section explains the problems with the previous algorithm used in the BOSS symbology. The following sections detail the different algorithms investigated for potential implementation.

Problems with the Previous Hybrid

As previously mentioned, there were two main issues that needed to be addressed regarding the previous hybrid algorithm. Together, these issues formulated the purpose and motivation for this study. The first was that pilots found the algorithm led the aircraft to be at low speeds for too long in brownout.[66] Therefore, there was a need to explore different ways to potentially reduce the amount of time spent at low speeds.

The second issue was that the hybrid algorithm was only designed to provide guidance for one specific approach (IP of 0.8Nm and 80kts). It happens to also provide acceptable guidance for few specific other approaches, but it lacks any robustness to handle much variance in IP conditions. This is because the hybrid was constrained with both a fixed D_t and a fixed V_t. When used with other IPs, it can develop unfavorable discontinuities. Figure 19 shows the acceleration plot for a faster approach using the Hybrid (80kts, 0.6Nm). The acceleration plot exemplifies the discontinuities formed at the transition between the constant deceleration and exponential deceleration portions. These discontinuities were not desired because they can create inconsistent behavior depending on the initial conditions. This problem was also seen in the piecewise constant deceleration algorithm which had a discontinuity at the transition point between the two
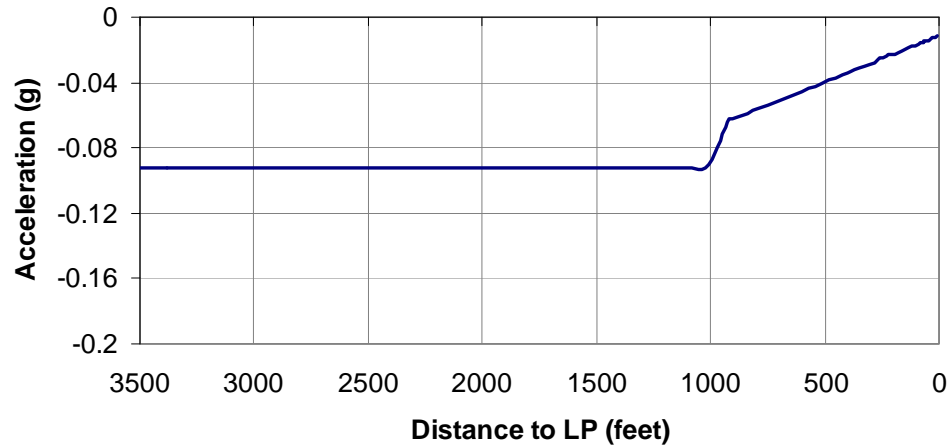
Figure 19: Deceleration profile of faster approach using previous Hybrid.

constant decelerations. Therefore, there was a need to develop the hybrid into an algorithm that could produce relatively consistent and smooth transitions between the constant deceleration and exponential deceleration portions.

Constant Attitude Algorithm

In the investigation of new algorithms, one worthy alternative was to use a Constant Attitude algorithm, as mentioned in the literature. This algorithm received positive reviews from pilots, and thus it was worth considering. The benefit of using this algorithm is that, when implemented in an attitude-augmented aircraft, it greatly reduced the amount of controlling required to complete the maneuver, because the pilot could keep the cyclic in the same position throughout the whole approach. It also provided a nice deceleration profile such that the majority of the deceleration occurred in the beginning and then decreased as the aircraft slowed. This is because most aircraft have a trim pitch profile like the one in Figure A8. However, the UH-60 has a very different trim pitch profile due to the stabilator on the tail of the aircraft. This stabilator is

automatically controlled via the flight control system. Thus as the aircraft slows, the stabilator changes deflection angles, which greatly changes the trim pitch attitude, as seen in Figure E1. Additionally, the BOSS symbology has been designed for rate-command systems, not attitude command systems, so the benefits of the constant attitude could not be realized. Additionally, as noted in the literature[63] there were pilot concerns that the deceleration led the aircraft to be slow and low for long periods of time. Therefore, it was decided not to pursue the constant attitude algorithm.

Constant Cyclic Position Algorithm

To achieve the same benefits of the Constant Attitude algorithm when used with an attitude-augmented system, it was thought to test a Constant Cyclic deceleration for a rate-command aircraft. This deceleration would allow the pilot to hold the cyclic in a constant position throughout the approach, which would allow for less controlling. A constant cyclic deceleration was tested in the simulator to investigate its utility and feasibility. Results showed that the constant cyclic led to a slower approach than the previous hybrid, and had comparable amounts of time spent in brownout. Additionally, due to the dynamics of the UH-60 and its stabilator, it was recommended not to use this approach, as it would likely not provide robust results for varying approach IPs.

Creating a New Hybrid

Another idea for a new algorithm was to pursue an adaptation of the previous Hybrid. But first it was necessary to develop a Hybrid capable of handling different initial velocities and distances from the LP. The previous Hybrid was limited because it

used fixed D_t and fixed V_t values. The new algorithm needed to use varying values of either the D_t or V_t. By varying either of these two parameters, smooth transitions between the constant deceleration and exponential deceleration could be achieved. Therefore, two proposed new hybrid algorithms were created. The first used a static V_t, with a dynamic (varying) D_t, and was named the Constant V_t Hybrid. The second used a static D_t, with a dynamic V_t, and was named the Constant D_t Hybrid.

To solve for either a dynamic V_t or D_t, data had to be gathered examining the transition distance and transition velocity under different IPs. This was done through the use of the Matlab GUI. A 10x4x6 full factorial design was used to collect two datasets, with the following factors: initial distance from LP (0.6-1.4Nm in 0.1 increments), initial speed (60-120kts in 20kt increments), and either V_t(15-30kts in 3kt increments) or D_t (250-1500ft in 250ft increments). For the first dataset, V_t was used as the third factor, and the GUI was used to solve for an appropriate D_t that led to a smooth transition between the constant and exponential portions of the algorithm. For the second dataset, D_t was used as the third factor, and the GUI was used to solve for V_t to provide the smooth transition. A total of 240 data points were collected for each dataset. Additionally for both datasets, time to touchdown, time spent under 20kts, and the maximum deceleration values were recorded.

Constant V_t Hybrid

Using the collected dataset, regression analysis was performed in Minitab to solve for D_t. The initial model used D_t as the response, and examined all possible factors and interactions as listed: D_o, V_o, V_t, D_o*V_o, D_o*V_t, V_o*V_t, D_o*D_o, V_o*V_o, V_t*V_t, $D_o*V_o*V_t$, D_o*V_o. Stepwise regression was performed to remove any insignificant factors or interactions. The final regression equation fit the model with an adjusted r-squared of

99%. The regression analysis can be seen in Figure E4 and the resulting equation can be seen in Equation C1.

This model was mapped using 4-D plots to examine the resultant D_t and deceleration time under varying D_o and V_o and V_t (Figure E7). The solution surface shows the calculated values for D_t that the algorithm uses to try to provide a smooth transition between the constant and exponential decelerations. From coloring of the plots it can be seen that reduction in the V_t can result in less time spent in the approach. With this algorithm, the transition to the exponential deceleration would always occur at the same V_t with a dynamic D_t calculated based on the IP parameters. However, V_t is a velocity based on the speed schedule. Therefore, the profile would switch at the point when the aircraft *should* be at V_t, but not necessarily when the aircraft speed was at V_t. This meant that if the aircraft was off speed schedule, the transition would appear to occur at different speeds. After discussion of this behavior with the AFRL, it was ruled better not to include this ambiguity, and thus the Constant V_t Hybrid was not used for the experiment.

Constant D_t Hybrid

The same regression procedure was completed for the Constant D_t dataset. The initial model used V_t as the response, and examined all possible factors and interactions as listed: D_o, V_o, D_t, D_o*V_o, D_o*D_t, V_o*D_t, D_o*D_o, V_o*V_o, D_t*V_t, $D_o*V_o*D_t$, D_o*V_o. Again a stepwise regression was performed to methodically remove the insignificant factors and interactions. The final equation fit the model with an adjusted r-squared of 98.1%. The regression analysis can be seen in Figure E5 and a form of the equation can be seen in Equation C6.

A set of 4-D plots were created to examine the solution surface area with the colored shading to provide temporal information (Figure E8). From examination of the

time-coloring, it was found that by using a lower D_t, the algorithm could quicken the approach. It was also found that lower values of D_t could result in lower amount of times spent below 20kts, as seen in Figure 20. These results were presented to the AFRL, and after further discussion, it was decided to use the Constant D_t Hybrid for the simulation with varying D_t values. However, the AFRL recommended modifying the algorithm such that it could handle closer distances better.
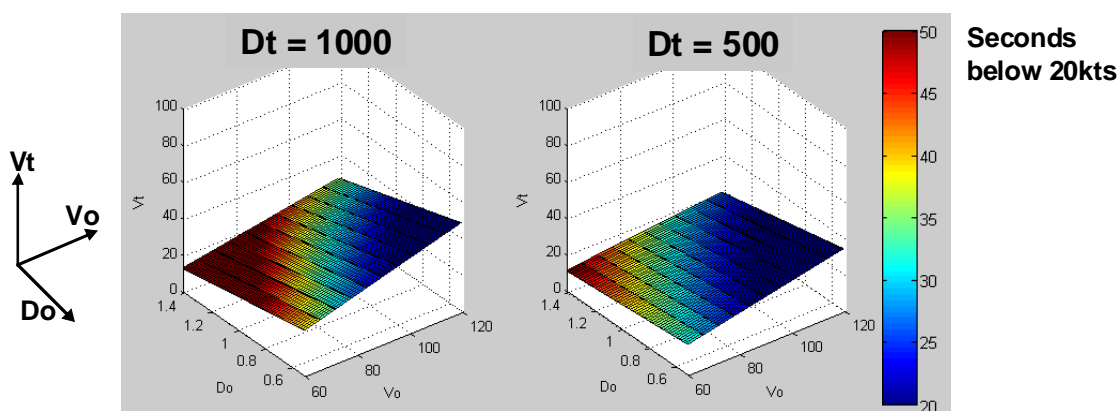
Figure 20: Differences in time below 20kts between 1000ft D_t and 500ft D_t.

Therefore, 48 more data points were collected between 0.3 and 0.4Nm. At this close of range, some initial velocities were not practical, which made the regression difficult to obtain a reasonable fit. Therefore, the dataset was filtered to reasonable deceleration values (0.04g – 0.14g). Regression was run using the full model to include all factors and interactions. Ten outliers were subsequently removed from the model to increase model accuracy. And replications of validation runs were added to strengthen the common approach profiles. The result was a model with a 98.5% adjusted r-squared value. The regression analysis can be seen in Figure E6 and the equation can be seen in Equation C7. This equation was programmed into the Matlab GUI, and tested using a variety of different starting positions and velocities. The plots showed that this new

Hybrid algorithm responded well to the IPs and provided relatively smooth and consistent transitions between the constant deceleration and exponential deceleration. Figure 21 shows the acceleration profile for the same approach as Figure 19 (80kts, 0.6Nm), but calculated using the Static D_t Hybrid. It can be seen that the new algorithm provides a much smoother transition between the constant deceleration and exponential deceleration portions.
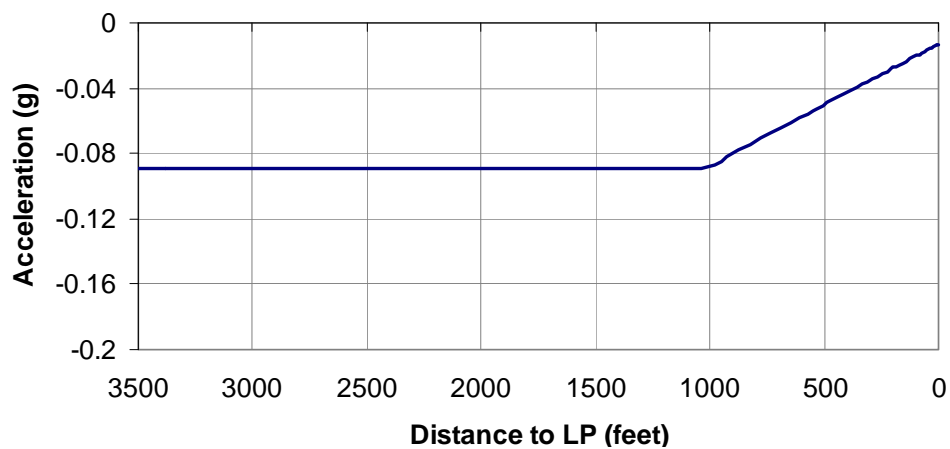
Figure 21: Deceleration profile of faster approach using Static Dt Hybrid.

CHAPTER VI. EXPERIMENTAL SETUP

Experimental Design

The experiment was designed as a 4x2 complete within-subject factorial design with one replication. The factors were the longitudinal speed guidance algorithm (four levels) and the approach (two levels).   This design was used because it was quite simple yet powerful since it tested all combinations of algorithms and approaches. The replication was included to help reduce variance and the possible presence of outliers in the data. In all, the design required a total of 16 data runs per pilot. The two factors are further detailed in the proceeding sections.
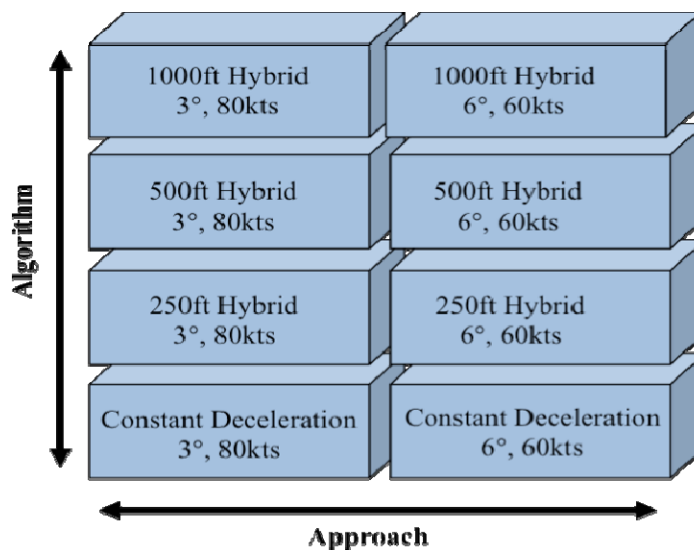
Figure 22: 4x2 experimental test matrix.

Factors

Longitudinal Guidance Algorithm

The purpose of the algorithm factor was to provide the pilot with four different levels of deceleration aggressiveness. Results from the informal AFRL study[58] revealed that pilots equally preferred the Constant Deceleration to the Hybrid. However, it was hypothesized that pilot preference would likely lie somewhere in between the Constant Deceleration and the Hybrid. Therefore, the Fixed D_t Hybrid was used to create two new algorithms that fell in between the Hybrid and the Constant Deceleration in terms of aggressiveness.

The baseline was the Fixed D_t Hybrid with a D_t of 1000ft and is referred to as the 1000ft Hybrid. This algorithm behaved just like the previous Hybrid, which had been the standard for the BOSS symbology. Therefore, this was deemed the least aggressive algorithm tested. The next algorithm was the Fixed D_t Hybrid with a D_t of 500ft and is referred to as the 500ft Hybrid. This was slightly more aggressive than the 1000ft Hybrid and was expected to produce less amounts of time below ETL. The next algorithm was the Fixed D_t Hybrid with a D_t of 250ft, and is referred to as the 250ft Hybrid. This algorithm was more aggressive than both the 1000ft Hybrid and 5000ft Hybrid and was thus expected to provide faster approach times and less time below ETL. The last algorithm tested was the Constant Deceleration, and was the most aggressive algorithm.
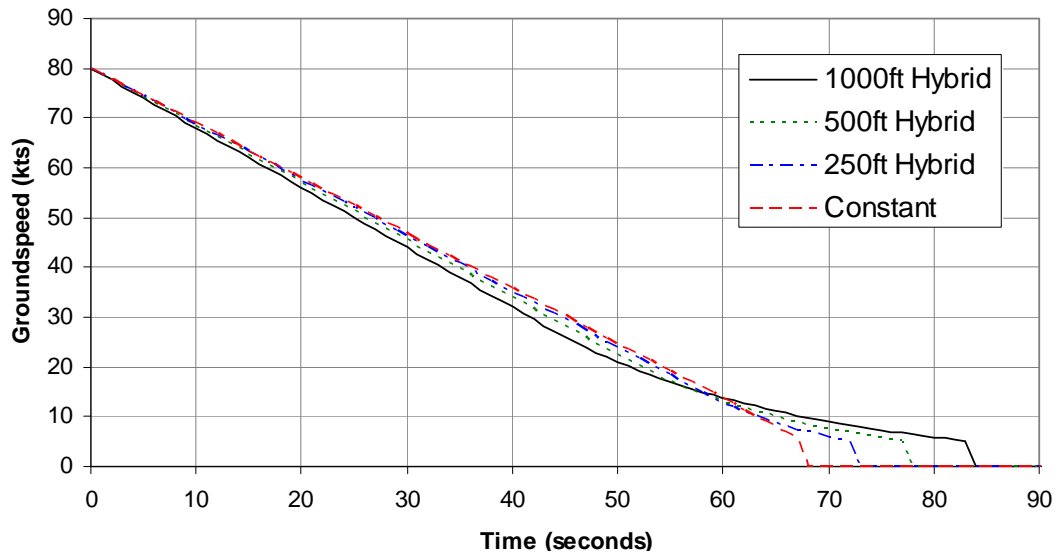
Figure 23: Velocity profiles for 3-degree approach.
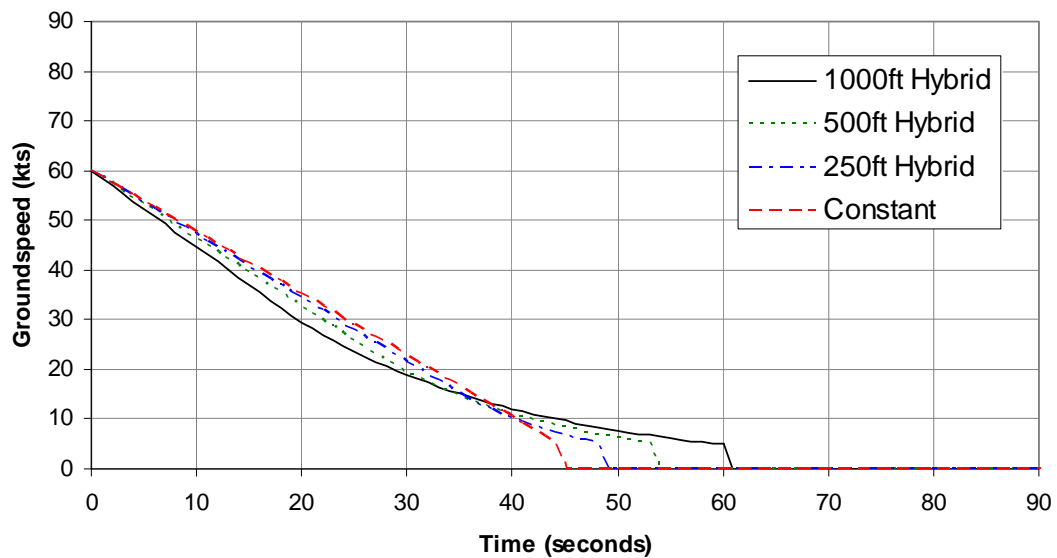
Figure 24: Velocity profiles for 6-degree approach.

Approach

Two approaches were used to test the deceleration algorithms under differing approach parameters (Figure 25). Both profiles started an altitude of 255 feet above the LP and began with an initial straight and level segment aligned on the correct heading for the final approach, which lasted for five seconds. Once the aircraft reached the final approach fix (FAF), a decelerating descent was initiated towards the LP. The aircraft continued the approach to arrive at the intended landing point with minimal airspeed, lateral drift, and rate of descent at touchdown. The maneuver ended once contact with the ground was made. Run cards for the two approaches can be seen in Figure F3 and Figure F4. The calculated V_t values for the approaches can be seen in Table F2 and Table F3.

The first approach was a shallow profile, and was identical to the approach that has been commonly used in the BOSS symbology studies.[36,58,66,56,57] It started the aircraft at 80 knots and began the descent and deceleration at 0.8 nautical miles from the LP, following a shallow three-degree glideslope. This approach is typically used to allow the pilot to maintain higher amounts of forward airspeed for longer periods of time.
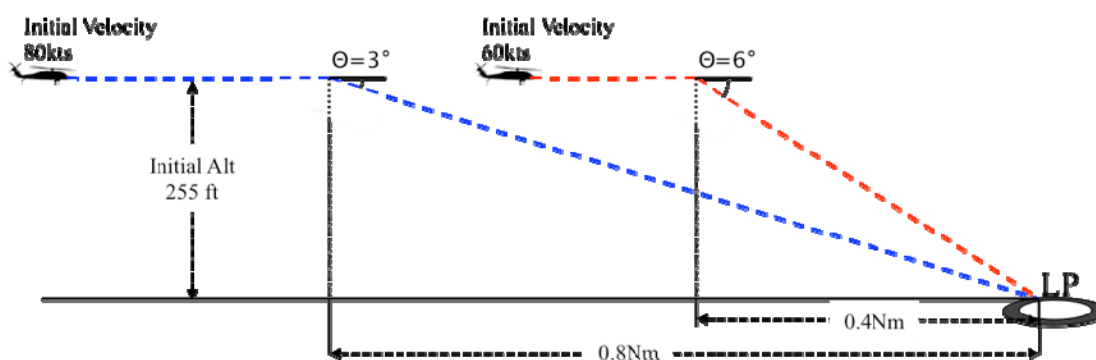
Figure 25: Approach profiles.

Note: Blue line – 3 deg approach, red line – 6 deg approach).

The second approach started the aircraft at 60 knots and began the descent and deceleration at 0.4 nautical miles from the LP on a six-degree glideslope. This glideslope is closer to a normal decent angle for an approach. Since the approach began closer to the LP, it took less time to complete the maneuver, and required slightly stronger decelerations and pitch angles to complete.

Blocking

The differences between some of the algorithms could be perceived as somewhat subtle at times, and therefore it was determined necessary to block the experiment on the algorithm factor. This way, the pilot flew all conditions for one algorithm before moving on to the next. It was believed this blocking would make it easier for the pilot to mentally sort out each algorithm and consequently provide more consistent and reliable data. The experiment was additionally blocked on the replication so the pilot flew a condition once and then immediately repeated it. This also was done to improve the pilot perception of each algorithm.

Run Matrix

A run matrix was developed to determine the run order for each pilot and to minimize any learning bias within the experiment. Learning bias is an inadvertent confounding factor in all experiments. Therefore, proper consideration had to be taken into the design of the matrix, such that the order in which the factors were presented to the pilots did not bias the results.

The best solution to mitigate any learning bias is to fully counterbalance the experiment such that every possible presentation order for the factors is presented an equal amount of times in the study. However, due to the design of the experiment (4x2),

it was not possible to make a fully counterbalanced matrix, as the algorithm factor with four levels had 24 (4!) possible ordering combinations, yet the experiment only had eight pilots. So the run matrix was instead designed using Latin Squares. A Latin Square is a square design (n by n) of values where each value occurs exactly once per row and exactly once per column.[68] This is a useful tool to use for matrix design when full counterbalancing is not feasible. For this experiment two Latin Square design options were available.

The first was an 8x8 Latin Square. Following this design, all eight factor combinations (4x2 = 8) were accounted for, and all eight pilots were accounted for. However, it required a randomization of the eight possible factor combinations, which meant that blocking on the algorithm would not be possible. Because of the requirement for blocking due to the difficulty in determining differences across algorithms, this design was not used.

The second design was multiple 4x4 Latin Squares. This accounted for the four levels of the algorithm factors, and four pilots. Because of its ability to incorporate blocking for the algorithm, this design was chosen, and was consequently repeated two times to accommodate the eight pilots. For each set, all columns of the 4x4 Latin Square were randomized, and then all rows but the first were randomized. Additionally, the approach was also randomized such that each pilot flew the two possible combinations of the approaches the same number of times within each algorithm block. The full run matrix for all eight pilots can be seen in Table F4.

Testing Procedure

Pilots

Pilots used in this study were required to have previous military rotorcraft flight training. They were invited to participate from all areas of the rotorcraft community including military and industry. The pilots voluntarily participated with no compensation provided for their service, and all complied with IRB experimental protocol. Further detailed information regarding the pilots can be found in the Pilot Demographics section.

Schedule

Table 2: Test Schedule

Session	Minutes
Forms	20
Pilot Briefing	50
Practice - Free Flight	40
Practice - All Approaches	60
Practice - Performance Evaluation Task	10
Break	60
Data Collection	70
Post Flight Debrief	20
TOTAL	5.5 hr

The study took approximately five and a half hours to complete (Table 2). The schedule was heavily biased towards training and practice to ensure adequate time for the pilots to become acquainted and proficient with the BOSS symbology. This schedule was also flexible to provide additional training for pilots as needed. The primary concern was to make certain pilots were competent for data collection. This was done to strengthen the integrity of the data.

Pre-Flight Questionnaire

A pre-flight questionnaire was administered to the pilots in order to collect pilot demographic and experience information. Pilots were asked to list flight hours, aircraft experience, test pilot training (if any), and brownout experience. A pairwise comparison was also included to obtain expert opinion on importance weighting for four TD metrics. These TD metrics were the vertical velocity, longitudinal velocity, lateral velocity, and position error. Results of this comparison were used to assess the landing performance of the pilots.

Training and Practice

Before data collection, the pilots had extensive training to become familiarized with the flight controls, display symbology, and flight model. Training was a vital aspect of this study for a number of reasons. The focus of the study, to investigate modifications to the speed guidance, was relatively focused in comparison to the overall learning curve of the BOSS symbology. In order for the pilots to be able to pick up on the differences between the speed guidance algorithms, it was imperative that a comfort level with flying the BOSS symbology be established first. Once the pilots were comfortable flying the BOSS symbology and their mental capacity was capable of focusing on specific aspects of the symbology, then training focused on establishing comfort levels with flying each

of the algorithms. All of this familiarization training was done to ensure consistency in performance during data collection to lessen the data variance.

The first part of training was a pilot briefing and lasted for slightly less than an hour. The presentation stepped through all aspects of the study relevant to the pilot including the purpose, the experimental design and associated factors, the BOSS symbology, the simulator and flight controls, the flight model, and the performance evaluation criteria. Pilots were encouraged to ask questions at any time throughout the presentation.

After the briefing the pilots flew the simulator in free flight for as long as needed to become familiar with the BOSS symbology. The pilots were first instructed to fly around and get a feel for the controls and the gains on the controls. This consisted of performing turns, descents, and decelerations. Then the pilots were then instructed to step through the BOSS symbology, one piece at a time, to watch it move. Once the pilots felt comfortable with the layout and movement of the symbology, they then were encouraged to fly approaches using a *dummy* algorithm. This algorithm was the Exponential Deceleration and was used during free flight because it enabled the pilots to become familiar with the guidance without biasing one algorithm from the study. During this time, the pilots practiced scan patterns and control strategies for performing the maneuver. The free flight training lasted anywhere from thirty minutes to an hour, depending on the pilots familiarity and comfort with the symbology.

After free flight, the pilots practiced all the approaches for the experiment. The 16 approaches were flown in the same order as presented for data collection. Pilot performance was critiqued by the experimenter, and helpful suggestions, strategies, and tactics were discussed as needed.

Performance Evaluation Task

Following the completion of the practice runs, every pilot completed a performance evaluation task. This was done to ensure all pilots were capable of performing up to an expected level. To complete the task, pilots had to fly the Constant Deceleration algorithm with the six-degree approach. This approach was expected to be the most difficult to perform, and thus the evaluation tested the pilots ability to handle the aircraft under an expected high workload scenario. During the approach, the experimenter closely examined the pilots' ability to stay on speed schedule while descending to the LP. Once the aircraft reached the ground, touchdown parameters were collected and checked to see if they were within the desired or adequate performance criteria. All pilots performed within acceptable performance criteria for the performance evaluation task.

Performance Evaluation Criteria

No quantitative performance criteria for flying the approaches were provided to the pilots. The pilots were simply asked to perform the maneuvers, while tracking the guidance cues to the best of their ability. However for TD, objective criterion was provided to the pilots, as seen in Table 3. The evaluative criterion was based on desired and adequate limits for the velocities and position of the aircraft at touchdown. Desired limits indicated optimal touchdown values that would result in a safe and preferred landing. Adequate limits indicated sufficient values that would be acceptable but not necessarily preferred. Anything beyond adequate was deemed hazardous and not indicative of a safe landing. Therefore, pilots were asked to try to stay within the desired boundary limits and not exceed the adequate boundary limits.

Table 3: TD performance evaluation criteria.

Variable	Desired	Adequate	Measure
Vertical Velocity	≤100 fpm	≤300 fpm	feet/min
Forward Velocity	≤5kts fwd	≤10kts fwd	knots
Aft Velocity	≤.5kt	≤1kts	knots
Lateral Velocity	≤.5kt	≤1kts	knots
Position Error	≤25ft from LP Center	≤50ft from LP Center	feet
Obstacle Contact	None	None	Acft Hits

Collected Objective Data

Numerous flight and environmental parameters were collected for data analyses. All parameters were recorded at 75Hz. Selected parameters included aircraft state information, brownout intensity, speed guidance values, and temporal parameters. A complete list of these parameters can be found in Table F1.

Collected Subjective Data

Subjective data was collected immediately following each repetition (after the pilot had flown the condition twice). Workload was assessed using the NASA Task Load Index (TLX) rating.[69] The TLX is a validated workload assessment tool and can be administered without the need for specialized pilot training such as an XP rating. It is a six question, post-flight subjective assessment aimed at evaluating six sub-components of

workload. These subcomponents are mental demand, physical demand, temporal demand, perceived performance, amount of effort required, and amount of frustration incurred. The answers to these questions are combined into a single TLX workload score. The NASA TLX rating sheet can be seen in Figure F1.

Handling qualities were assessed using the Cooper-Harper Handling Qualities Rating (HQR)[70]. This also is a validated assessment tool primarily used for studies examining flight control issues. It is a formal evaluation and requires the pilot to have been previously trained through formal methods (test pilot school) to adequately evaluate and provide an HQR value. The rating uses a decision tree format to determine the level of handling qualities experienced. To determine an HQR value, the pilot verbally stepped through the tree, explaining reasoning, and then ultimately gave a single HQR score. The HQR rating sheet can be seen in Figure F2.

Data Collection

During data collection, no one was permitted to be in the simulator lab except for the pilot and the experimenter. The data collection took roughly an hour to complete. During this time, the pilot flew the 16 approaches and completed TLX and HQR ratings following the completion of a repetition. The pilot was also encouraged to take notes as well as verbalize any additional comments.

Post Flight Debrief

Following the completion of the data collection, the pilots were given a post flight questionnaire that served as the formal debrief of the study. The experimenter went through the questionnaire with the pilots beforehand and answered any questions

regarding its content. The questionnaire took between fifteen and thirty minutes to complete.

The first section of the questionnaire asked the pilots to rate each of the algorithms in terms of comfort for use in both non-threat and threat environments. To provide these ratings, the pilot had to critically assess each algorithm in terms of controllability and temporal performance. The next section was an algorithm ranking, in which the pilots ranked each algorithm [1-best, 4-worst] in terms of overall preference. This assessment required the pilots to evaluate each algorithm from a broad perspective and derive a preferential order among them. Pilots were also encouraged to provide additional comments regarding each algorithm. Upon completion, the pilots and the experimenter informally discussed the experiment.

Pilot Task Analysis

The first segment required the pilot to keep the aircraft straight and level for five seconds, flying the aircraft towards the FAF. The pilot was visually heads down on the VSD display watching the FPM and cross checking with the vertical speed tape to make sure the aircraft was flying straight and level. Once the aircraft reached the final approach fix (FAF), the longitudinal acceleration caret appeared off the left wing of the FPM, indicating that speed guidance turned on. At that point the pilot initiated a descent and deceleration towards the landing point using the VSD symbology.

The descent was initiated by dropping the collective, which in turn lowered the position the FPM. Concurrently, the pilot used left and right cyclic to move the FPM left and right. The pilot manipulated both the collective and the left/right cyclic to place the FPM over the LP marker. This set up the aircraft on the correct glideslope and the correct lateral profile to intercept the LP.

The deceleration was initiated by pulling back on the cyclic, which pitched the aircraft up. This action could be seen in the symbology, as the iron wings pitched up above the horizon line, and the longitudinal acceleration caret dropped below the left wing of the FPM, indicating deceleration. The speed error tape then started to either grow or shrink depending on if the pilot was on the correct deceleration profile. Through the approach, the pilot adjusted the pitch of the aircraft in order to null out any speed error that appeared.

Visually, the pilot was focusing on the FPM, keeping it over the LP marker, and checking for any speed error that appeared off the left wing. This design created a nice central location for the pilot to focus attention without having to continually cross check other symbology.

Once the aircraft decelerated below 30 knots, the FPM became dashed, indicating to the pilot that it was soon time to transition to the HSD. The FPM remained dashed until 20 knots, at which point it disappeared. The pilot could transition at anytime in between. The point of transition to HSD was highly dependent on pilot preference. Some transitioned as soon as the FPM went dashed, and some waited until the FPM disappeared before transitioning to the HSD. In order to make the transition, pilots were asked to hold what they had, and not to make any strong inputs while transitioning. This helped to reduce mental workload associated with switching to the HSD control task.

After transitioning to the HSD, the pilot used the acceleration ball and target speed cup to manage both the longitudinal (speed) and lateral profiles. The ball moved in the same directions as the cyclic (left cyclic moved the ball left, forward cyclic moved the ball forward, etc). The control strategy was to keep the acceleration ball inside the target speed cup. As the aircraft continued the approach, the target speed cup moved towards the center of the screen, indicating deceleration. The speed guidance algorithm determined the rate at which the cup moved. As the aircraft slowed, the display scaled

down twice. When rescaling occurred, the velocity vector, acceleration ball, target speed cup, and homeplate symbol all *jumped* on the screen.

The vertical profile was managed using the vertical speed tape and the rising ground symbol. Pilots were instructed to maintain roughly the same vertical speed from the VSD when the FPM was over the LP marker. This provided the approximate correct vertical speed to stay on the glideslope. However, if the aircraft reached the ground too early, the pilots were instructed to zero out the vertical speed so that the aircraft could make it to the LP before touching down. Likewise, if the aircraft arrived at the LP too high, the pilots were instructed to come to a hover and drop down over the LP. Because there was no definitive vertical guidance provided to the pilot on the HSD, the vertical profile was secondary to the longitudinal profile. However, constant crosschecks to the vertical speed tape were necessary in order to adequately manage the vertical speed. As the aircraft slowed through ETL, more torque power was required to maintain the same descent speed. Additionally, as the aircraft neared the ground, the aircraft encountered ground effect, which significantly reduced the amount toque power required. While in ground effect, the pilot had to continually reduce the collective to maintain a descent.

As the aircraft approached the LP, the homeplate symbol moved towards the center of the screen indicating that the aircraft was nearing the LP. Once the homeplate symbol fell below the target speed cup, pilots were instructed to track the top half of the homeplate symbol using the acceleration ball. This set up the aircraft to reach the LP on target with minimal forward speed. Once the homeplate was in the center of the display, the pilot zeroed out any undesired velocities (lateral or aft) by controlling the acceleration ball and dropped the collective at an acceptable rate until TD occurred. The simulation then paused at TD indicating the end of a run.

Simulation Hardware

Computers

Two dedicated Linux machines were used to support the simulation. One machine was used to drive the flight model, outside visuals, and sensor vision. The other machine was used to drive the symbology and to collect the data. A video overlay box was used to overlay the VSD symbology over the synthetic sensor display image.

Outside Visual Displays

The entire maneuver was a heads down task, meaning the pilot did not have to look at the out the window (OTW) view in order to complete the maneuver. However, the cockpit was configured with OTW 19" LCD monitors (Figure 27). The OTW field of view (FOV) was approximately 80°x 20°, presented on these displays.

Panel Mounted Displays

The instrument panel was configured with three PMDs. The center and left PMDs were used in the experiment to display the VSD and HSD. These two displays had shrouds on either side of the displays such that the viewing area matched that of common cockpit displays (6"x8"). The right display was used during checkout flights, but was turned off and unused for the experiment.

Flight Controls

<u>**Cyclic**</u>

The cyclic (Figure 26a) was self-centering and installed on the right side of the cockpit in a side-arm configuration. The grip and button layout followed a generic rotorcraft design. This layout is not congruent with actual the H-60 cyclic, which uses a center-stick. However, based on expert opinion from qualified XPs, the side stick was sufficient for completing the approach and landing tasks without sacrificing realism a significant amount.

<u>**Collective**</u>

The collective was standard and positioned on the left side of the cab (Figure 26b). It was balanced to prevent unintended upward or downward movement. The height was adjustable and as was the movement friction to ensure the motion felt comfortable to the pilot.

Figure 26: Pilot controls.

Note: (a) cyclic, (b) collective, (c) pedals

Pedals

The rudder pedals (Figure 26c) were standard spring-to-center pedals. These were not essential to the task, as the approach and landing could be performed with feet off the pedals. However, they were functional in case pilots wanted to correct any sideslip error. The pedals were adjustable to accommodate pilots of all heights.

Switches

The simulator had a selection of buttons and switches located on the controls and the instrument panel. However, most were unused for this study. One switch on the instrument panel provided the experimenters the ability to quickly switch through the algorithms, but was only used for checkout of the simulator. During data collection, the trigger button on the cyclic reset the aircraft position back to the IP.

Figure 27: Simulation cab layout.

Note: Helmet was not used in this experiment.

Experimenter's Station

The experimenter's station was located directly behind the simulator cab. It was equipped with three monitors and a keyboard and mouse. The station was configured with a KVM switch so both computers needed to run the simulator could be accessed. This setup allowed the experimenter to direct and execute all aspects of the experiment from the station. Additionally, two of the displays showed the VSD and HSD symbology, so the experimenter could closely watch the pilot fly each approach without having to glance over the shoulder of the pilot.

Simulation Software

BOSS Symbology

A previous BOSS flight symbology version was used, along with the symbology drivers, and associated graphics software for displaying them on the panel mounted displays. This BOSS version was comparable to the version that was flight validated from the brownout landings at YPG. The only difference was that the version used for this simulation lacked a vertical speed guidance box located on the vertical speed tape.

Outside Visual Environment

RIPTIDE was the simulation environment that tied together the helicopter model, the control stick interfaces, and the terrain database. RIPTIDE generated the OTW view as well as integrated the flight model into the system.

Simulated Brownout

The brownout effect was done through a simple shading variable. The shading intensity was driven using a function of altitude and airspeed. The initial conditions for brownout were approximately 100 feet and 20 knots airspeed. As the aircraft decelerated and descended closer to the ground, the brownout became more severe, and eventually fully enveloped the aircraft in brownout with zero outside visibility. The brownout equation can be seen in Equation C9.
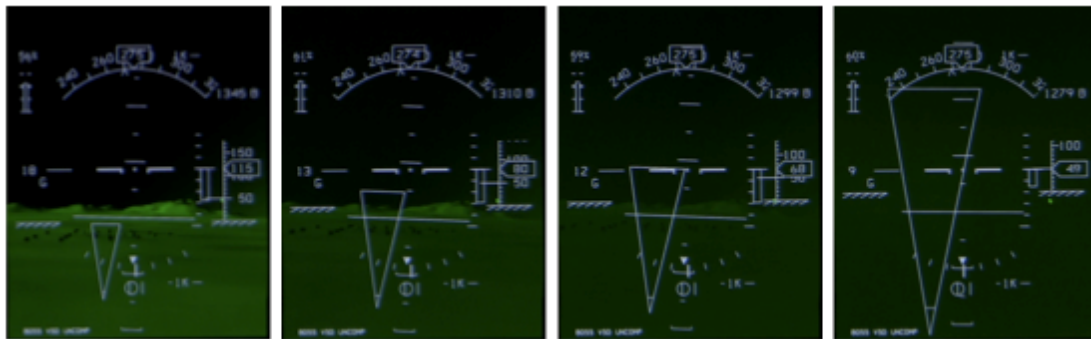
Figure 28: Brownout effect on the VSD.

Flight Model

The GENHEL flight model was used for the simulation. This flight model was the most advanced rotorcraft flight model available and provided high-level model dynamics for the maneuvers to be performed in the study. The model included non-linear cross coupling between the controls, individual rotor blade dynamic modeling, effective translational lift modeling, and ground effect modeling.[71, 67]

Experimental Validation

Software Validation

The flight model was tested to ensure it behaved in accordance to a known validated GENHEL model. In order to do this, data was collected for a set of control inputs for each of the flight controls. The control deflection data was then fed into both models and aircraft state variables (pitch, roll, and yaw) were plotted. Through close inspection, it was determined that both behaved identically, indicating that the model was correct.

To validate the symbology code, an XP who had flown the YPG flight tests test flew the symbology to verify the two versions behaved the same. All pieces of the symbology were closely examined during additional flight trials to make sure they behaved accordingly.

Hardware Validation

The flight controls were all tested extensively to check for proper performance. Raw signals from the controls were first examined to make sure the potentiometers were working correctly. Then limits within the software were checked to verify the controls were set to the appropriate boundaries. Lastly, an XP flew the controls, doing simple control displacements (full deflection, half deflection, etc), to make sure the controls behaved accordingly with the flight model.

Maneuver Validation

The maneuvers were flown by at various airspeeds to determine the best selection of initial parameters to be used. Through this validation testing, it was found that the

airspeed had to drop by twenty knots for the six-degree approach in order to make it safely controllable. Thus from this validation, the two maneuvers (3deg/80kts, 6deg/60kts) were selected and verified.

Data Validation

Once the simulator was running correctly, a military-trained checkout pilot flew each of the maneuvers in the study to collect a full dataset. The data was first inspected to make sure each metric was collecting the correct output. Then the data was analyzed to make sure all metrics had reasonable outputs throughout the approach. Finally, the data was analyzed in the same manner that actual data collected from the study was analyzed. This was done to check the analysis methods and to compare the collected data to the mathematical model predictions.

CHAPTER VII. ANALYSIS AND RESULTS

Pilot Demographics

Eight military-trained rotorcraft pilots participated in the simulation. Seven of the participants were male, and one was female. Four of the participants were from the Air Force, two from the Army, one from the Navy, and one from industry. Six were XPs with an experimental rating from the US Navy Test Pilot School, and two were current operational pilots. A breakdown of the pilot flight hours can be seen in Table 4. The majority (6) was H-60 pilots, one was an AH-64 pilot, and one was a CH-47 pilot. Additionally, every pilot had experienced brownout in real world situations (Min: 2, Max: 300).

Table 4: Breakdown of pilot flight hours.

Type	Min Hours	Max Hours	Average Hours
Fixed Wing	100	600	344
Combat	0	1200	234
Non-Combat	150	4000	1881
Total	700	4000	2841

<u>Objective Data</u>

The following section presents the results of the objective data. The analyses include RMS error, temporal metrics, maximum pitch and deceleration values, pilot control frequency, and touchdown performance.

Each individual analysis dataset was comprised of n=128 data points (16 runs per pilot, for 8 pilots). All parametric analysis was done using a general linear model analysis of variance (GLM ANOVA) in Minitab. The model tested the approach, algorithm, and the algorithm-approach interaction as factors. Additionally if significance was found, pairwise comparisons were performed using Tukey's Method for the levels within the algorithm factor to determine individual significance. All significance was determined using α=0.05. Minitab printouts for all the analyses can be found in Appendix G. Results

The data is presented graphically using cumulative histograms. These plots are useful in examining spread and trend information from continuous data. Each line is comprised of 16 data points, representing all the data for one algorithm, sorted from low to high (8 pilots with 2 runs each per algorithm equates to 16 data points). Note that there is a 17th data point at zero percent, which is simply a replication of the first data point. Plots of significant metrics are shown in the results section and all other plots can be found in Appendix G. Results

RMS Speed Error

To evaluate pilot ability to stay on speed schedule during the approach, root mean squared (RMS) error was calculated for the speed. The RMS error calculation can be seen in Equation C8. Because the pure errors were squared, the RMS error treated deviations either above or below the desired speed the same. This was needed for

absolute error without any confounding from both positive and negative values. Additionally because of the squaring, the RMS error forgave small deviations from the desired track but penalized large deviations.

Results revealed no significant differences across the algorithms (p-value = 0.329), the approaches (p-value = 0.453), and their interaction (p-value = 0.523). The RMS speed error data for the 3-degree and 6-degree approaches can be seen in Figure G4 and Figure G5. The RMS error was relatively low (98.4% of the data was under 5kts), and the algorithms averaged between only 1.8-2.2 knots error throughout the approach. This is an indicator that the pilots were able to track the speed guidance cues and stay on speed schedule with a good level of proficiency, regardless of the algorithm.

Temporal Analysis

The temporal analysis evaluated different time segments within the approach. In particular, this analysis aimed to quantify the differences between the algorithms in the amount of time spent in the approach and in brownout.

The overall time in approach was analyzed to examine the overall differences in time between the algorithms. Results were significant for both algorithm (p-value = 0.000) and the approach (p-value = 0.000). No significance was found for the interaction effect (p-value = 0.939). Expectedly, the approach was significant as the two approaches took different amounts of time to complete. The cumulative histograms for both approaches can be seen in Figure 29 and Figure 30. From comparison of the two it can be seen that the 6-degree approach was associated with faster approach times.

For the algorithms, pairwise comparisons revealed that Constant Deceleration and the 250ft Hybrid took significantly less amounts of time to fly than the baseline 1000ft Hybrid (p-value = 0.0000 and p-value = 0.0012). Additionally the Constant Deceleration was also significantly quicker than the 500ft Hybrid (p-value = 0.0013). No significant

Table 5: Improvements on overall approach time.

Algorithm	Average Time Reduction from Baseline (percentage)
Constant Deceleration	12.8%*
250ft Hybrid	9.3%*
500ft Hybrid	3.40%
1000ft Hybrid (baseline)	N/A

* denotes significance against the 1000ft Hybrid

Table 6: Improvements for time in heavy brownout.

Algorithm	Average Time Reduction from Baseline (percentage)
Constant Deceleration	30.8%*
250ft Hybrid	21.5%*
500ft Hybrid	8.70%
1000ft Hybrid (baseline)	N/A

* denotes significance against the 1000ft Hybrid

differences were found between the 500ft Hybrid and 1000ft Hybrid (p-value = 0.4739). The improvements in comparison to the baseline can be seen in Table 5.

The time spent in heavy brownout was calculated to evaluate how long pilots spent at low speeds in brownout conditions. Heavy brownout was determined as the time when brownout intensity was greater than 50%. Result of the GLM ANOVA showed that the algorithm was significant (p-value = 0.000), but the approach and the interaction effect were not (p-value = 0.145 and p-value = 0.978). Pairwise comparisons further revealed that the Constant Deceleration and the 250ft Hybrid spent significantly less amounts of time in heavy brownout in comparison to the 1000ft Hybrid (p-value = 0.0000 and p-value = 0.0001). The Constant Deceleration was also significant against the

500ft Hybrid (p-value = 0.0001). No significant differences were found between the 500ft Hybrid and the 1000ft Hybrid (p-value = 0.2884). Improvements from the baseline can be seen in Table 6.

The time spent below 20 knots was also calculated to see how long pilots spent at speeds roughly below ETL. These results were very similar to those of the time spent in brownout. This is due to the strong correlation between the likelihood of brownout forming at speeds below ETL. As with the time in brownout, from the GLM ANOVA results, it was found that algorithm was significant (p-value = 0.000) while the approach and the interaction were not significant (p-value = 0.121 and p-value = 0.988). The pairwise comparisons revealed that the Constant Deceleration spent significantly less amounts of time below 20kts than both the 500ft Hybrid and the 1000ft Hybrid (p-value = 0.0001 and p-value = 0.0000). The 250ft Hybrid also spent significantly less amounts of time below 20kts than both the 500ft Hybrid and the 1000ft Hybrid (p-value = 0.0253 and p-value = 0.0000). No significant differences were found between the 500ft Hybrid and the 1000ft Hybrid. The average improvements from the baseline can be seen in Table 7.

Table 7: Improvements for time spent below 20kts.

Algorithm	Average Time Reduction from Baseline (percentage)
Constant Deceleration	32.3%*
250ft Hybrid	24.2%*
500ft Hybrid	10.80%
1000ft Hybrid (baseline)	N/A

* denotes significance against the 1000ft Hybrid
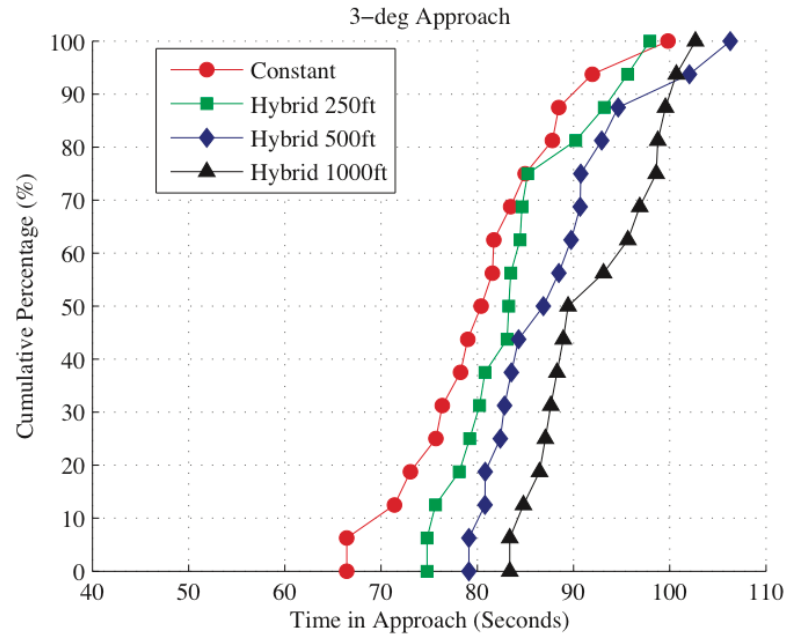
Figure 29: Time spent in approach, 3-degree approach.
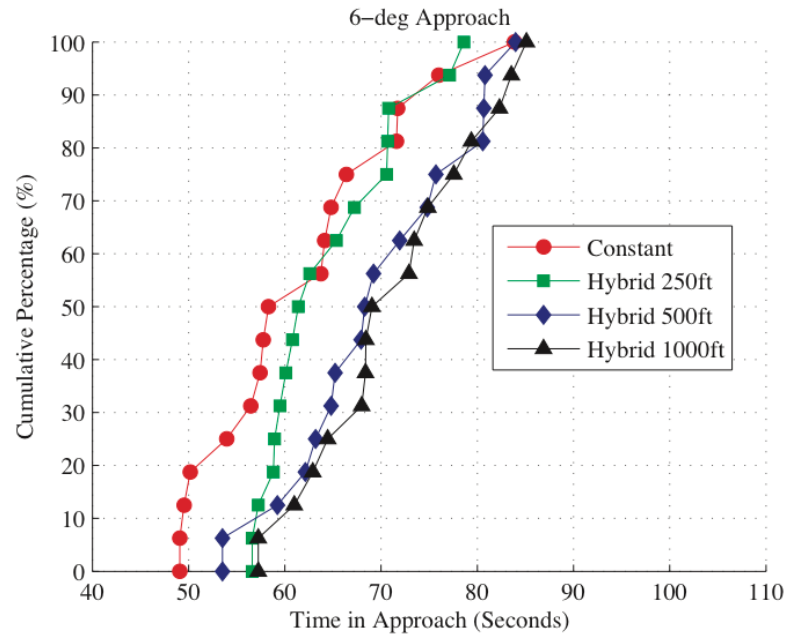
Figure 30: Time spent in approach, 6-degree approach.
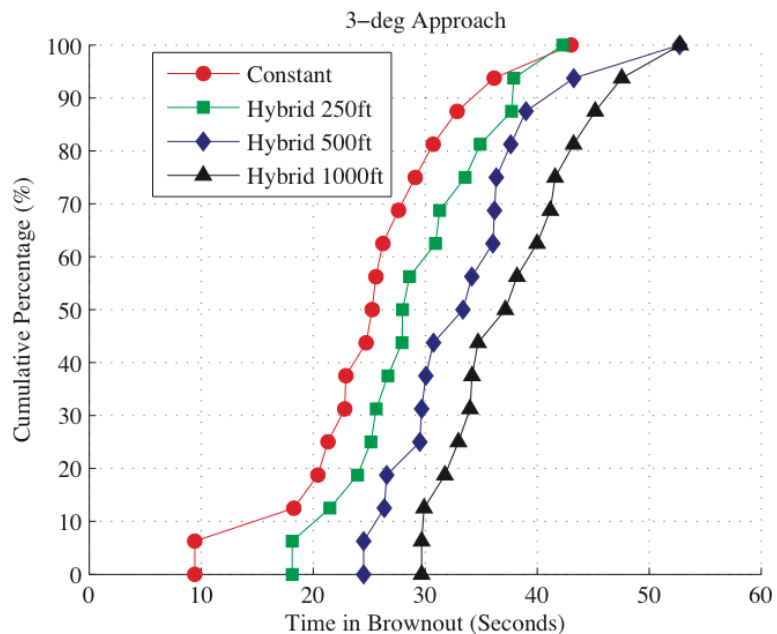
Figure 31: Time spent in heavy brownout, 3-degree approach.
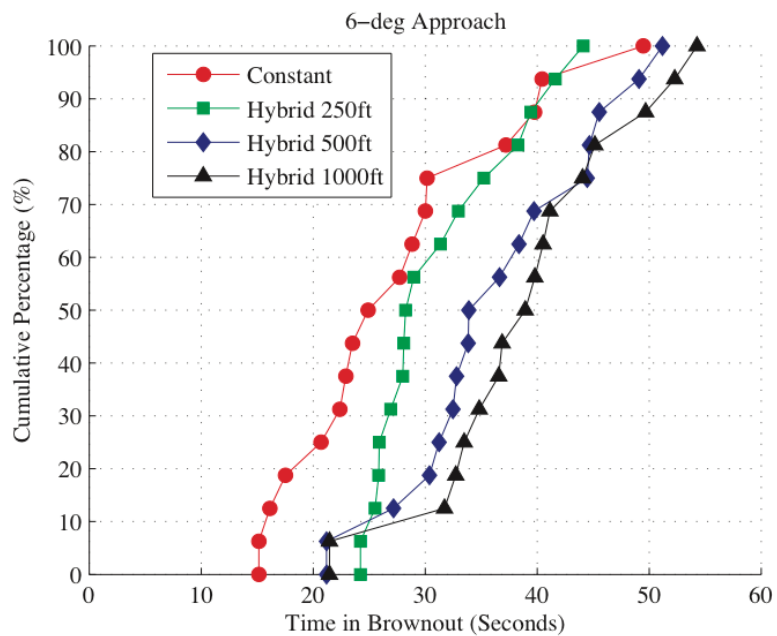
Figure 32: Time spent in heavy brownout, 6-degree approach.
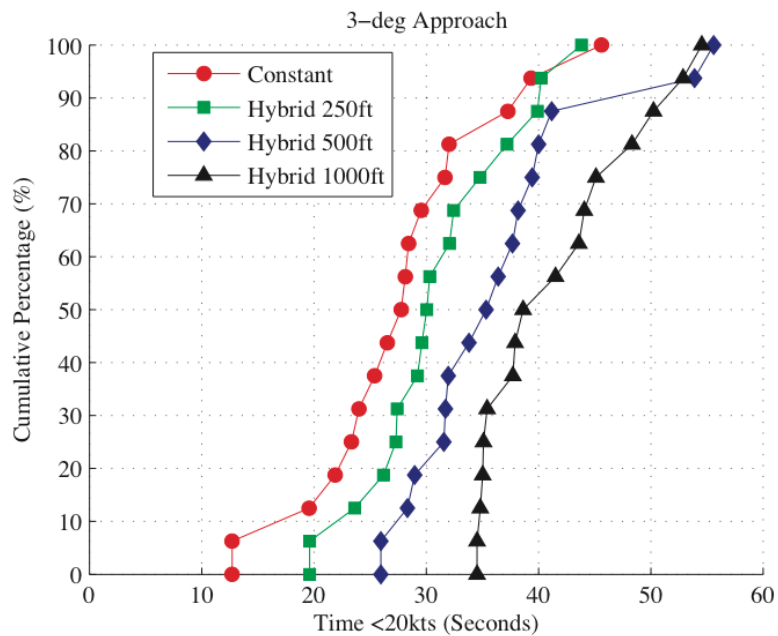
Figure 33: Time below 20kts, 3-degree approach.
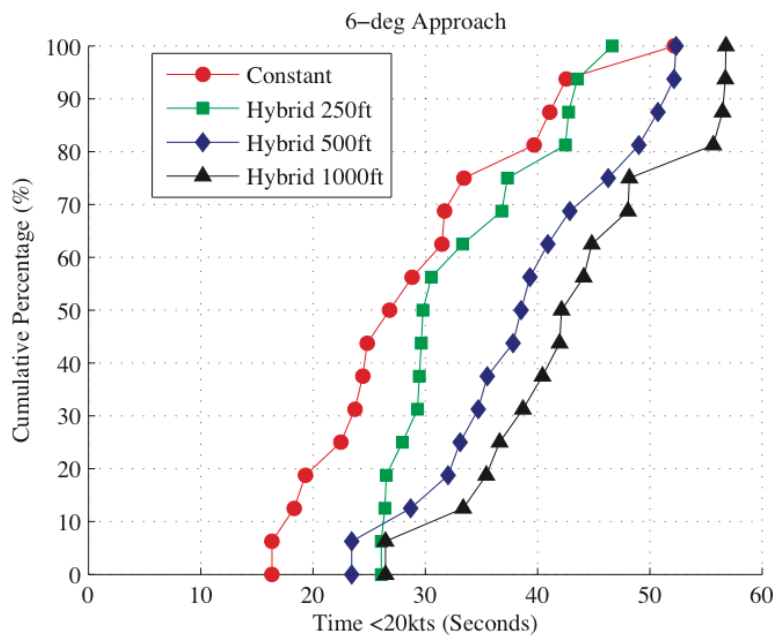
Figure 34: Time below 20kts, 6-degree approach.

Touchdown Performance

It was believed that touchdown behavior could provide a culminating glimpse into how the symbology performed in guiding the pilot safely to the LP, as it served as the final criteria for acceptability since safe touchdown was the main goal of the approach guidance. A comprehensive score analysis, developed at the Operator Performance Laboratory in a previous rotorcraft study,[30] was used to assess the overall performance of each display by examining multiple TD performance factors combined into a single score. The TD metrics included for the comprehensive score were the position error, vertical velocity, longitudinal velocity, and lateral velocity.

To create the comprehensive TD score, all the metric values were standardized to fit the interval [0, 1] (Figure 35). Standardization for data used the two performance levels (desired and adequate) for each metric. If the data point fell within the desired limits, then the data was standardized to a maximum value of 1. If the data fell between the desired and adequate limits, the data was standardized following a linear model between 1 and 0. Beyond the adequate limits, and the data was standardized with the minimum value of 0. Once the four metrics were standardized, the weights derived from the pilot pairwise comparisons were applied to each metric (Table 8). The sums of the weighted and standardized data then provided an overall comprehensive score for each.

The results of the TD comprehensive score revealed that all TDs were exceptionally good (Table 9). In fact, out of the 128 data runs performed in the study, 122 of the TDs were within all the desired TD parameters. Individual analyses of each TD parameter as well as analysis for the TD score were performed. Though not surprisingly, no significant results were found for any of the metrics.
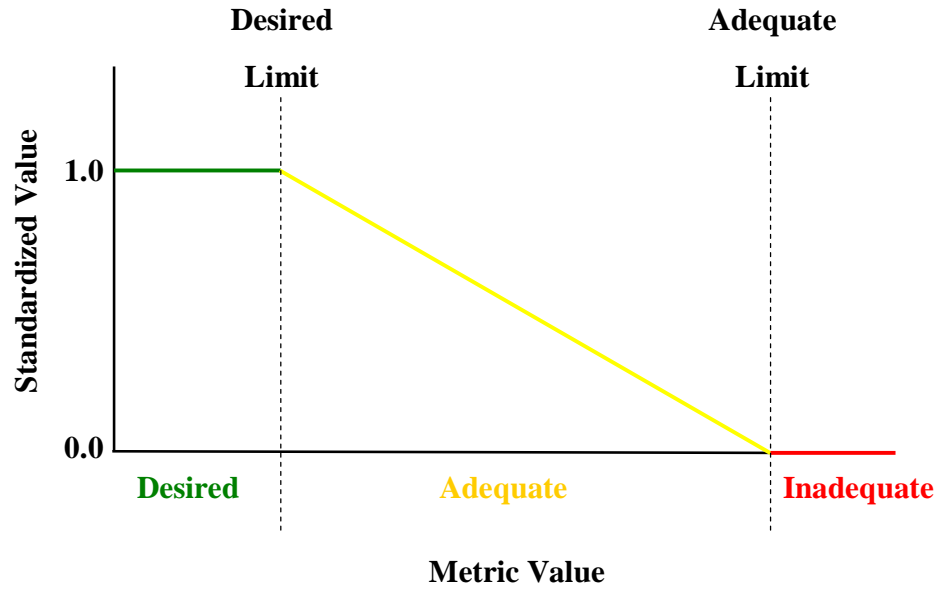
Figure 35. Standardization of data.

Table 8: TD metric pairwise comparison results.

Metric	Weighting
Position Error	14%
Vertical Velocity	22%
Longitudinal Velocity	21%
Lateral Velocity	43%

Table 9: Comprehensive TD score.

Algorithm	Average TD Score (%)
Constant Deceleration	98.3%
250ft Hybrid	99.7%
500ft Hybrid	99.8%
1000ft Hybrid	98.2%

Maximum Pitch

The maximum pitch was calculated for heavy brownout to see how much pitch the pilots had to input while in DVE conditions. This helped to provide the other side of the story regarding the approaches. The goal was to reduce the time, but also to maintain reasonable levels of aggression, which could be defined through the pitch of the aircraft. The data for both approaches can be seen in Figure 36 and Figure 37.

Results found the algorithm to be significant (p-value = 0.000) but not the approach or the interaction effect (p-value = 0.068 and p-value = 0.552). The pairwise comparisons revealed further that the Constant Deceleration resulted in significantly higher amounts of pitch than the 500ft Hybrid and the 1000ft Hybrid (both p-value = 0.0000). The 250ft Hybrid also was associated with significantly higher amounts of pitch than the 500ft Hybrid and the 1000ft Hybrid (p-value = 0.0053 and p-value = 0.0000). No significant differences were found between the 500ft Hybrid and the 1000ft Hybrid. The average maximum pitches achieved can be viewed in Table 10. Notably, these were all less than 12 degrees, which was the limit that Garren et al.[49] found pilots did not like to exceed in IMC conditions.

Table 10: Maximum pitch in DVE.

Algorithm	Average Max Pitch in DVE (degrees)
Constant Deceleration	11.4*
250ft Hybrid	11.0*
500ft Hybrid	10.1
1000ft Hybrid (baseline)	9.5

* denotes significance against the 1000ft Hybrid
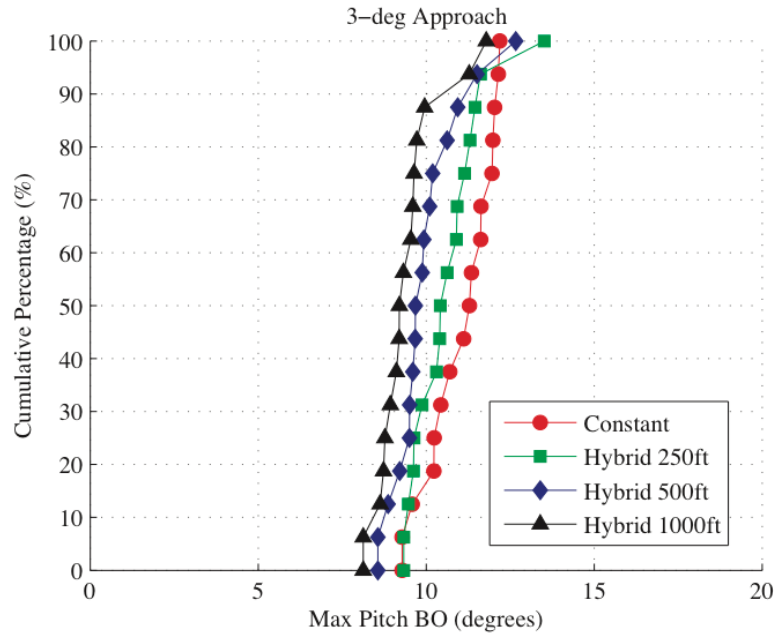
Figure 36: Maximum pitch in DVE, 3-degree approach.
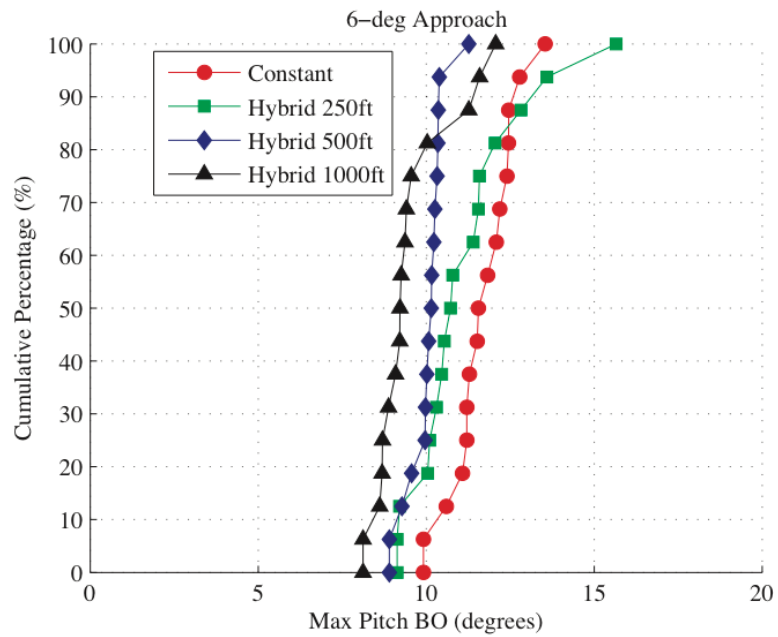
Figure 37: Maximum pitch in DVE, 6-degree approach.

Maximum Deceleration

The maximum deceleration level achieved in heavy brownout was also computed. The data can be seen in Figure 38 and Figure 39. This metric is highly correlated to the maximum pitch since pitching the aircraft up increases deceleration. Thus results matched those of the maximum pitch, as the algorithm was significant (p-value = 0.000) while the approach and the interaction effect were not (p-value = 0.129 and p-value = 0.732). The pairwise also agreed with the results of the maximum pitch, as both the Constant Deceleration and the 250ft Hybrid had significantly higher maximum deceleration values in comparison to both the 500ft Hybrid (p-value = 0.000 and p-value = 0.0273) and the 1000ft Hybrid (p-value = 0.0000 and p-value = 0.0000). Again no significant differences were found between the 500ft Hybrid and the 1000ft Hybrid.

The averages of the maximum decelerations for each algorithm can be seen in Table 11. These averages exceed the typical deceleration limits that Garren et al.[49] found pilots reached during IMC flight. However, as it was noted from the study, the deceleration was limited due to the pilots' hesitancy to pitch higher than 12 degrees. Unlike the aircraft's 8 degree hover pitch tested in the study, the H-60 has a hover pitch of about 3 degrees. This allows for substantially more nominal pitch to decelerate the aircraft while still remaining under the 12-degree pitch threshold. Thus it was expected that the deceleration maximums achieved would be slightly higher.

Table 11: Maximum deceleration in DVE.

Algorithm	Average Max Deceleration in DVE (g)
Constant Deceleration	0.11*
250ft Hybrid	0.10*
500ft Hybrid	0.09
1000ft Hybrid (baseline)	0.08

* denotes significance against the 1000ft Hybrid
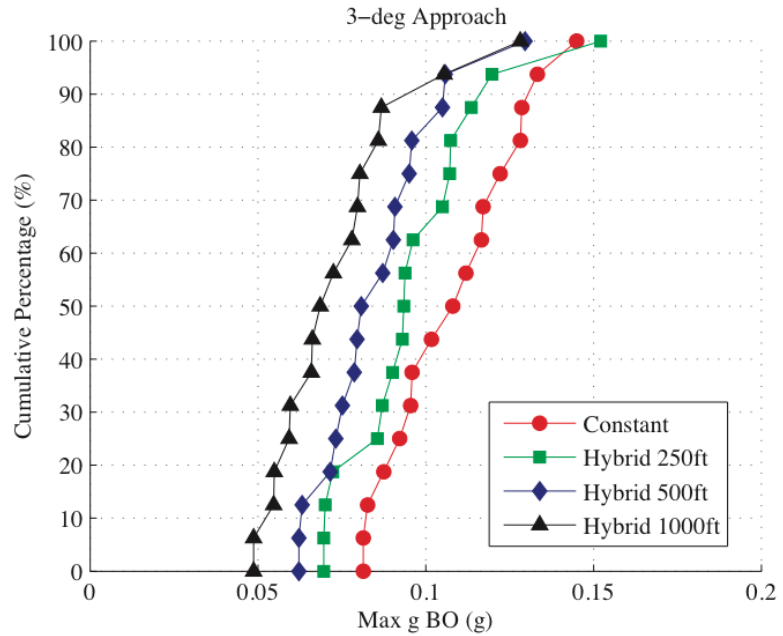
Figure 38: Maximum deceleration in DVE, 3-degree approach.
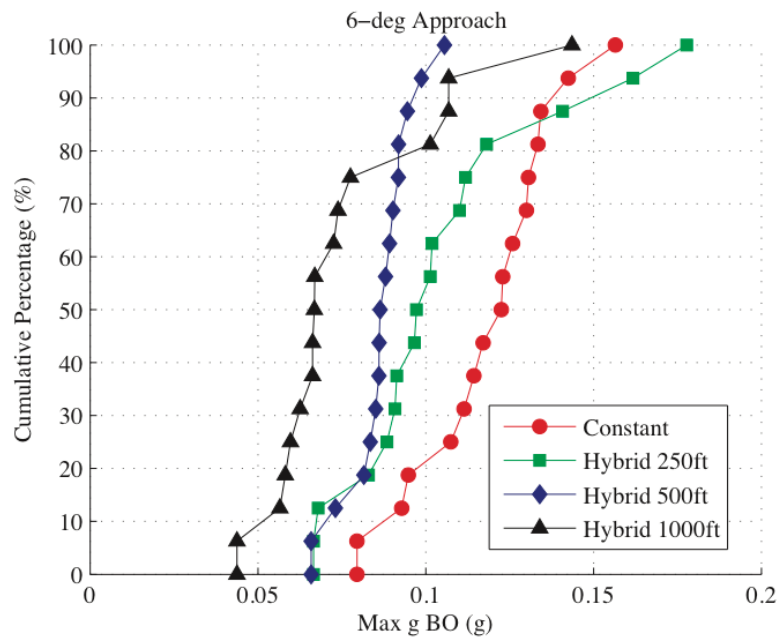
Figure 39: Maximum deceleration in DVE, 6-degree approach.

Fourier Control Analysis

To evaluate the pilot control behavior, Fourier analysis was completed on the deflections of the controls. This analysis used sine waves to estimate a signal and then calculated the amplitudes of the control inputs across different frequencies. Over-controlling or high workload can be interpreted as large amplitudes in the high frequencies on a Fourier amplitude spectrum plot. It was hoped that this analysis would be able to objectively reveal subtle differences in the controllability of the different algorithms. The analysis summed the power data below 1Hz (low amounts of controlling) and summed all the power data above 1Hz (higher amounts of controlling). Then a power ratio was computed by dividing the high power by the low power. The ratio was used to analyze the controlling tendency across the algorithms, as higher values of the ratio signals more amounts of over-controlling. This analysis method was derived from a previous control theory course.[72]

The main area of interest for the Fourier analysis was for the longitudinal cyclic, which commands the pitch of the aircraft consequently the longitudinal deceleration However, no significant differences were found between the algorithms for the power ratios (p-value = 0.610). The average power ratio values for each algorithm can be found in Table 12. There was a significant difference between the approaches (p-value = 0.000), as the longitudinal cyclic frequency power ratio was significantly higher for the 3-degree approach than for the 6-degree approach. On average, the 3-degree had a higher power ratio by 0.06. This is slight, but suggests that the 3-degree approach lead the pilot to over-control more during the approach. No significance was found for the interaction effect (p-value = 0.323).

Table 12: Longitudinal cyclic frequency power ratios.

Algorithm	Average Frequency Power Ratio
Constant Deceleration	0.50
250ft Hybrid	0.50
500ft Hybrid	0.51
1000ft Hybrid (baseline)	0.49

Note: Lower ratios indicate more low-frequency controlling

Analyses were also performed on the lateral cyclic control and the collective control during the approaches. Again no significant differences were found between the algorithms or interaction effects for either of the control movements. But the approach was found to be significant (lateral cyclic p-value = 0.000; collective p-value = 0.000). The power ratios for both were significantly higher for the 6-degree approach. The higher amount of controlling for the collective is likely due to the more demanding vertical profile of the 6-degree approach. Likewise, more controlling of the collective results in more rotational torque changes, which can change the yaw in the aircraft. Most pilots flew the approach with feet off the pedals, thus yaw would be corrected through use of the lateral cyclic, which would concur with the higher lateral values.

Subjective Data

For the NASA-TLX metric, the dataset was comprised of n=64 data points (8 ratings per pilot for 8 pilots). Cooper-Harper HQR was only administered to the XPs, and therefore the datasets were comprised of n=48 data points (8 ratings per pilot for 6 pilots). The algorithm comfort ratings and preference rankings were comprised of n=32 data points (4 ratings per pilot for 8 pilots).

Parametric analysis was completed for the NASA-TLX using a GLM ANOVA in Minitab. The model tested the approach, algorithm, and the algorithm-approach interaction as factors. Additionally if significance was found, then pairwise comparisons were performed using Tukey's Method for the levels within the algorithm factor to determine individual significance. All significance was determined using α=0.05. Minitab results for all the analyses can be found in the Appendix G. Results.

NASA TLX

The NASA-TLX rating evaluated six subcomponents of workload to derive an overall workload assessment. Results showed no significant differences in the TLX computed workload for the approach, algorithm or the interaction effect (p-value = 0.136, p-value = 0.258 and p-value = 0.950 respectively), indicating that all the algorithms and approaches required roughly the same amount of workload. The average TLX workload scores for each of the algorithms can be seen in Table 13.

Table 13: NASA-TLX workload ratings.

Algorithm	Average TLX Workload
Constant Deceleration	6.20
250ft Hybrid	5.50
500ft Hybrid	5.10
1000ft Hybrid (baseline)	5.30

The six subcomponents were also tested for significance. Temporal demand was the only subcomponent that was significant, for the algorithm factor (p-value = 0.046). On average, the Constant Deceleration was associated with higher levels of temporal

demand, as seen in Table 14. However, it is deemed marginally significant as the pairwise comparisons between the algorithms revealed no significant differences. Additionally, examination of the boxplot provided no clear trend among the data (Figure G36).

Table 14: NASA-TLX temporal demand.

Algorithm	Average Temporal Demand
Constant Deceleration	7.2
250ft Hybrid	5.7
500ft Hybrid	5.7
1000ft Hybrid (baseline)	5.5

Cooper-Harper HQR

The Cooper-Harper HQR examined the handling qualities characteristics of the algorithms. The averages of the ratings provided can be seen in Table 15. Results show that the algorithms fell in between an HQR of 3.5 and 4. A rating of 3 indicates that the aircraft characteristics were fair with some mildly unpleasant deficiencies, and that minimal pilot compensation was needed for desired performance. Values under 3.5 are classified as Level 1 handling qualities. A rating of 4 indicates that there are some minor but annoying deficiencies, and that moderate pilot compensation was needed for desired performance. Values over 3.5 and less than 6.5 can be classified as Level 2 handling qualities. These results show that, though extremely close to the Level 1 threshold, all algorithms were at Level 2 handling qualities.

Table 15: Cooper-Harper HQR.

Algorithm	Average HQR
Constant Deceleration	4.0
250ft Hybrid	3.5
500ft Hybrid	3.8
1000ft Hybrid (baseline)	3.7

Note: Lower HQR values indicate better handling qualities.
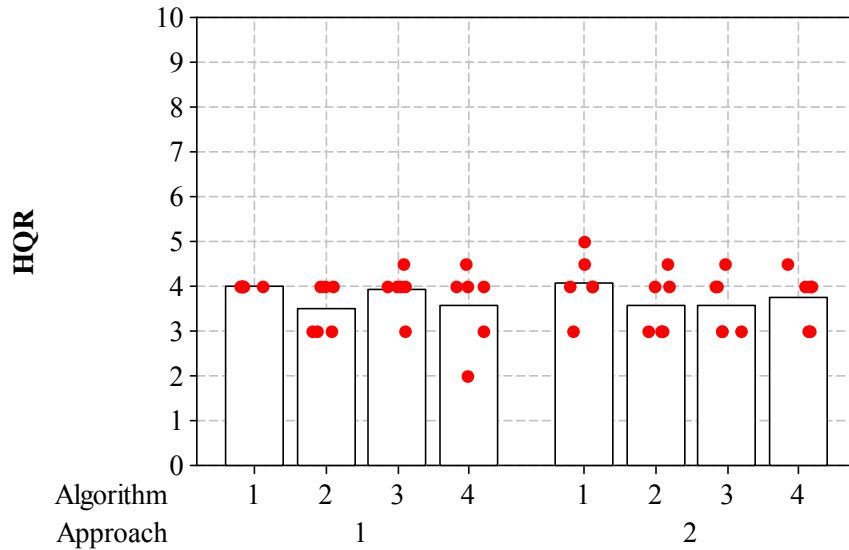
Figure 40: Bar chart for HQR.

Note: Dot plots represent raw data. Lower HQR values indicate better handling qualities.

Algorithm Comfort

The algorithms were rated to assess how comfortable the pilots were with the algorithms if used for brownout landings in both non-threat environments and threat environments. Figure 41 and Figure 42 show the results with bar plots. The averages of the algorithms for each environment can be seen in Table 16 and Table 17. A score of 3 indicated that the pilot would be "moderately comfortable" using the algorithm. Results showed a consistent trend for both environments. The 250ft Hybrid was associated with the highest comfort levels, followed by the 500ft Hybrid, and the 1000ft Hybrid, while the Constant Deceleration was associated with the lowest comfort scores.

Table 16: Non-threat environment comfort levels.

Algorithm	Average Non-Threat Comfort Level
Constant Deceleration	2.5
250ft Hybrid	3.8
500ft Hybrid	3.6
1000ft Hybrid (baseline)	3.3

Table 17: Threat environment comfort levels.

Algorithm	Average Threat Comfort Level
Constant Deceleration	2.1
250ft Hybrid	3.3
500ft Hybrid	2.8
1000ft Hybrid (baseline)	2.4

Scale: 1 (very uncomfortable) to 5 (very comfortable)
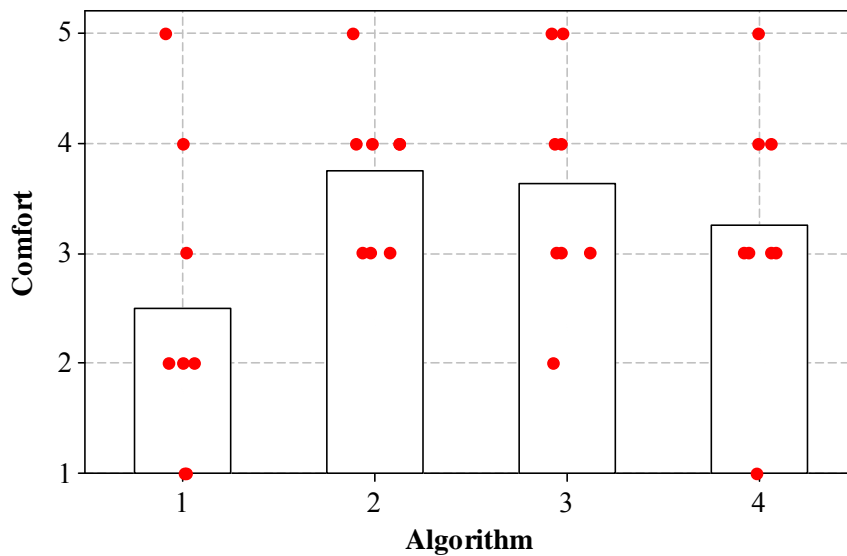
Figure 41: Bar chart with dot-plots for comfort levels in non-threat environments.
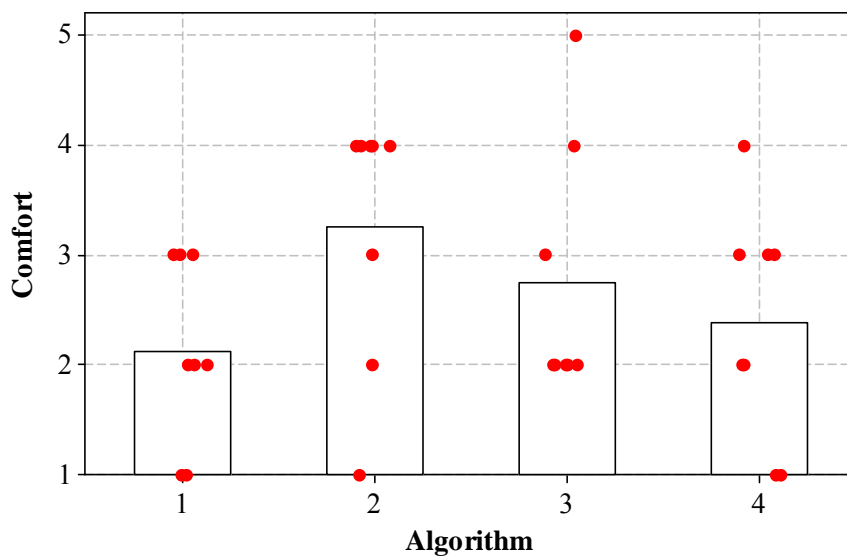
Figure 42: Bar chart with dot-plots for comfort level in threat environments.

Note: Scale from 1 to 5 (1 is very uncomfortable, 5 is very comfortable)

Algorithm Preference Ranking

Pilots additionally ranked the algorithms to determine pilot preference. The most preferred was ranked with a value of 1 while the least preferred was ranked with a value of 4. The data can be seen in Figure 43, and the averaged results can be seen in Table 18. Lower averages equate to the algorithm being more preferred. These results agree with the comfort level ratings in that, on average, the 250ft Hybrid was most preferred, followed by the 500ft Hybrid, then the 1000ft Hybrid, and the Constant Deceleration was least preferred.
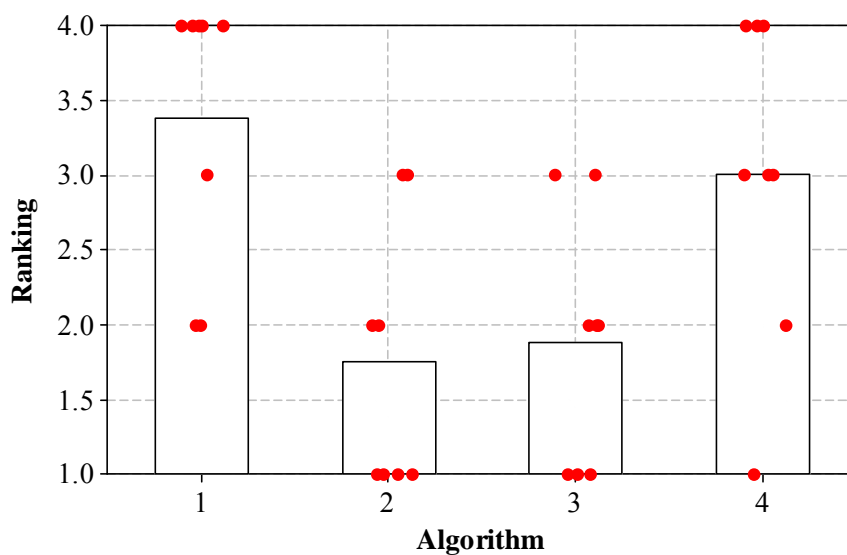
Figure 43: Bar chart with dot-plot for algorithm preference ranking.

Note: Lower ranking values indicate more preferred.

Table 18: Algorithm preference ranking.

Algorithm	Average Preference Ranking
Constant Deceleration	3.4
250ft Hybrid	1.8
500ft Hybrid	1.9
1000ft Hybrid (baseline)	3.0

Pilot Comments

The following section details additional pilot comments regarding the individual algorithms tested. These are provided to show the trend in pilot attitude toward each algorithm.

Pilots had positive comments for the 250ft Hybrid, indicating that it provided a fast, but still manageable deceleration profile.

- Relatively easy to fly

- Good balance between getting to the LZ in a timely manner, but under control and not feeling rushed

- Comfortable, yet expeditious

- Fast after scale change, but still controllable

The 500ft Hybrid also received positive comments, but some with regards to it providing a slow profile.

- Very easy to fly but too slow to decel initially – the approach seems to take too long

- Speed could be increased slightly but overall felt the most comfortable

- Seemed the easiest to control at start of approach, leading to a good setup and easier endgame

- Best mix of speed and controllability

The 1000ft Hybrid also received positive comments for ease of flight, but was also remarked as being slow.

- Seemed easiest to control at all phases of approach

- Felt the slowest and was easy to control, but took a while to get to the LZ

- Doghouse speed at the end of the approach was way too slow

- Way too slow

The Constant Deceleration on the other hand was remarked as being too fast and difficult to control.

- Felt slightly too fast which led to a less controlled approach

- Too fast

- If it is too fast it could induce over control – PIO

- Hardest to control, seemed faster and hardest to catch up to

Discussion of Results

The results of this study were promising in that the data tended to correlate well to the predicted behavior. The four algorithms provided the pilot with guidance that created four different distinct deceleration profiles. These differences between the profiles can be summarized objectively using the temporal and pitch/deceleration results. As the level of aggressiveness of the maneuver increased, the time to complete the maneuver (and time spent at low speeds) decreased, but at the cost of increased pitch values (and hence deceleration values) in brownout conditions. However, in comparison to pitch limits found in the literature, the average maximum pitch values achieved did not exceed the pitch limits reported for pilots flying in IMC conditions. The maximum deceleration values were slightly higher than reported in the literature, but that can be attributed to the

difference in aircraft hover characteristics as discussed in the previous section. The pilots proficiently tracked the speed guidance cues to a high degree of performance with all the algorithms, and thus no significant differences in RMS speed error were found across the algorithms. Additionally, no significant differences were found in control behavior between the algorithms, indicating that the pilot control was not significantly affected through use of more aggressive profiles. Lastly, TD performance exceeded expectations as almost all landings met desired performance criteria. No significance was reported for any TD metric across the algorithms. Overall objectively, it was found that it appears possible to improve the approach characteristics to provide a quicker approach without exceeding performance limits of the aircraft or sacrificing landing performance. However, these results must be coupled with the subjective data in order appreciate the entire human-machine system.

Throughout the experiment, the pilots provided a wealth of subjective data through use of formal rating techniques, questionnaires, and comments. To mitigate any sort of pilot preferential biases regarding deceleration methods, the algorithm identities were masked from the pilot and further randomized in presentation order. During experimentation, pilots completed workload ratings and handling quality ratings for the algorithms. No significant differences were found in the computed workload rating, and the ratings were midrange, indicating moderate but not severe workload. A subcomponent was found to be marginally significant. Temporal demand was associated with higher ratings for the Constant Deceleration, which supports the comments that the rate of closure for approach was too fast. The handling qualities for all algorithms were rated with HQR values between 3.5 and 4, indicating Level 2 handling qualities. The 250ft Hybrid was associated with the lowest HQR, while the Constant Deceleration was associated with the highest. But considering the task of flying a rate-command rotorcraft platform into severe brownout conditions, all of these ratings show that the symbology and guidance greatly aided in maintaining pilot SA for precise control of the aircraft.

Post flight evaluations assessed the comfort levels for the algorithms in threat and non-threat environments. The following trend was exhibited for both environments: 250ft Hybrid was the highest scored, followed by the 500ft Hybrid, 1000ft Hybrid, and the lowest scored was the Constant Deceleration. The averaged values indicated varying levels of moderate comfort, but no algorithms were very uncomfortable or very comfortable. An algorithm ranking established the 250ft Hybrid as the most preferred, followed close by the 500ft Hybrid, then the 1000ft Hybrid, and lastly the Constant Deceleration as least preferred. The pilots comments further strengthen the findings of the subjective data, in that the pilots remarked that the 250ft Hybrid to be fast but controllable, the 500ft Hybrid to be easy to control but slightly too slow, the 1000ft Hybrid to be much too slow, and the Constant Deceleration to be too fast.

These subjective findings culminate into the following understanding: regardless of the algorithm, on average the task required a moderate amount of workload in which pilots felt only moderately comfortable. However, as the Yerkes-Dodson law[73] explains, the level of arousal needs to be moderate in order to achieve the optimum level of performance from the pilot. Too low of workload, and the pilot performance suffers due to lack of focus and boredom. Too high of workload, and the performance degrades due to over-arousal and the inability to manage the required tasks. Therefore, from the subjective feedback, it appears that this study adequately saturated the pilot with task demands to sufficiently invoke a high level of performance.

From this performance, it can be seen that the pilots unquestionably preferred a faster approach as compared to the baseline (1000ft Hybrid). However, the Constant Deceleration led to pilot discomfort and higher temporal demand, thus being deemed too fast. The 500ft Hybrid was well received with positive comments regarding its ease, but was commented as potentially being too slow. This is further confirmed by the lack of statistical difference in temporal parameters between it and the 1000ft Hybrid. The 250ft Hybrid consistently scored the highest in the pilot preference rankings, pilot comfort

ratings, and handling quality ratings. It also provided a significant reduction in the amount of time spent at low speeds (and in brownout), and was within the pitch tolerances derived from the literature.

SECTION VIII. CONCLUSIONS

This study sought to improve the deceleration guidance used within the BOSS symbology framework, to provide the pilot with intuitive guidance cues to enable the safe landing of rotorcraft in brownout, zero-visibility conditions. The prior deceleration guidance cue was flight-validated in actual brownout conditions, but was deemed too slow for comfort in a brownout environment. Therefore there was a need to develop a new deceleration algorithm that could provide a faster approach with less time spent in brownout that was still controllable and manageable. Additionally, the previous deceleration algorithm was not robust in its ability to provide consistent guidance at variable starting distance from the LP and starting velocities. Thus there was a need to develop a more robust algorithm that could provide consistent guidance at a dynamic range of initial distances and velocities.

A mathematical model was developed in Matlab to compute the behavior of the deceleration guidance for different deceleration algorithms. An interface was developed to aid in the quick manipulation of the varying parameters input into the deceleration algorithms. New algorithms were investigated to test for capability and feasibility for the rate-command H-60 platform. The investigation found that a simple and effective method for reduction in the amount of time spent at low speeds could be achieved through manipulation of parameters within the previous algorithm. The previous algorithm, known as the 1000ft Hybrid, utilized a constant deceleration until a point in which it transitioned to an exponential deceleration. This transition point was defined with a D_t of 1000ft and a V_t of 30kts. By altering the D_t to a closer distance, the approach could be quickened and less time could be spent at low speeds. Through modeling and regression analysis, a new algorithm was developed, capable of calculating a reasonable V_t that allowed for a smooth transition between the constant deceleration and exponential

deceleration parts of the algorithm for varying initial distances and velocities. Two new algorithms were formed by manipulating the D_t within the new algorithm: 250ft Hybrid and the 500ft Hybrid. Four algorithms were tested in a formal simulation study. These four, in ordering of least aggressive to most aggressive, were: 1000ft Hybrid, 500ft Hybrid, 250ft Hybrid, and a pure Constant Deceleration.

Eight highly skilled pilots participated in the simulation study using a generic fixed-base simulator with a high-fidelity rotorcraft H-60 model. Results found that as the aggressiveness of the algorithm increased, the time spent at low speeds and in brownout significantly decreased, and concurrently the pitch of the aircraft (and resulting deceleration) significantly increased. Though the maximum pitch values achieved were within reasonable limits for DVE flight according to previous literature. The maximum deceleration rates were slightly higher than recommended from the literature, but the disparity was due to differences in aircraft characteristics and thus is expected to be within reason. The Constant Deceleration and 250ft Hybrid were found to significantly reduce the amount of time spent at low speeds (below 20kts) by 32% and 24% respectively. All landings were satisfactory, regardless of the algorithm, with over 95% meeting all desired landing performance criteria.

The algorithms were all classified with Level 2 handling qualities characteristics, though it should be noted the values were on the lower threshold, nearing Level 1. No significant differences were found in the subjective workload metric between the algorithms. But pilot preferences and algorithm ranking all trended towards the same conclusion: the 250ft Hybrid was the most desired, followed by the 500ft Hybrid, then the 1000ft Hybrid, and finally the Constant Deceleration. Pilot comments found that the 250ft Hybrid was a good balance between arriving at the LP quickly and still being manageable in terms of controllability. The Constant Deceleration was found to be too fast and difficult to maintain consistently. The 500ft Hybrid was praised for its ease, but criticized for its tendency to drag out the approach. The 1000ft Hybrid was also deemed

easy in terms of controllability, but very poor in terms of how long it required the aircraft to spend in brownout.

Results of this study positively show the capability of the 250ft Hybrid algorithm in significantly reducing the amount of time spent at low speeds when the aircraft is most unstable and brownout is most prevalent. The 250ft Hybrid also received the highest preference ranking and the highest comfort ratings for both threat and non-threat environments. Additionally, the new developed algorithm provides the robustness for more consistent guidance from dynamic starting distances and velocities. Thus substantial evidence has been presented that the deceleration guidance within the BOSS symbology could be improved through use of the new deceleration guidance algorithm with a 250ft D_t. Subsequent validation flights in an H-60 platform will have to be performed to confirm these findings.

APPENDIX A. BROWNOUT BACKGROUND
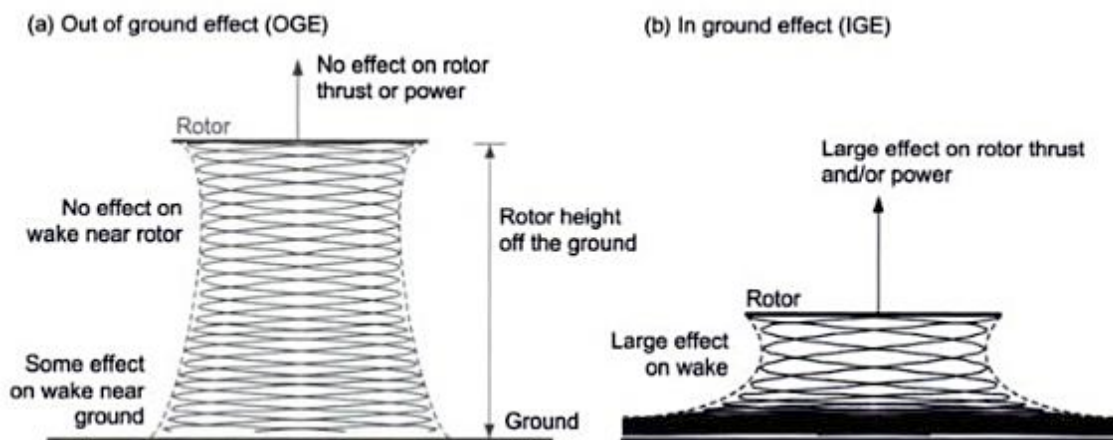
Figure A1: Rotor downwash behavior in and out of ground effect.

Source: Leishman[8]
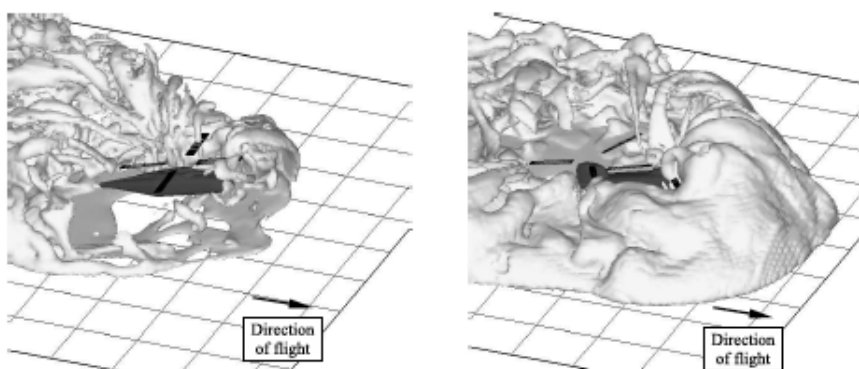
Figure A2: Distribution of dust density for single and tandem rotor configurations.

Source: Phillips and Brown[10]
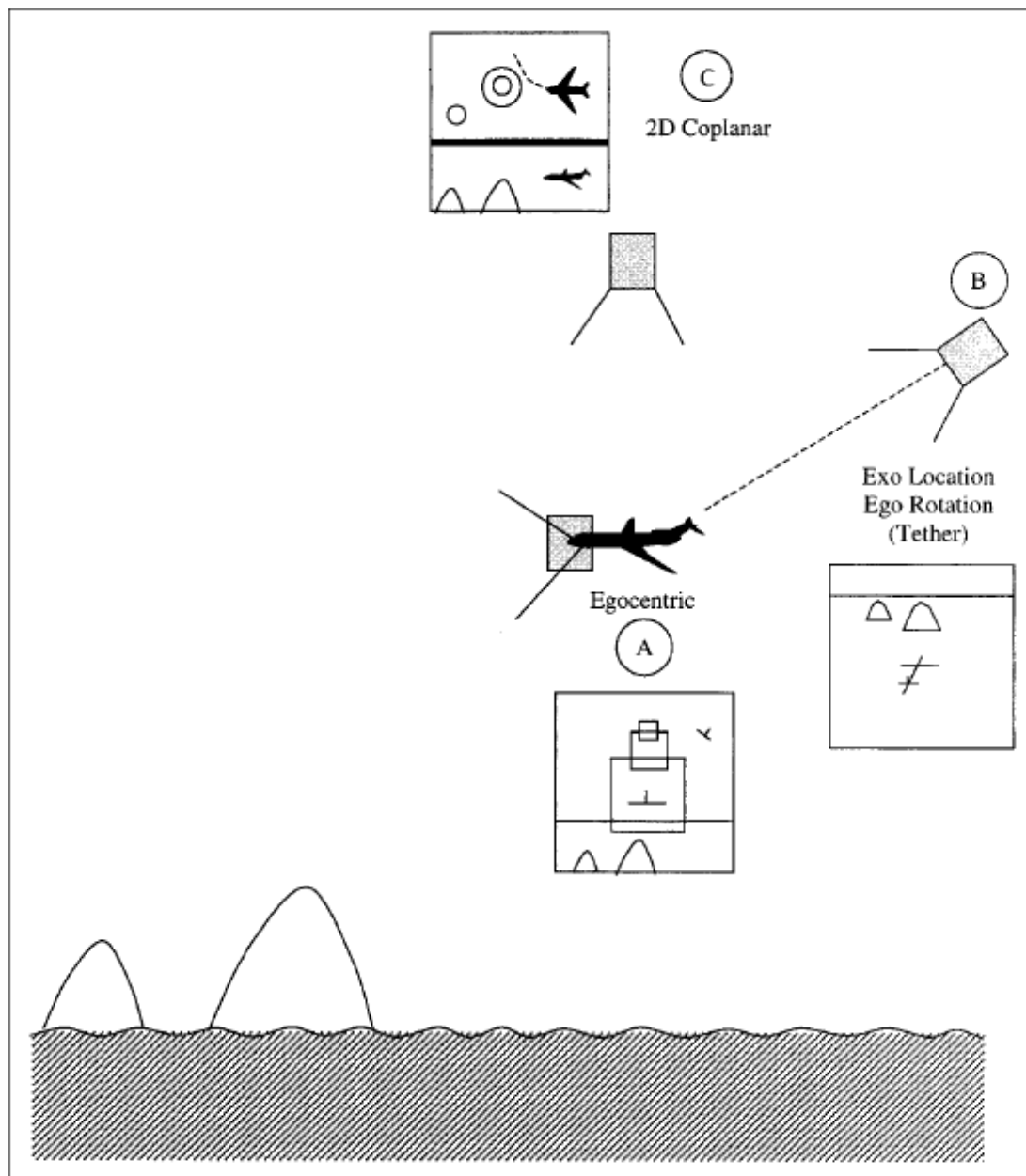
Figure A3: Types of display perspectives.

Figure A4: BOSS symbology overlaid on top of FLIR sensor imagery.

Source: Harrington et al.[35]

Figure A5: Comparison of OTW and Sandblaster mmW radar display.

Source: Colucci[5]
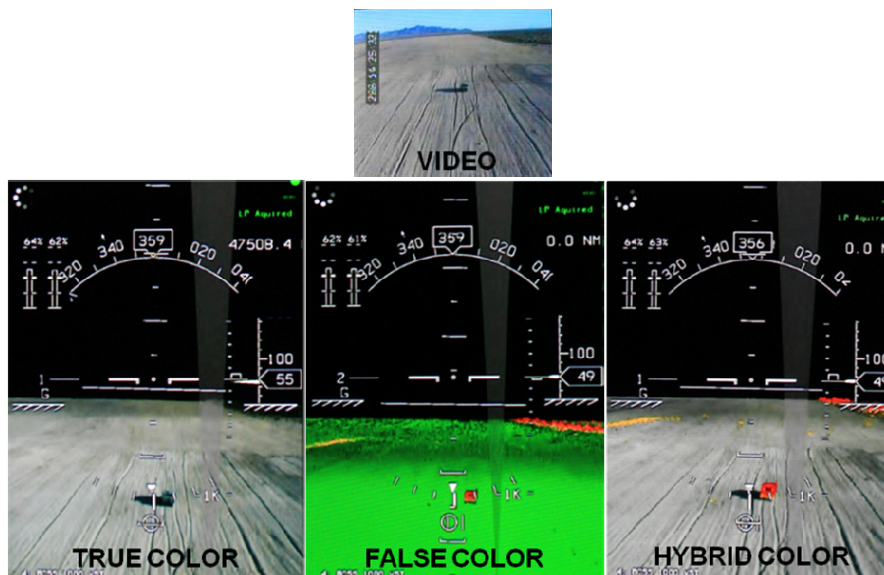
Figure A6: BOSS symbology overlaid on top of LADAR imagery.

Note: The smaller image represents the true video-captured image. The following three
images are LADAR imagery with different coloring schemes.

Source: Harrington et al.[36]
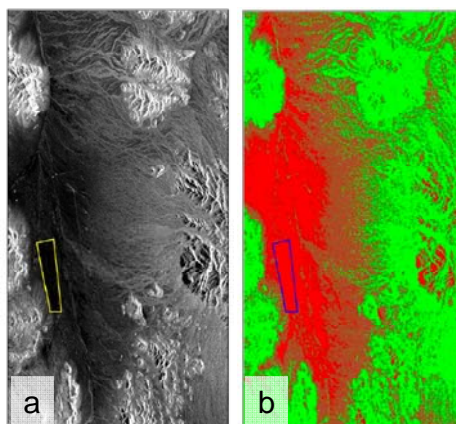
Figure A7: Polarimetric brownout algorithm.

Note: (a) Grey-scale polarimetric image, (b) Image after brownout algorithm.

Source: Rabaja[13]
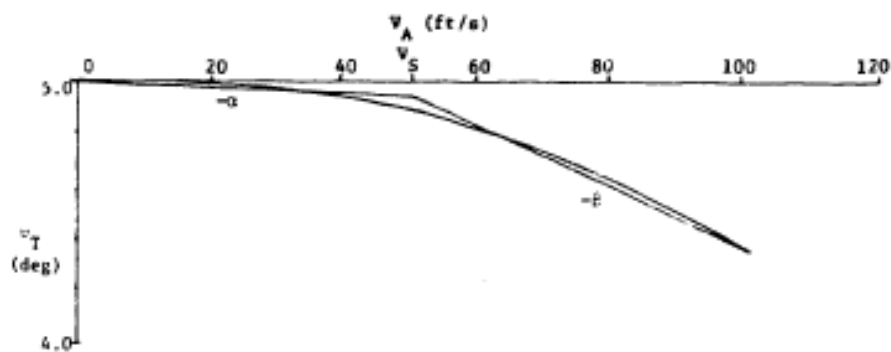
Figure A8: Trim pitch attitude versus airspeed.
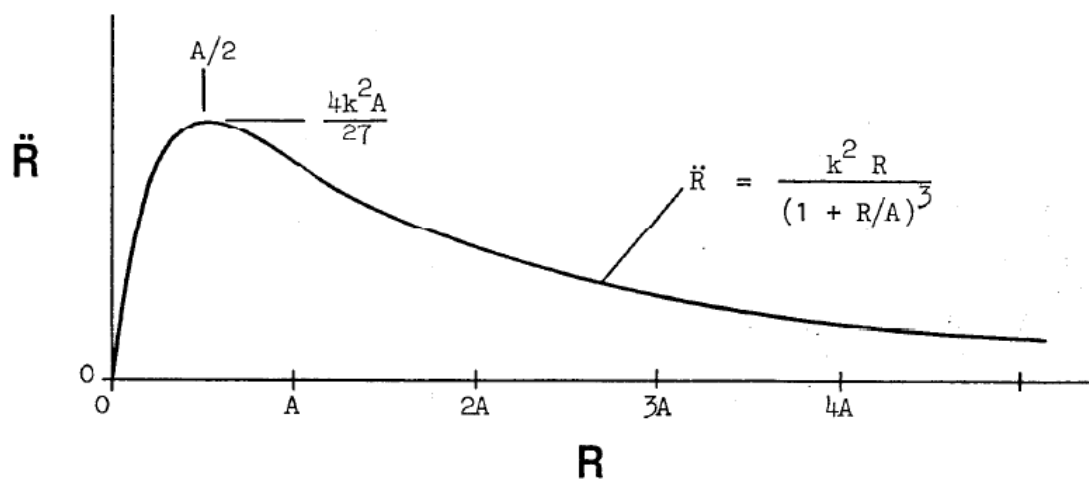
Figure A9: Manual deceleration model, deceleration profile.

APPENDIX B. BOSS SYMBOLOGY
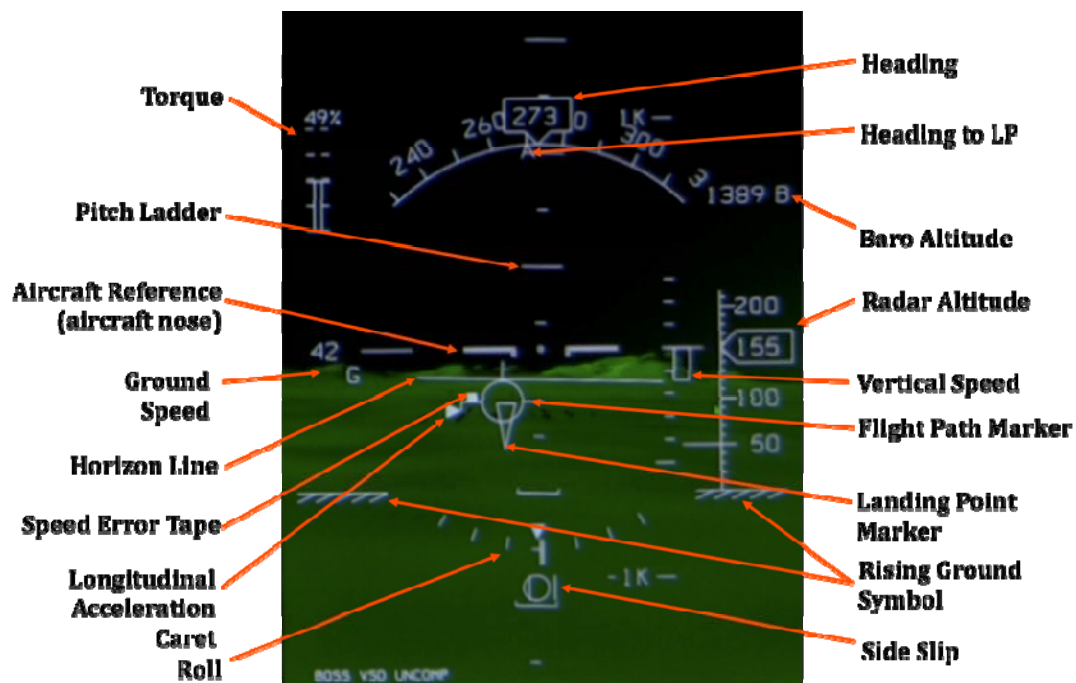
Figure B1: BOSS VSD symbology.
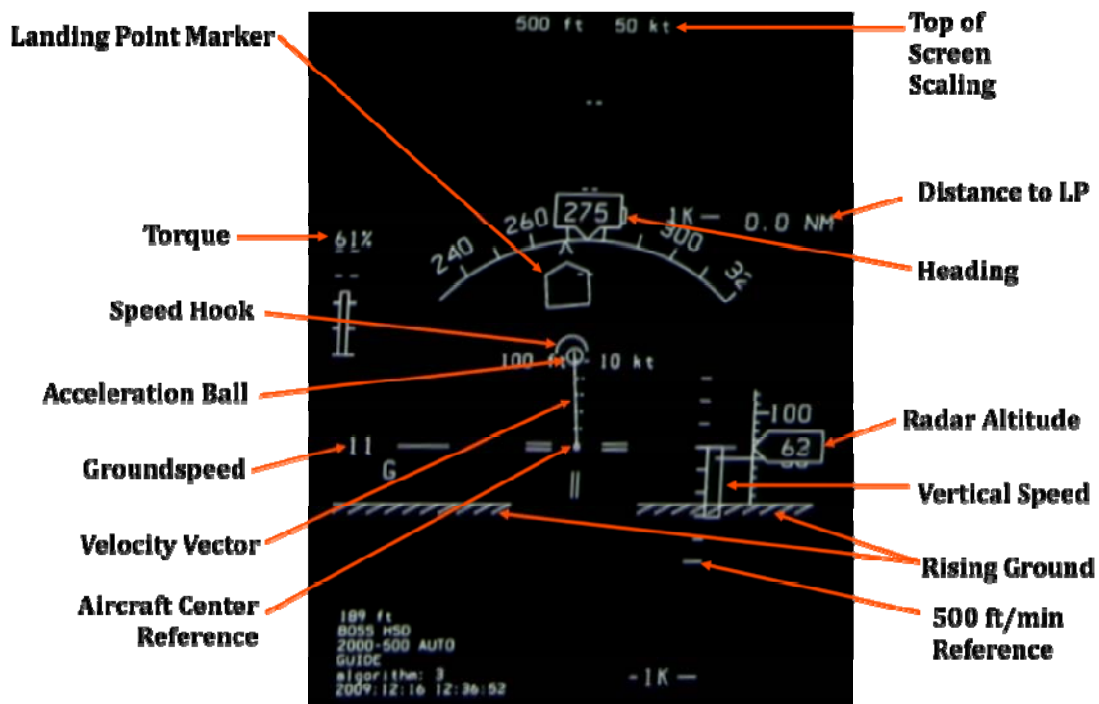
Figure B2: BOSS HSD symbology.

APPENDIX C. EQUATIONS

$$V_c = V_o * \left(\frac{D}{D_o} \right)$$

V_c = Commanded velocity (ft/sec)
V_o = Initial velocity (ft/sec)
D = Current distance to LP (ft)
D_o = Initial distance to LP (ft)

Equation C1: Exponential deceleration algorithm.

$$a = -\frac{1}{2} \left(\frac{Vo^2}{Do} \right)$$

$$V_c = \sqrt{V_o^2 + 2a(D_o - D)}$$

V_c = Commanded velocity (ft/sec)
V_o = Initial velocity (ft/sec)
D = Current distance to LP (ft)
D_o = Initial distance to LP (ft)

Equation C2: Constant deceleration algorithm.

$$If(D \geq D_t)$$

$$a = -\frac{V_o^2 - V_t^2}{D_o - D_t}$$

$$V_c = \sqrt{V_o^2 + 2a*(D_o - D_t)}$$

$$If(D < D_t)$$

$$a = -\frac{1}{2}\left(\frac{V_t^2}{D_t}\right)$$

$$V_c = \sqrt{V_t^2 + 2a*(D_t - D)}$$

V_c = Commanded velocity (ft/sec)

V_o = Initial velocity (ft/sec)

V_t = Transition velocity (ft/sec)

D = Current distance to LP (ft)

D_o = Initial distance to LP (ft)

D_t = Transition distance (ft)

Equation C3: Piecewise constant deceleration algorithm.

$$If (D \geq D_t)$$

$$a = -\frac{V_o^2 - V_t^2}{D_o - D_t}$$

$$V_c = \sqrt{V_o^2 + 2a*(D_o - D_t)}$$

$$If (D < D_t)$$

$$V_c = \left(\frac{D}{D_t}\right)*V_t$$

V_c = Commanded velocity (ft/sec)

V_o = Initial velocity (ft/sec)

V_t = Transition velocity (ft/sec)

D = Current distance to LP (ft)

D_o = Initial distance to LP (ft)

D_t = Transition distance (ft)

Equation C4: Hybrid deceleration equations

$$D_t = 2186 - 0.335*D_o - 23.7*V_o - 26.7*V_t + 0.00142*D_o*V_o + 0.0177*D_o*V_t ...$$
$$- 0.000075*D_o*V_o*V_t + 0.0773*V_o*V_o + 0.353*V_t*V_t$$

V_o = Initial velocity (ft/sec)

V_t = Transition velocity (ft/sec)

D_o = Initial distance to LP (ft)

D_t = Transition distance (ft)

Equation C5: Constant V_t Hybrid regression equation.

$$V_t = -14.4 + 0.0193 * D_t + 0.00348 * D_o + 0.292 * V_o - 0.000004 * D_t * D_o \ldots$$
$$+ 0.000207 * D_t * V_o - 0.000032 * D_o * V_o$$

V_o = Initial velocity (ft/sec)

V_t = Transition velocity (ft/sec)

D_o = Initial distance to LP (ft)

D_t = Transition distance (ft)

Equation C6: Initial Constant D_t Hybrid regression equation.

$$V_t = 14.6 + 0.0251 * D_t - 0.00251 * D_o + 0.101 * V_o - 0.000003 * D_t * D_o \ldots$$
$$+ 0.000151 * D_t * V_o - 0.000006 * D_o * V_o$$

V_o = Initial velocity (ft/sec)

V_t = Transition velocity (ft/sec)

D_o = Initial distance to LP (ft)

D_t = Transition distance (ft)

Equation C7: Final Constant D_t Hybrid regression equation.

$$RMS\_SpdErr = \sqrt{\frac{\sum_{i=1}^{n}(V - V_c)^2}{n}}$$

V_c = Commanded Velocity (kts)

V = Current Velocity (kts)

n = Total number of data points

Equation C8: RMS speed error calculation.

$$\alpha_{alt} = \frac{(h_{rad} - 50)}{50} \ni \alpha_{alt}[0,1]$$

$$\alpha_{spd} = \frac{(V - 10)}{10} \ni \alpha_{spd}[0,1]$$

$$\alpha_{brownout} = (1 - \alpha_{alt}^2)(1 - \alpha_{spd}^2)$$

h_{rad} = current altitude above ground (ft)

V = current velocity (kts)

Equation C9: Brownout simulation function.

APPENDIX D. MATLAB-SIMULINK MODELING
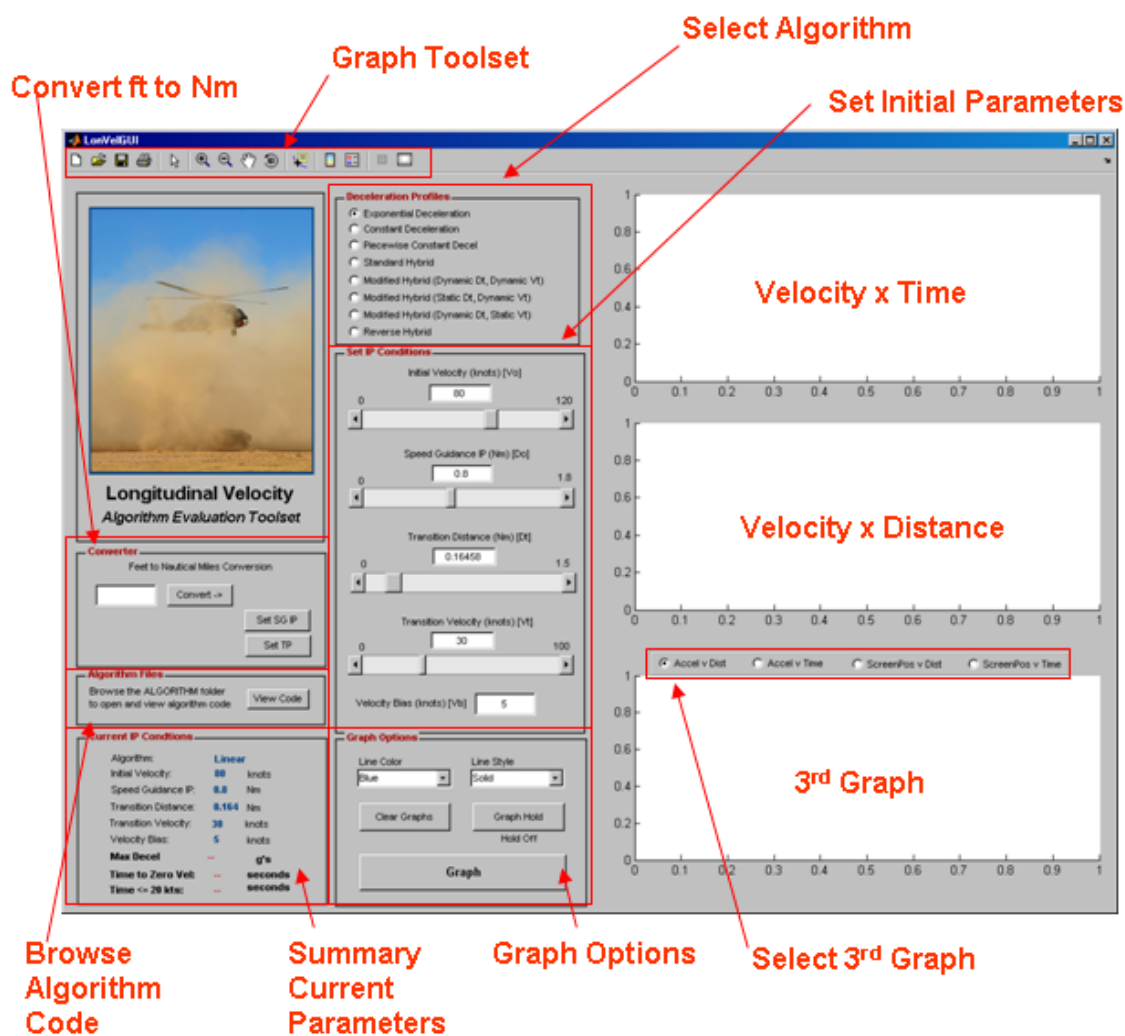
Figure D1: Algorithm toolset GUI Interface.
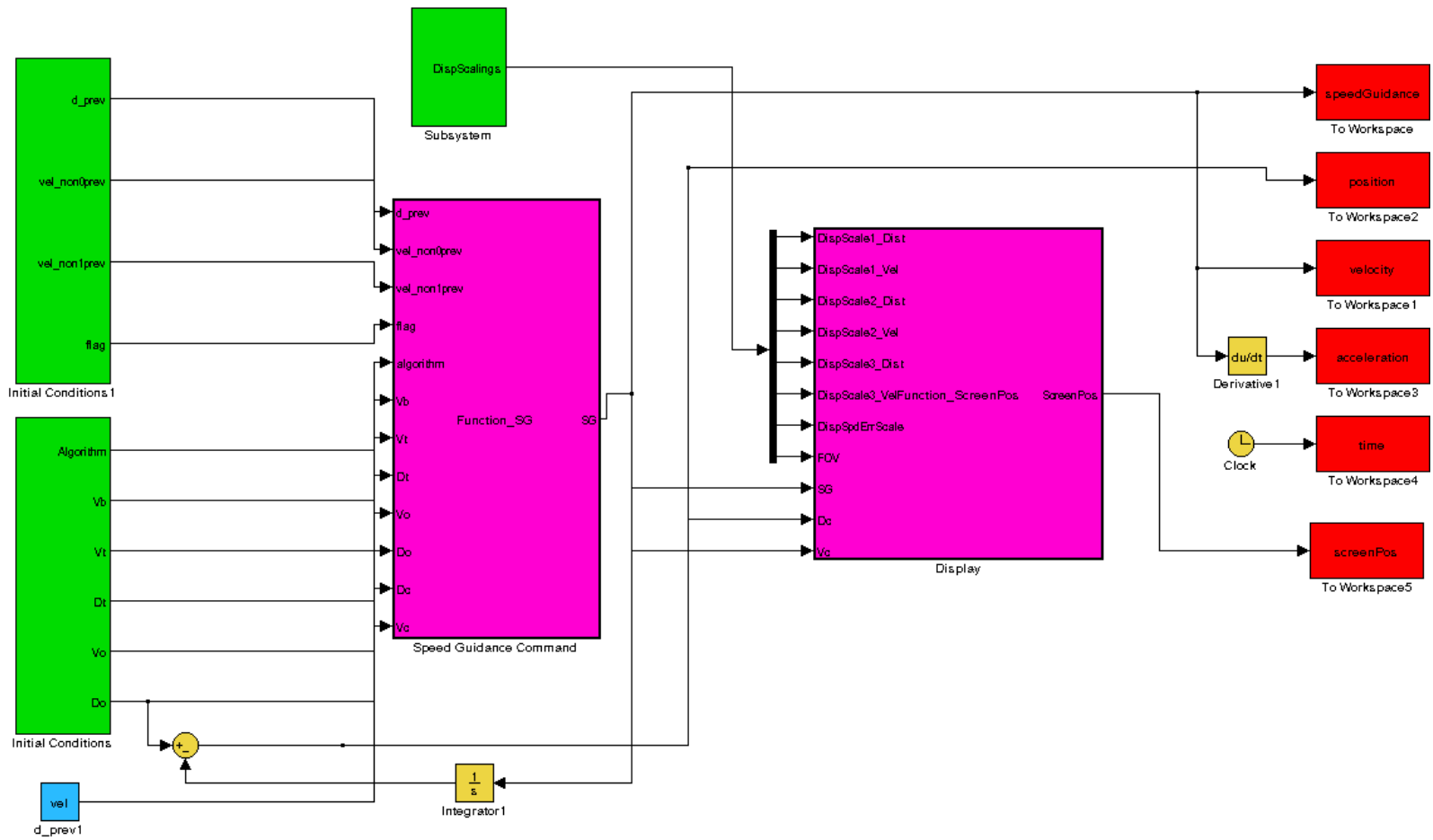
Figure D2: Matlab Simulink model.

APPENDIX E. ALGORITHM DEVELOPMENT
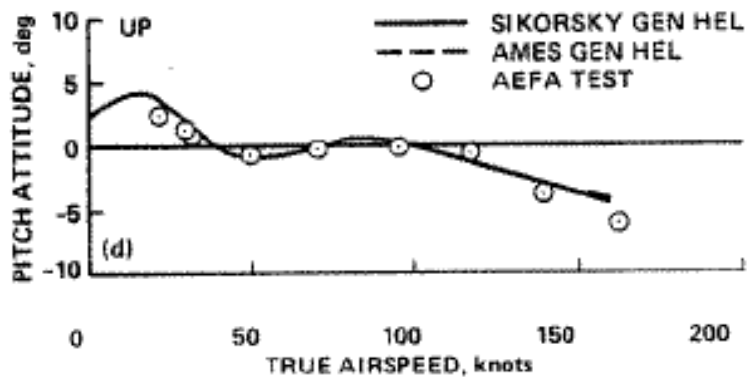
Figure E1: UH-60 trim pitch versus airspeed.

Source: Ballin[67]
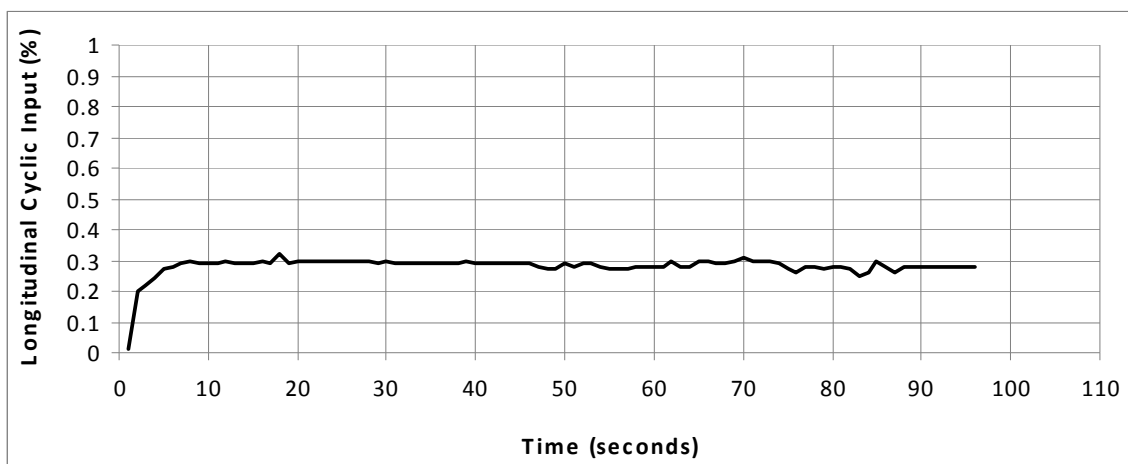
Figure E2: Longitudinal cyclic input versus time.
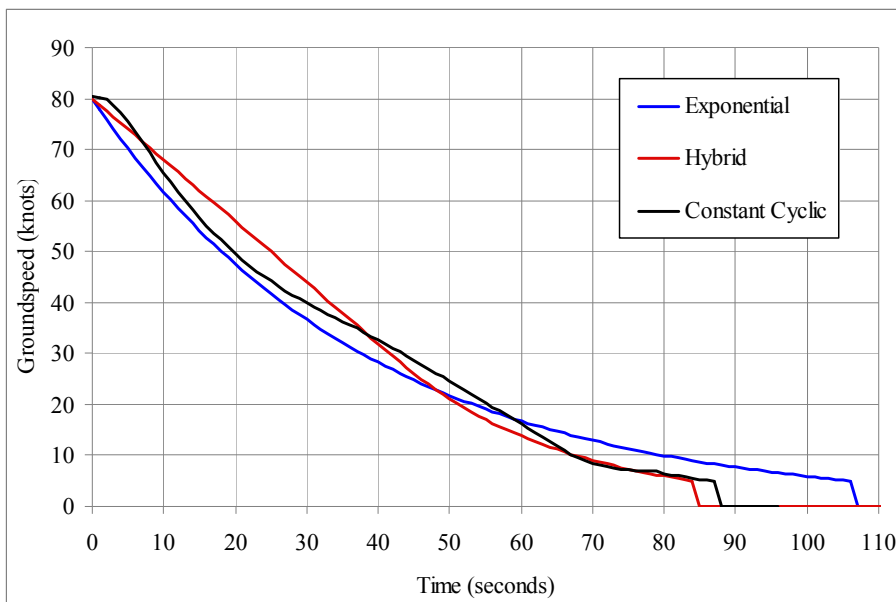
Figure E3: Constant cyclic profile versus hybrid and exponential profiles.

Regression Analysis: Dt versus Do, Vo, ...

```
The regression equation is
Dt = 2186 - 0.335 Do - 23.7 Vo - 26.7 Vt + 0.00142 Do*Vo + 0.0177 Do*Vt
     - 0.000075 Do*Vo*Vt + 0.0773 Vo*Vo + 0.353 Vt*Vt


Predictor        Coef      SE Coef        T       P
Constant        2185.8       122.5     17.85   0.000
Do            -0.33529     0.01568    -21.38   0.000
Vo           -23.6604       0.9738    -24.30   0.000
Vt           -26.666         4.326     -6.16   0.000
Do*Vo        0.00141958   0.00008483   16.73   0.000
Do*Vt        0.0176558     0.0003517   50.21   0.000
Do*Vo*Vt    -0.00007522   0.00000176  -42.84   0.000
Vo*Vo        0.077272      0.003030    25.50   0.000
Vt*Vt        0.35314       0.05386      6.56   0.000


S = 53.5580    R-Sq = 99.1%    R-Sq(adj) = 99.0%
```

Figure E4: Regression analysis for Fixed Vt algorithm.

Regression Analysis: Vt versus Dt, Do, Vo, Dt*Do, Dt*Vo, Do*Vo

```
The regression equation is
Vt = - 14.4 + 0.0193 Dt + 0.00348 Do + 0.292 Vo - 0.000004 Dt*Do
        + 0.000207 Dt*Vo - 0.000032 Do*Vo


Predictor          Coef     SE Coef        T      P
Constant        -14.417       3.062    -4.71  0.000
Dt             0.019253    0.002115     9.10  0.000
Do            0.0034761   0.0004512     7.70  0.000
Vo              0.29165     0.01812    16.10  0.000
Dt*Do       -0.00000364  0.00000023   -15.94  0.000
Dt*Vo        0.00020666  0.00001056    19.56  0.000
Do*Vo       -0.00003155  0.00000258   -12.21  0.000


S = 2.63717   R-Sq = 98.2%   R-Sq(adj) = 98.1%
```

Figure E5: Regression analysis for initial Fixed Dt algorithm.

Regression Analysis: Vt versus Dt, Do, Vo, Dt*Do, Dt*Vo, Do*Vo

```
The regression equation is
Vt = 14.6 + 0.0251 Dt - 0.00251 Do + 0.101 Vo - 0.000003 Dt*Do + 0.000151 Dt*Vo
        + 0.000006 Do*Vo


Predictor          Coef     SE Coef        T      P
Constant         14.598       1.917     7.62  0.000
Dt             0.025111    0.001406    17.86  0.000
Do            -0.0025131   0.0003967   -6.33  0.000
Vo              0.10078     0.01639     6.15  0.000
Dt*Do       -0.00000320  0.00000025   -12.72  0.000
Dt*Vo        0.00015099  0.00001366    11.05  0.000
Do*Vo        0.00000636  0.00000216     2.94  0.004


S = 1.75908   R-Sq = 98.5%   R-Sq(adj) = 98.5%
```

Figure E6: Regression analysis for final Fixed Dt algorithm.
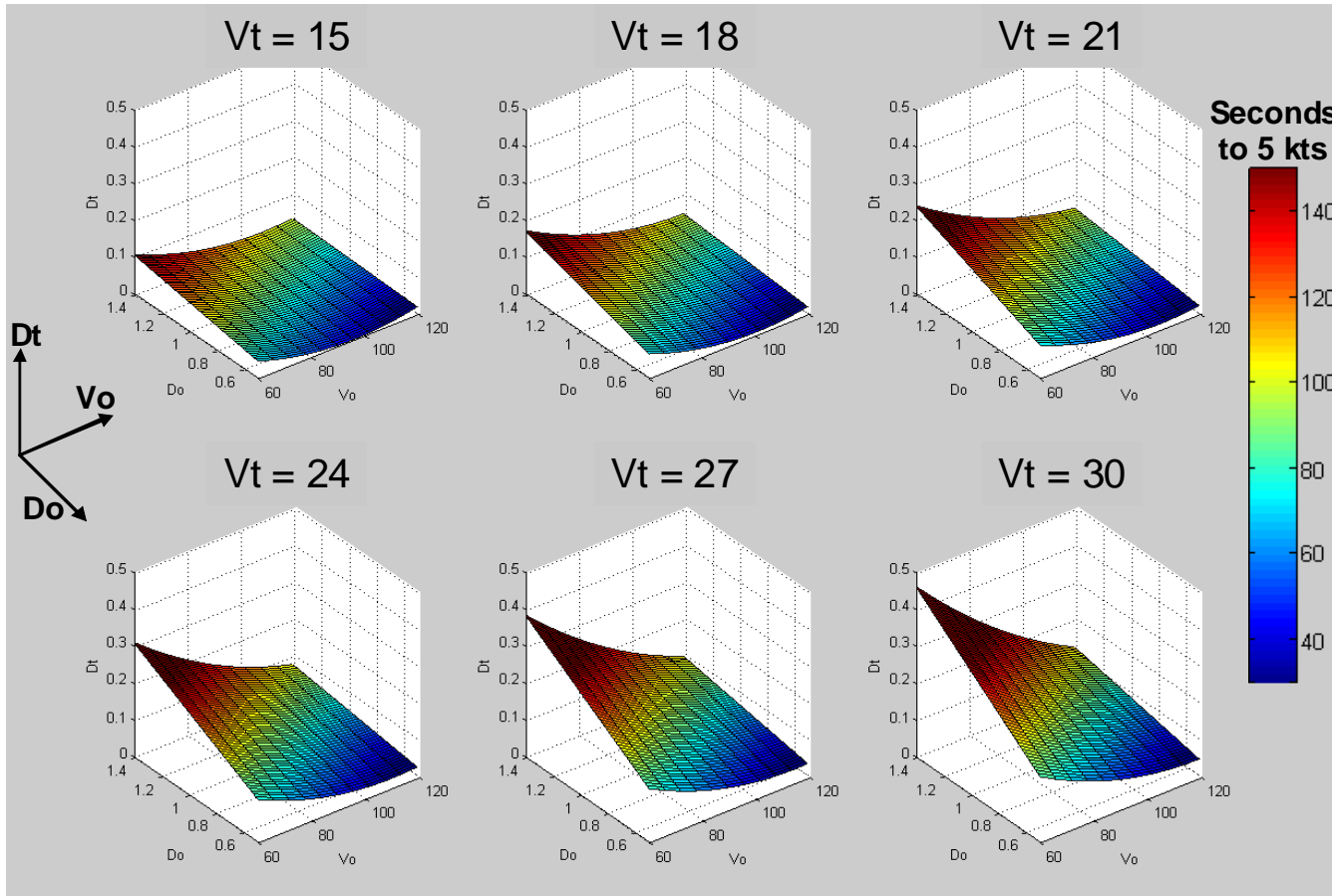
Figure E7: 4-D plots of Constant Vt Hybrid.
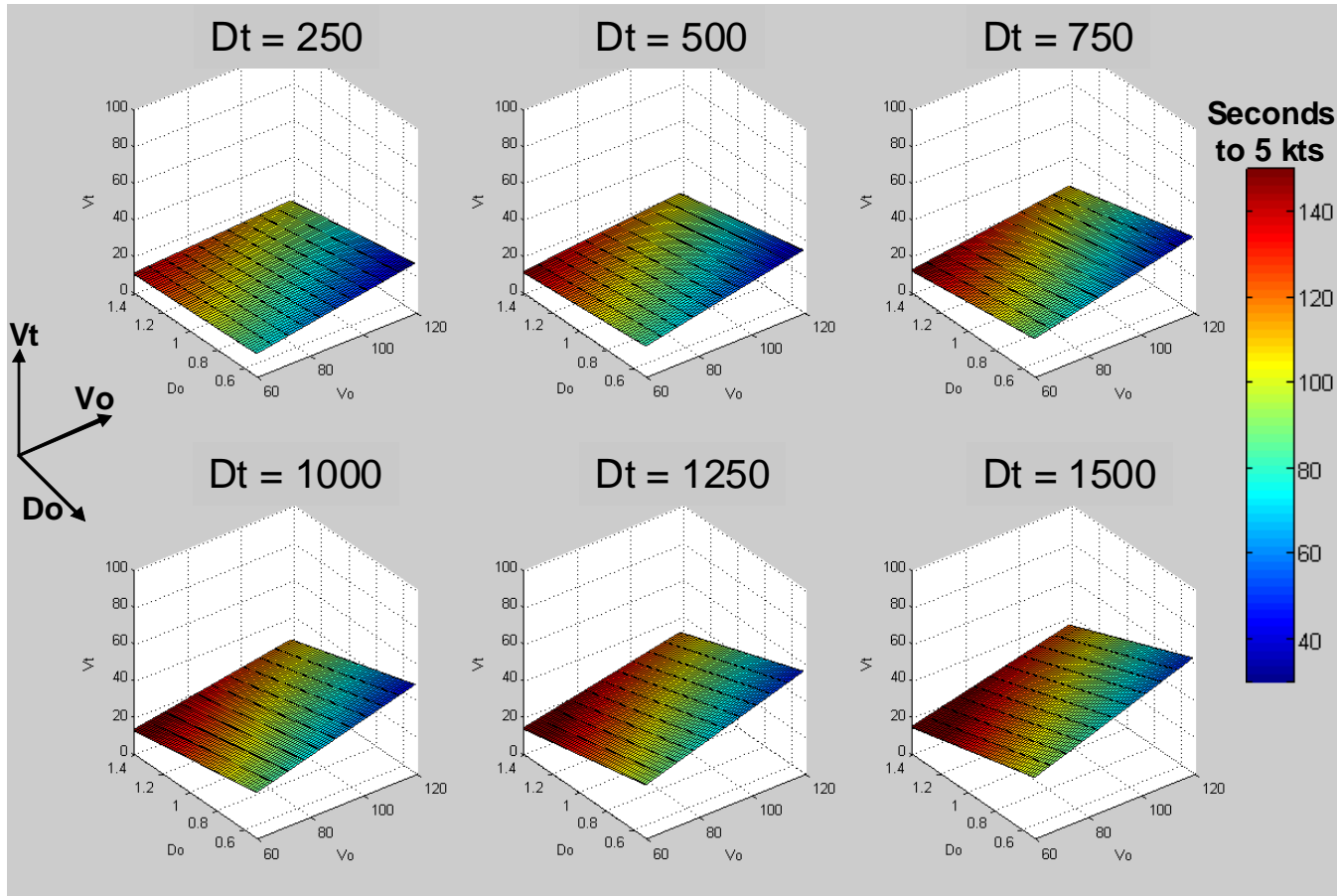
Figure E8: 4-D plots for Constant Dt Hybrid.

APPENDIX F. EXPERIMENTAL SETUP

Table F1: Data collection parameters.

Parameter	Units
Date	[year:month:day]
Timestamp	[hour:minute:second]
Pilot Number	integer
Algorithm	integer [1-4]
Approach	integer [1-2]
Run	integer [1-16]
Time	seconds
Time Since Start of Speed Guidance	seconds
LP - X	feet
LP - Y	feet
LP - Z	feet
Aircraft - X	feet
Aircraft - Y	feet
Aircraft - Z (baro altitude)	feet
Radar Altitude	feet
Distance to LP	feet
Vertical Velocity	feet/minute
Vertical Acceleration	feet/second/second
Lateral Velocity	knots
Longitudinal Velocity	knots
Ground Speed	knots
Ground Speed Acceleration	g's
Brownout Intensity	percentage
Speed Guidance Commanded Speed	knots
Speed Error	knots
Altitude Error	RMS feet
Heading Error	RMS degrees
Cross Track (Lateral) Error	RMS feet
Aircraft Pitch	degrees
Aircraft Roll	degrees
Aircraft Heading	degrees
Longitudinal Cyclic	percentage
Lateral Cyclic	percentage
Torque (Collective)	percentage
Pedal Inputs	Percentage
Speed Guidance Flag	binary [0 1]
Algorithm Transition Flag	binary [0 1]

RATING SCALE DEFINITIONS

Title	Endpoints	Descriptions
MENTAL DEMAND	Low/High	How much mental and perceptual activity was required (e.g., thinking, deciding, calculating, remembering, looking, searching, etc.)? Was the task easy or demanding, simple or complex, exacting or forgiving?
PHYSICAL DEMAND	Low/High	How much physical activity was required (e.g., pushing, pulling, turning, controlling, activating, etc.)? Was the task easy or demanding, slow or brisk, slack or strenuous, restful or laborious?
TEMPORAL DEMAND	Low/High	How much time pressure did you feel due to the rate or pace at which the tasks or task elements occurred? Was the pace slow and leisurely or rapid and frantic?
EFFORT	Low/High	How hard did you have to work (mentally and physically) to accomplish your level of performance?
PERFORMANCE	Good/Poor	How successful do you think you were in accomplishing the goals of the task set by the experimenter (or yourself)? How satisfied were you with your performance in accomplishing these goals?
FRUSTRATION LEVEL	Low/High	How insecure, discouraged, irritated, stressed and annoyed versus secure, gratified, content, relaxed and complacent did you feel during the task?

MENTAL DEMAND

Low   High

PHYSICAL DEMAND

Low   High

TEMPORAL DEMAND

Low   High

PERFORMANCE

Good   Poor

EFFORT

Low   High

FRUSTRATION

Low   High
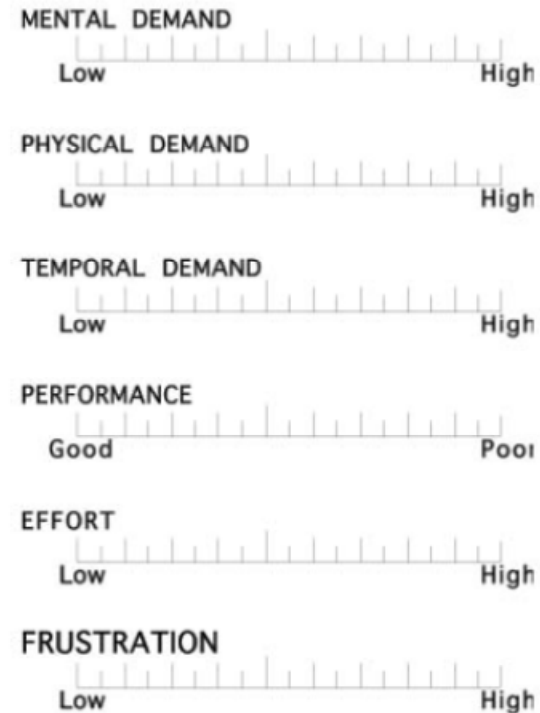
Figure F1: NASA TLX rating sheet.

Source: Hart and Staveland[69]
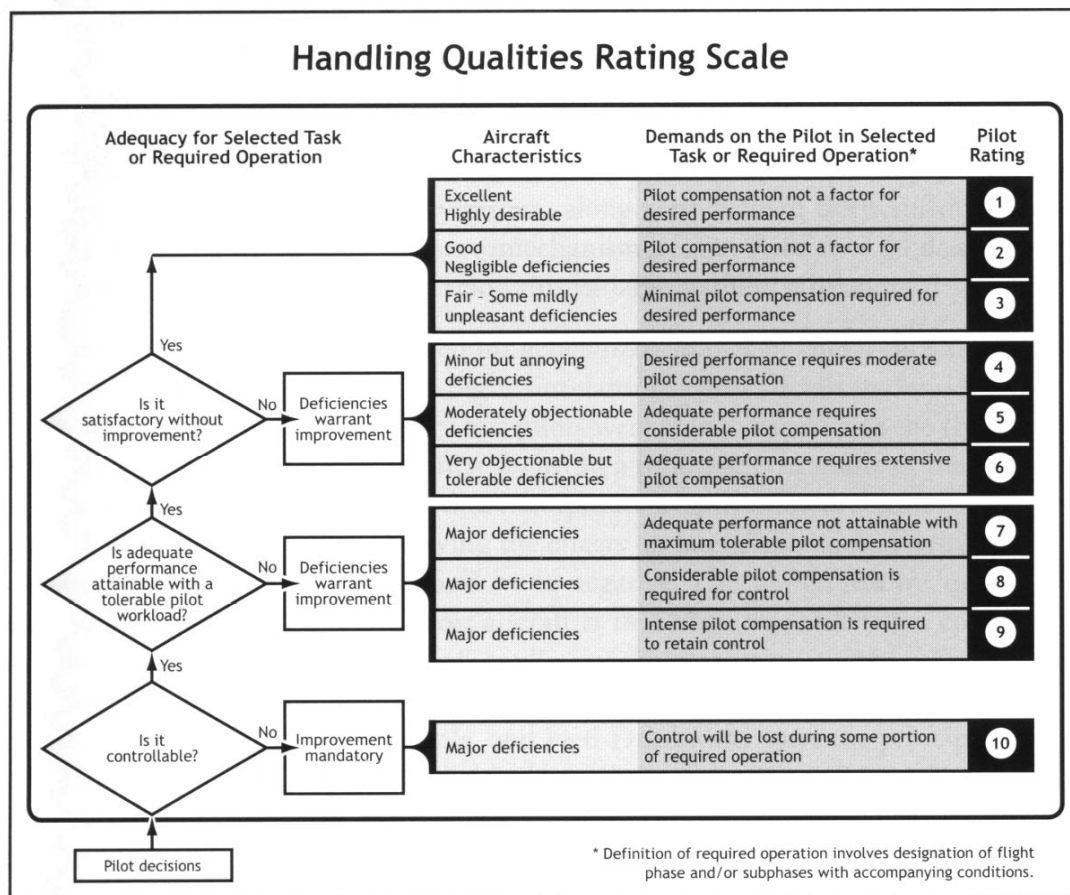
Figure F2: Cooper-Harper HQR sheet.

Source: Cooper and Harper[70]

Entry Alt: 1485 MSL
Entry Speed: 80 knots
FAF: 0.8 Nm
Glideslope: 3 degrees

DTL
Descent to Land

Plan View

Touchdown

LP

Follow speed guidance

Start descent and deceleration

FAF

5 seconds level flight

IP
1485 MSL
80 KTS

Side View

FAF

IP   80 knots   255 ft AGL
      1485 MSL

3°   LP

Fly initial heading at specified airspeed and altitude until speed guidance starts, at which point begin a deceleration and a descent to the LP. Continue to fly the approach, following the speed guidance cue. At the LP null out any undesired velocities, and touchdown within acceptable performance standards.

Figure F3: 3-degree approach run card.
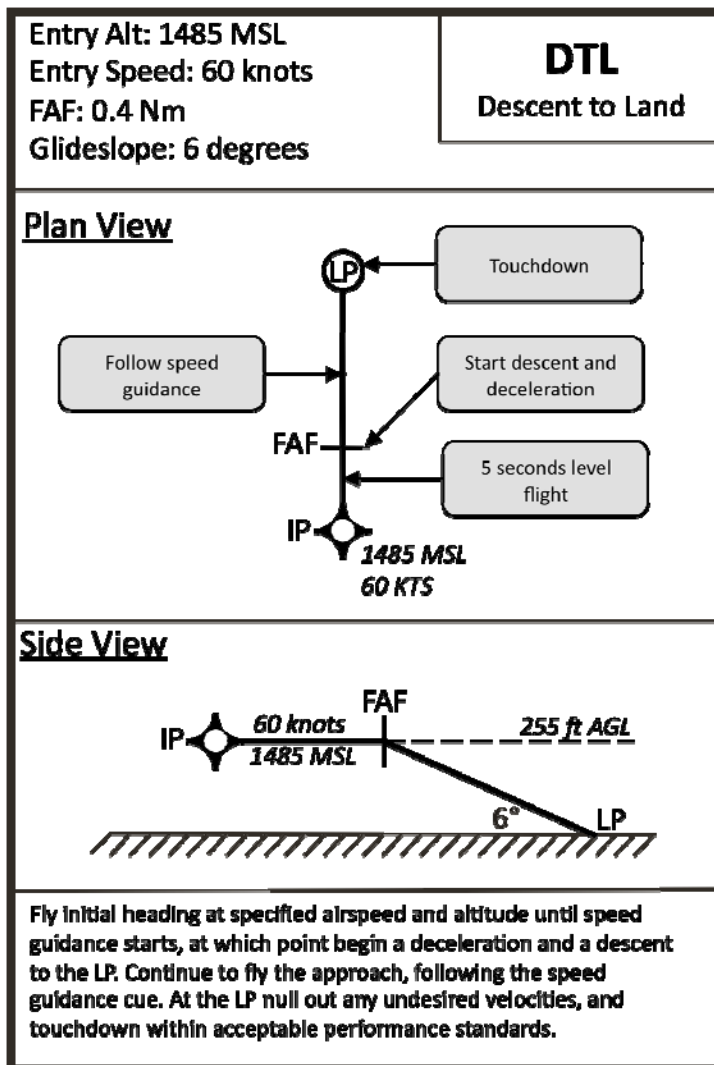
Figure F4: 6-degree approach run card.

Table F2: Calculated V_t for 3-degree approach.

| 3-deg, 80kts, 0.8 Nm ||
Dt (ft)	Vt (kts)
1000	30.15
500	20.99
250	16.41

Table F3: Calculated V_t for 6-degree approach.

6-deg, 60kts, 0.4 Nm	
Dt (ft)	**Vt (kts)**
1000	31.58
500	21.78
250	16.87

Table F4: Pilot run matrix.

Run	Pilot															
	1		2		3		4		5		6		7		8	
	Alg	*App*	*Alg*	*App*	*Alg*	*App*	*Alg*	*App*	*Alg*	*App*	*Alg*	*App*	*Alg*	*App*	*Alg*	*App*
1	1	1	2	1	3	1	4	2	4	2	3	1	1	2	2	1
2	1	1	2	1	3	1	4	2	4	2	3	1	1	2	2	1
3	1	2	2	2	3	2	4	1	4	1	3	2	1	1	2	2
4	1	2	2	2	3	2	4	1	4	1	3	2	1	1	2	2
5	3	2	4	2	1	2	2	1	2	1	1	2	3	1	4	2
6	3	2	4	2	1	2	2	1	2	1	1	2	3	1	4	2
7	3	1	4	1	1	1	2	2	2	2	1	1	3	2	4	1
8	3	1	4	1	1	1	2	2	2	2	1	1	3	2	4	1
9	4	1	1	2	2	2	3	1	1	1	4	1	2	2	3	2
10	4	1	1	2	2	2	3	1	1	1	4	1	2	2	3	2
11	4	2	1	1	2	1	3	2	1	2	4	2	2	1	3	1
12	4	2	1	1	2	1	3	2	1	2	4	2	2	1	3	1
13	2	2	3	1	4	1	1	2	3	2	2	2	4	1	1	1
14	2	2	3	1	4	1	1	2	3	2	2	2	4	1	1	1
15	2	1	3	2	4	2	1	1	3	1	2	1	4	2	1	2
16	2	1	3	2	4	2	1	1	3	1	2	1	4	2	1	2

APPENDIX G. RESULTS
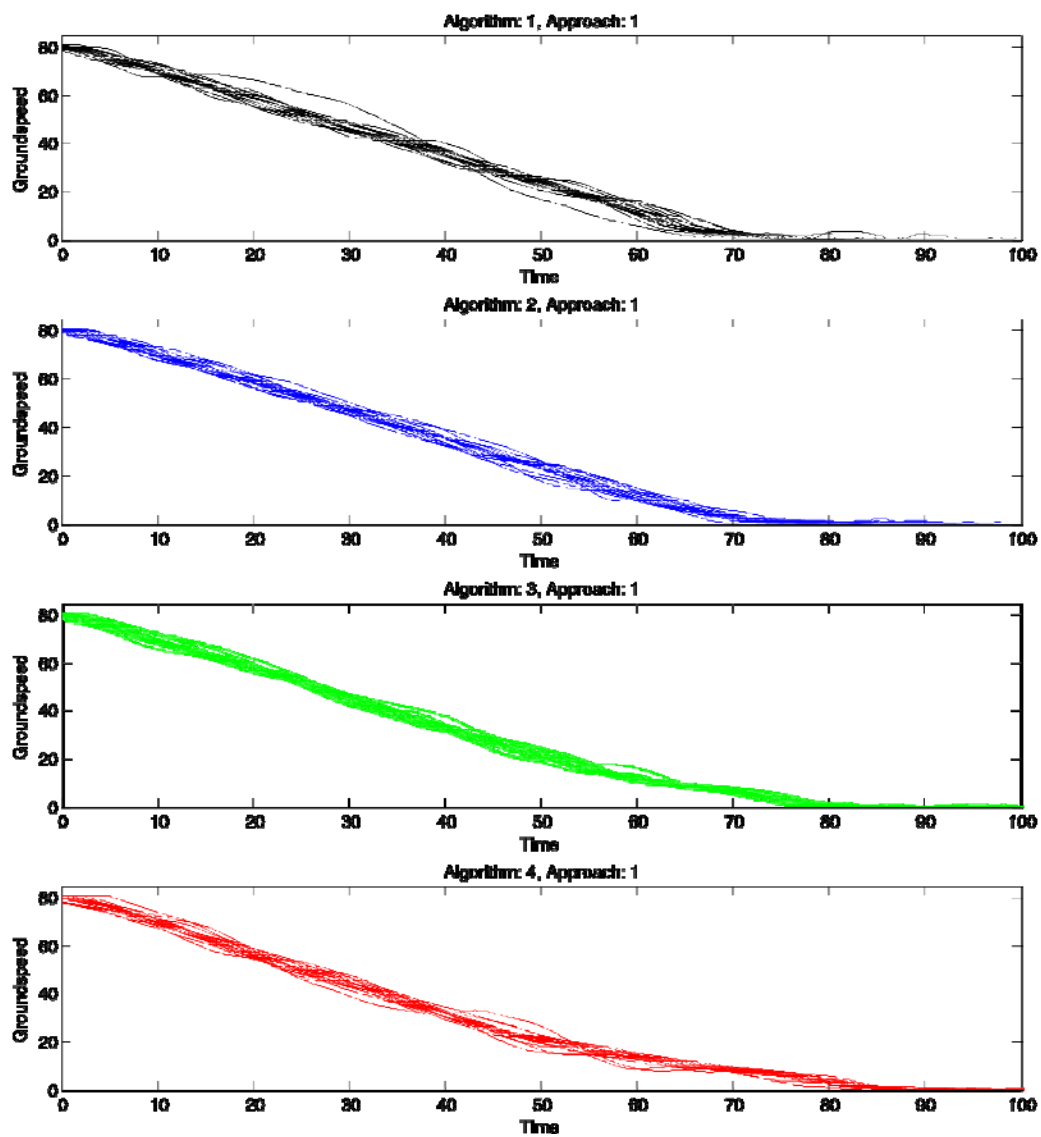
Figure G1: Collected deceleration profiles for 3-degree approach.

Algorithm: (1) Constant Decel (2) 250ft Hybrid (3) 500ft Hybrid (4) 1000ft Hybrid
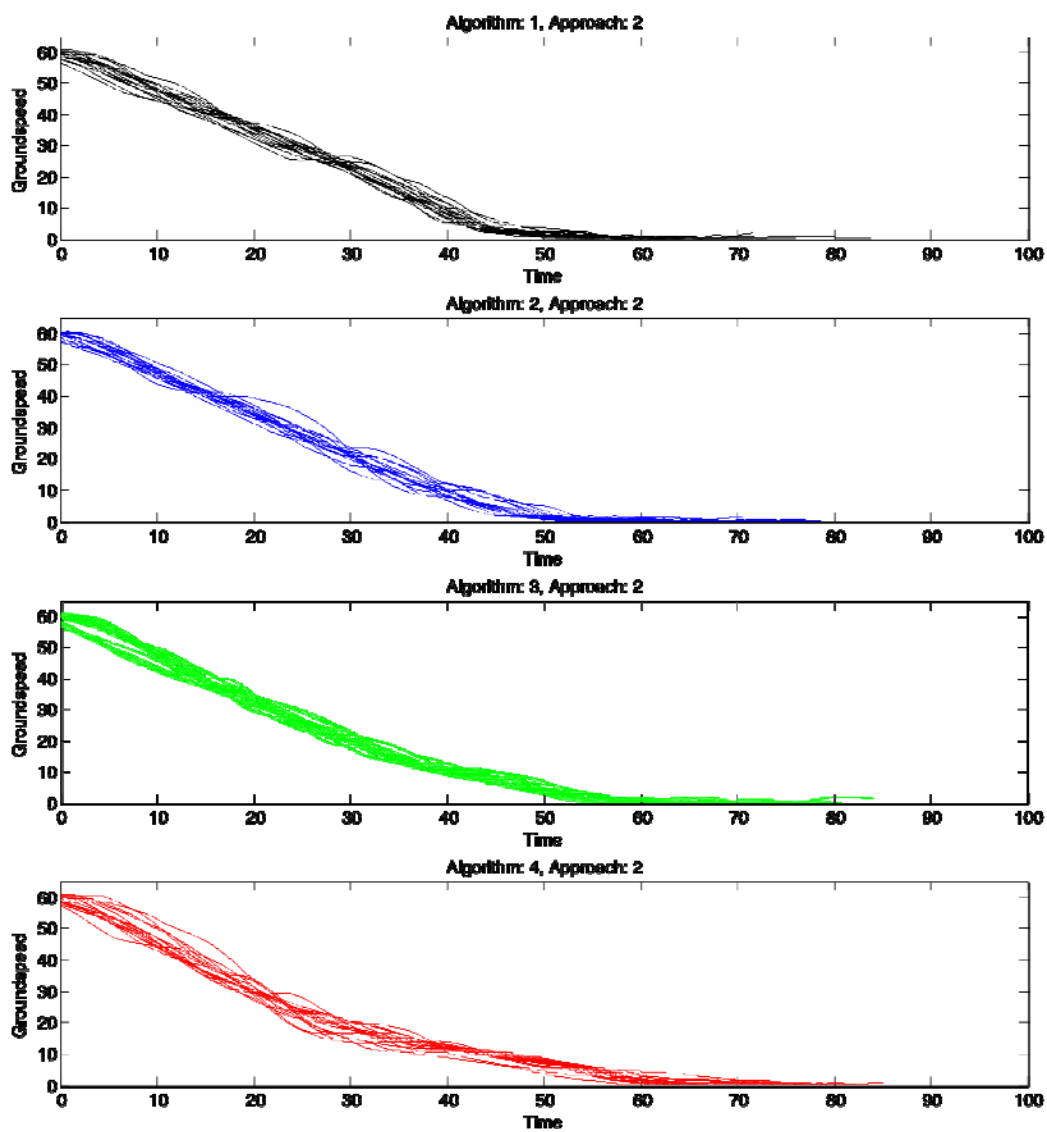
Figure G2: Collected deceleration profiles for 6-degree approach.

Algorithm: (1) Constant Decel (2) 250ft Hybrid (3) 500ft Hybrid (4) 1000ft Hybrid

General Linear Model: RMS SpdErr versus Algorithm, Approach

```
Factor      Type    Levels  Values
Algorithm   fixed        4  1, 2, 3, 4
Approach    fixed        2  1, 2


Analysis of Variance for RMS SpdErr, using Adjusted SS for Tests

Source              DF      Seq SS     Adj SS   Adj MS     F      P
Algorithm            3      3.1848     3.1848   1.0616   1.16  0.329
Approach             1      0.5193     0.5193   0.5193   0.57  0.453
Algorithm*Approach   3      2.0690     2.0690   0.6897   0.75  0.523
Error              120    110.0334   110.0334   0.9169
Total              127    115.8065


S = 0.957573   R-Sq = 4.99%   R-Sq(adj) = 0.00%
```

Figure G3: GLM ANOVA analysis for RMS speed error.
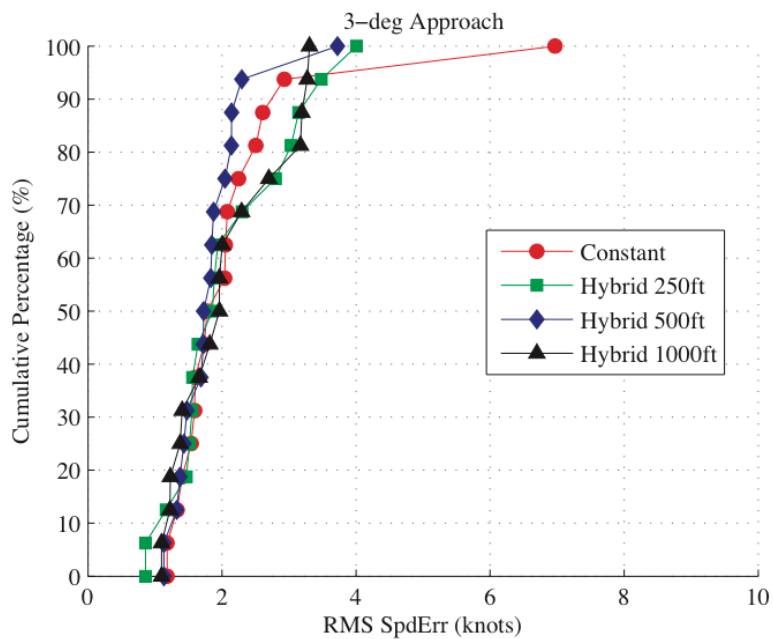
Figure G4: Cumulative histogram of RMS speed error, 3-degree approach.
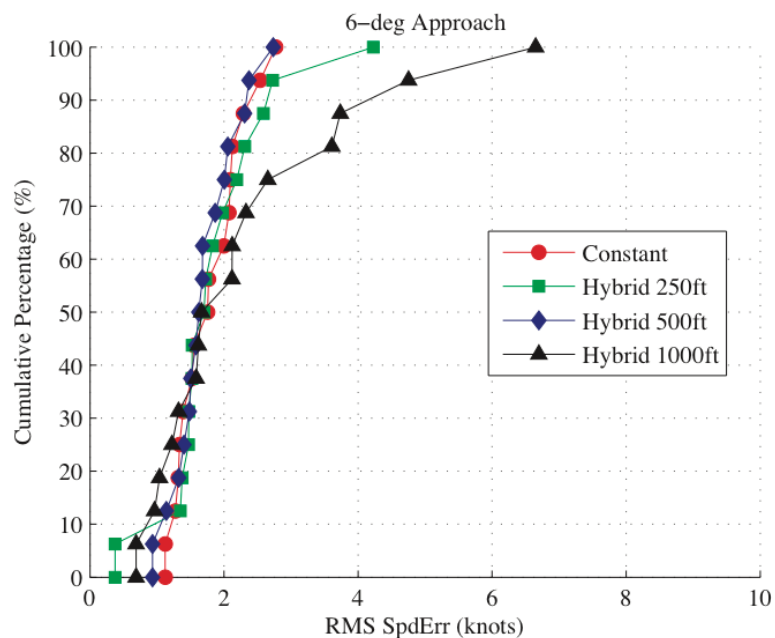
Figure G5: Cumulative histogram of RMS speed error, 6-degree approach.

General Linear Model: Time in Approach versus Algorithm, Approach

```
Factor      Type    Levels   Values
Algorithm   fixed        4   1, 2, 3, 4
Approach    fixed        2   1, 2


Analysis of Variance for Time in Approach, using Adjusted SS for Tests

Source               DF    Seq SS     Adj SS    Adj MS       F       P
Algorithm             3    2114.9     2114.9     705.0   11.09   0.000
Approach              1   12141.5    12141.5   12141.5  191.03   0.000
Algorithm*Approach    3      25.6       25.6       8.5    0.13   0.939
Error               120    7626.9     7626.9      63.6
Total               127   21908.9


S = 7.97228   R-Sq = 65.19%   R-Sq(adj) = 63.16%
```

Figure G6: GLM ANOVA analysis for time spent in approach.

Table G1: Algorithm pairwise comparison for time in approach.

Tukey's Pairwise Comparison p-values				
	Constant	250ft Hybrid	500ft Hybrid	1000ft Hybrid
Constant	X			
250ft Hybrid	0.4854	X		
500ft Hybrid	0.0013	0.0861	X	
1000ft Hybrid	0.0000	0.0012	0.4739	X

```
General Linear Model: Time in BO versus Algorithm, Approach

Factor      Type    Levels  Values
Algorithm   fixed        4  1, 2, 3, 4
Approach    fixed        2  1, 2


Analysis of Variance for Time in BO, using Adjusted SS for Tests

Source              DF    Seq SS    Adj SS   Adj MS      F      P
Algorithm            3   2706.56   2706.56   902.19  15.47  0.000
Approach             1    125.63    125.63   125.63   2.15  0.145
Algorithm*Approach   3     11.65     11.65     3.88   0.07  0.978
Error              120   6997.36   6997.36    58.31
Total              127   9841.20


S = 7.63618   R-Sq = 28.90%   R-Sq(adj) = 24.75%
```

Figure G7: GLM ANOVA analysis for time spent in brownout.

Table G2: Algorithm pairwise comparison for time spent in brownout.

Tukey's Pairwise Comparison p-values				
	Constant	250ft Hybrid	500ft Hybrid	1000ft Hybrid
Constant	X			
250ft Hybrid	0.2370	X		
500ft Hybrid	0.0001	0.0484	X	
1000ft Hybrid	0.0000	0.0001	0.2884	X

General Linear Model: Time <20kts versus Algorithm, Approach

```
Factor     Type   Levels  Values
Algorithm  fixed       4  1, 2, 3, 4
Approach   fixed       2  1, 2


Analysis of Variance for Time <20kts, using Adjusted SS for Tests

Source             DF     Seq SS    Adj SS    Adj MS      F      P
Algorithm           3    3637.08   3637.08   1212.36  18.53  0.000
Approach            1     159.81    159.81    159.81   2.44  0.121
Algorithm*Approach  3       8.65      8.65      2.88   0.04  0.988
Error             120    7849.64   7849.64     65.41
Total             127   11655.19


S = 8.08787   R-Sq = 32.65%   R-Sq(adj) = 28.72%
```

Figure G8: GLM ANOVA analysis for time spent under 20kts.

Table G3: Algorithm pairwise comparison for time spent under 20 kts.

Tukey's Pairwise Comparison p-values				
	Constant	250ft Hybrid	500ft Hybrid	1000ft Hybrid
Constant	X			
250ft Hybrid	0.3131	X		
500ft Hybrid	0.0001	0.0253	X	
1000ft Hybrid	0.0000	0.0000	0.1075	X

General Linear Model: TD LatVel versus Algorithm, Approach

```
Factor      Type    Levels  Values
Algorithm   fixed       4   1, 2, 3, 4
Approach    fixed       2   1, 2


Analysis of Variance for TD LatVel, using Adjusted SS for Tests

Source              DF    Seq SS    Adj SS    Adj MS      F      P
Algorithm            3   0.12707   0.12707   0.04236   1.16  0.330
Approach             1   0.09382   0.09382   0.09382   2.56  0.112
Algorithm*Approach   3   0.04544   0.04544   0.01515   0.41  0.744
Error              120   4.39935   4.39935   0.03666
Total              127   4.66568


S = 0.191471   R-Sq = 5.71%   R-Sq(adj) = 0.21%
```

Figure G9: GLM ANOVA analysis for lateral velocity at TD.

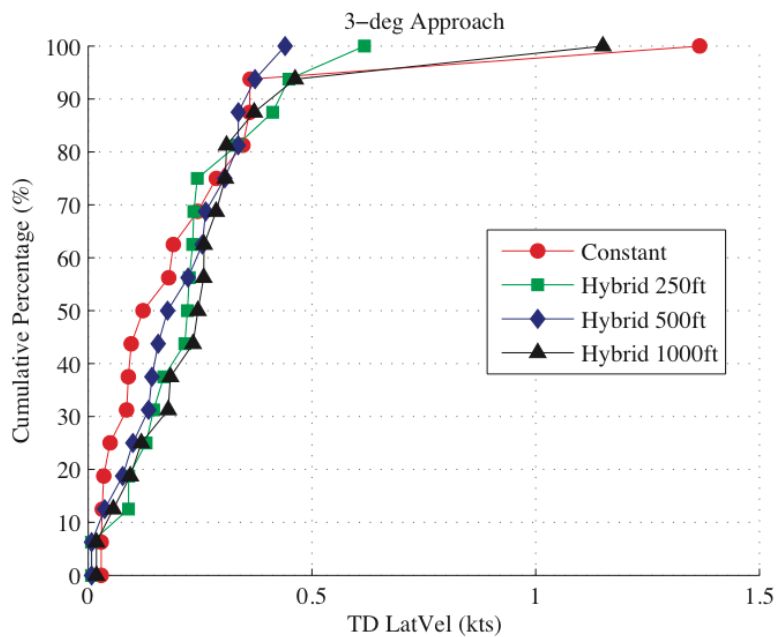Figure G10: Cumulative histogram of lateral velocity at TD, 3-degree approach.

Figure G11: Cumulative histogram of lateral velocity at TD, 6-degree approach.

Figure G12: GLM ANOVA analysis for longitudinal velocity at TD.

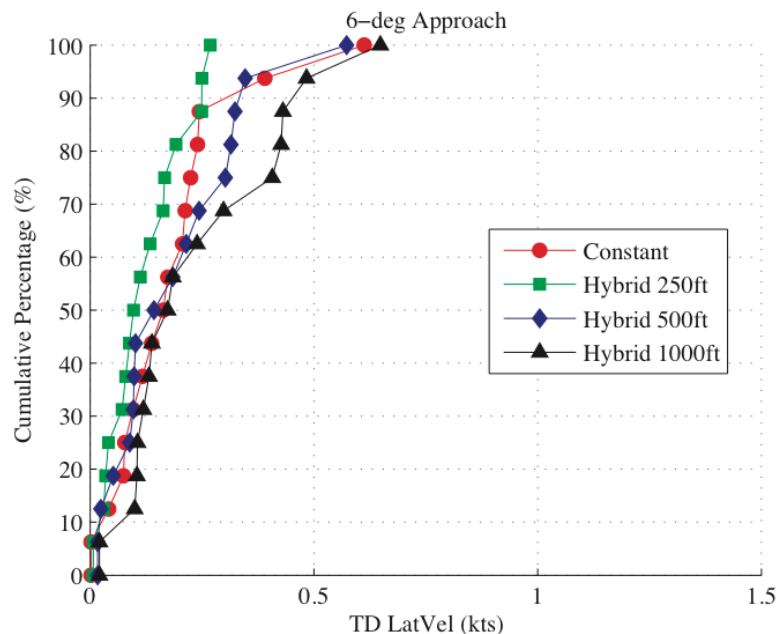Figure G13: Cumulative histogram of longitudinal velocity at TD, 3-degree approach.

Figure G14: Cumulative histogram of longitudinal velocity at TD, 6-degree approach.

```
General Linear Model: TD PosErr versus Algorithm, Approach

Factor      Type    Levels  Values
Algorithm   fixed        4  1, 2, 3, 4
Approach    fixed        2  1, 2


Analysis of Variance for TD PosErr, using Adjusted SS for Tests

Source              DF   Seq SS   Adj SS   Adj MS     F     P
Algorithm            3    47.81    47.81    15.94  0.42  0.743
Approach             1    31.07    31.07    31.07  0.81  0.370
Algorithm*Approach   3    43.66    43.66    14.55  0.38  0.768
Error              120  4607.81  4607.81    38.40
Total              127  4730.35


S = 6.19664   R-Sq = 2.59%   R-Sq(adj) = 0.00%
```

Figure G15: GLM ANOVA analysis for position error at TD.
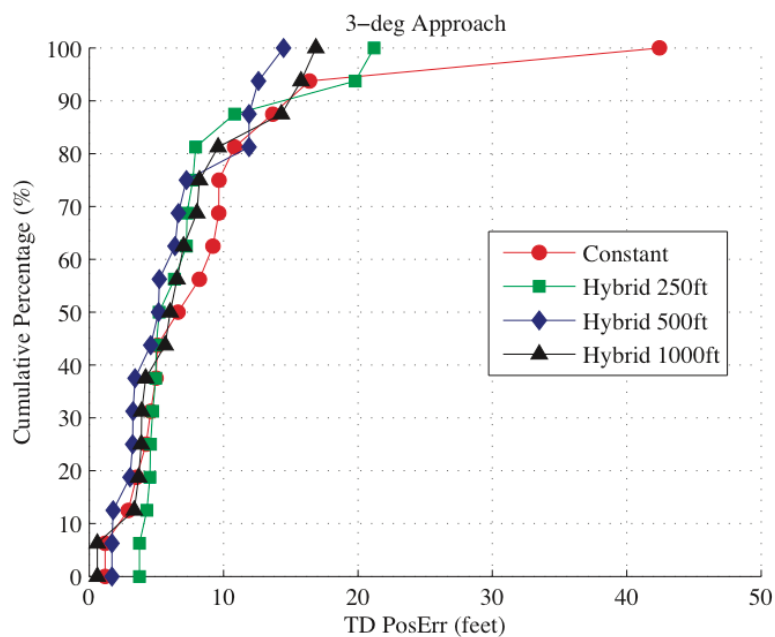
Figure G16: Cumulative histogram of position error at TD, 3-degree approach.
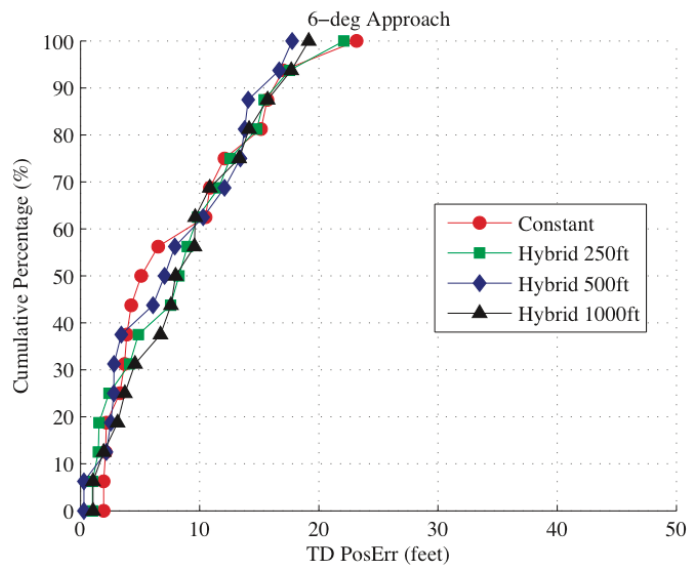
Figure G17: Cumulative histogram of position error at TD, 6-degree approach.

General Linear Model: TD V/S versus Algorithm, Approach

```
Factor      Type    Levels  Values
Algorithm   fixed       4   1, 2, 3, 4
Approach    fixed       2   1, 2


Analysis of Variance for TD V/S, using Adjusted SS for Tests

Source               DF     Seq SS    Adj SS   Adj MS      F      P
Algorithm             3     4883.5    4883.5   1627.8   2.04  0.112
Approach              1      702.3     702.3    702.3   0.88  0.350
Algorithm*Approach    3     1265.4    1265.4    421.8   0.53  0.663
Error               120    95665.6   95665.6    797.2
Total               127   102516.7


S = 28.2350   R-Sq = 6.68%   R-Sq(adj) = 1.24%
```
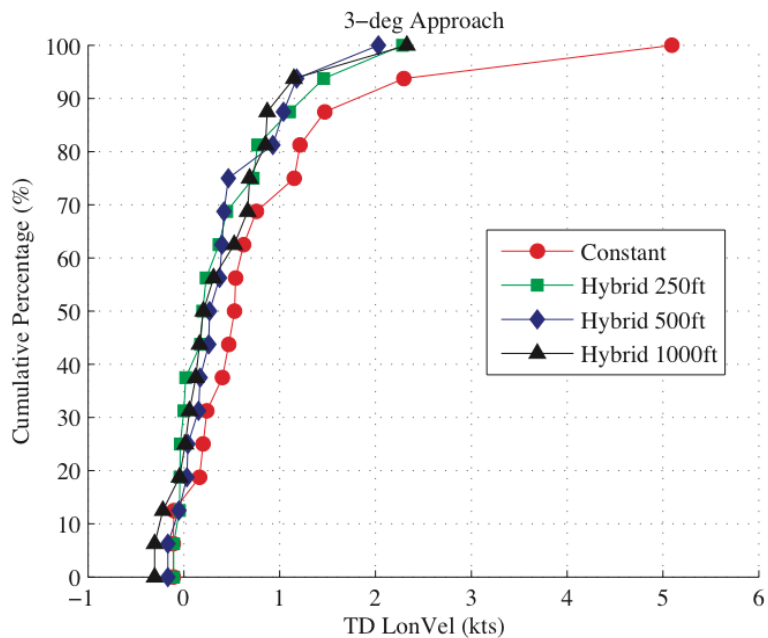
Figure G18: GLM ANOVA analysis for vertical velocity at TD.

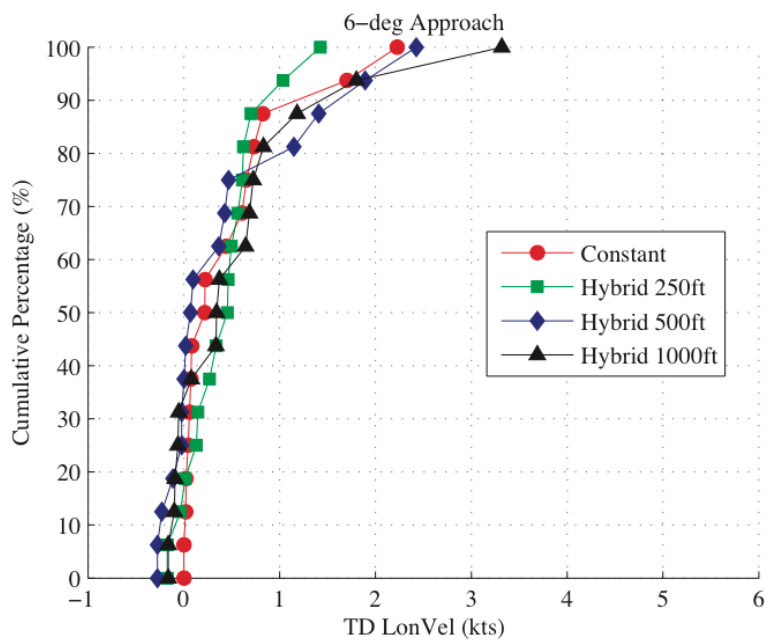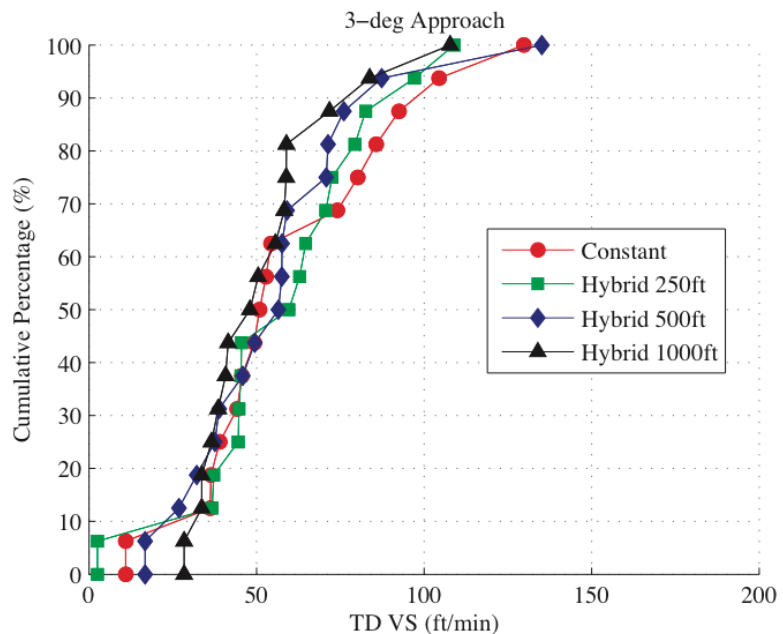Figure G19: Cumulative histogram of vertical speed at TD, 3-degree approach.
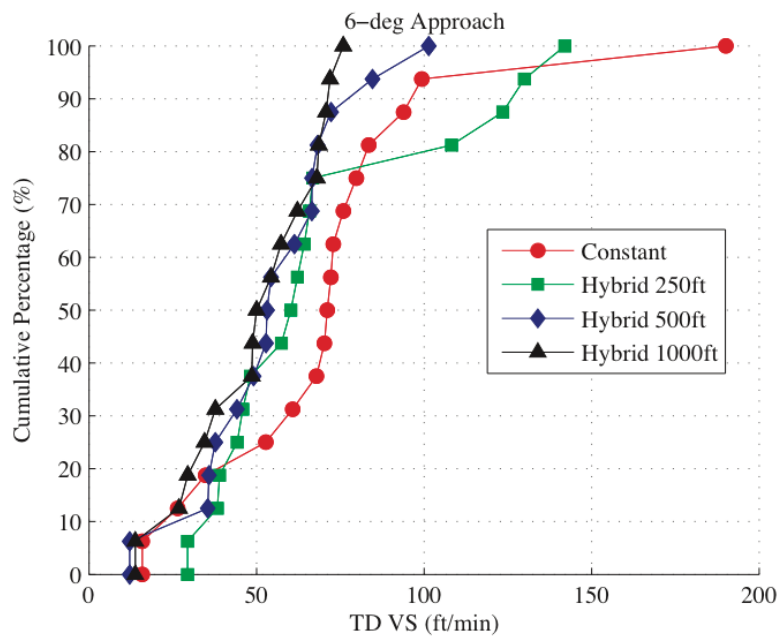
Figure G20: Cumulative histogram of vertical velocity at TD, 6-degree approach.

General Linear Model: TD Score versus Algorithm, Approach

```
Factor      Type   Levels  Values
Algorithm   fixed       4  1, 2, 3, 4
Approach    fixed       2  1, 2


Analysis of Variance for TD Score, using Adjusted SS for Tests

Source             DF    Seq SS    Adj SS    Adj MS     F      P
Algorithm           3  0.006810  0.006810  0.002270  0.69  0.558
Approach            1  0.003644  0.003644  0.003644  1.11  0.294
Algorithm*Approach  3  0.003316  0.003316  0.001105  0.34  0.798
Error             120  0.393103  0.393103  0.003276
Total             127  0.406873


S = 0.0572351   R-Sq = 3.38%   R-Sq(adj) = 0.00%
```

Figure G21: GLM ANOVA analysis for comprehensive TD score.

General Linear Model: Max Pitch BO versus Algorithm, Approach

```
Factor      Type   Levels  Values
Algorithm   fixed       4  1, 2, 3, 4
Approach    fixed       2  1, 2


Analysis of Variance for Max Pitch BO, using Adjusted SS for Tests

Source             DF   Seq SS   Adj SS  Adj MS      F      P
Algorithm           3   71.716   71.716  23.905  21.14  0.000
Approach            1    3.830    3.830   3.830   3.39  0.068
Algorithm*Approach  3    2.388    2.388   0.796   0.70  0.552
Error             120  135.729  135.729   1.131
Total             127  213.663


S = 1.06352   R-Sq = 36.48%   R-Sq(adj) = 32.77%
```

Figure G22: GLM ANOVA analysis for max pitch in brownout.

Table G4: Algorithm pairwise comparison for max pitch in brownout.

Tukey's Pairwise Comparison p-values				
	Constant	250ft Hybrid	500ft Hybrid	1000ft Hybrid
Constant	X			
250ft Hybrid	0.2721	X		
500ft Hybrid	0.0000	0.0053	X	
1000ft Hybrid	0.0000	0.0000	0.1894	X

General Linear Model: Max g BO versus Algorithm, Approach

```
Factor      Type   Levels  Values
Algorithm   fixed       4  1, 2, 3, 4
Approach    fixed       2  1, 2


Analysis of Variance for Max g BO, using Adjusted SS for Tests

Source              DF     Seq SS     Adj SS     Adj MS      F      P
Algorithm            3  0.0276169  0.0276169  0.0092056  20.56  0.000
Approach             1  0.0010478  0.0010478  0.0010478   2.34  0.129
Algorithm*Approach   3  0.0005765  0.0005765  0.0001922   0.43  0.732
Error              120  0.0537350  0.0537350  0.0004478
Total              127  0.0829762


S = 0.0211611   R-Sq = 35.24%   R-Sq(adj) = 31.46%
```

Figure G23: GLM ANOVA analysis for maximum deceleration in brownout.

Table G5: Algorithm pairwise comparison for maximum deceleration in brownout.

Tukey's Pairwise Comparison p-values				
	Constant	250ft Hybrid	500ft Hybrid	1000ft Hybrid
Constant	X			
250ft Hybrid	0.0875	X		
500ft Hybrid	0.0000	0.0273	X	
1000ft Hybrid	0.0000	0.0000	0.1552	X

```
General Linear Model: Lon Cyclic Power versus Algorithm, Approach

Factor      Type    Levels  Values
Algorithm   fixed       4   1, 2, 3, 4
Approach    fixed       2   1, 2


Analysis of Variance for Lon Cyclic Power Ratio APP, using Adjusted SS for
     Tests

Source              DF    Seq SS     Adj SS     Adj MS      F      P
Algorithm            3  0.008633   0.008633   0.002878   0.61  0.610
Approach             1  0.112451   0.112451   0.112451  23.82  0.000
Algorithm*Approach   3  0.016607   0.016607   0.005536   1.17  0.323
Error              120  0.566564   0.566564   0.004721
Total              127  0.704255


S = 0.0687122   R-Sq = 19.55%   R-Sq(adj) = 14.86%
```

Figure G24: GLM ANOVA analysis for longitudinal cyclic power ratio.

Figure G25: Cumulative histogram of longitudinal cyclic frequency power ratio, 3-degree approach.

Figure G26: Cumulative histogram of longitudinal cyclic frequency power ratio, 6-degree approach.

Figure G 27: GLM ANOVA analysis for lateral cyclic power ratio.
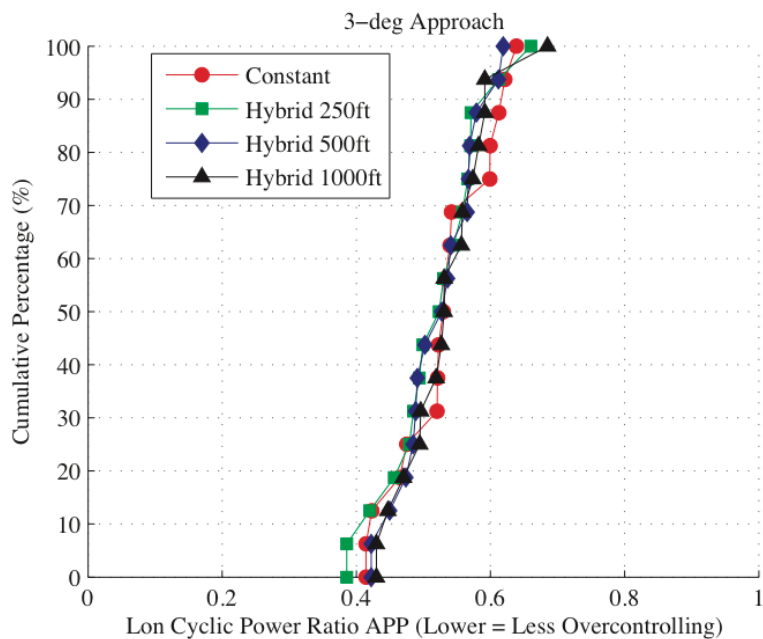
Figure G28: Cumulative histogram of lateral cyclic power ratio, 3-degree approach.
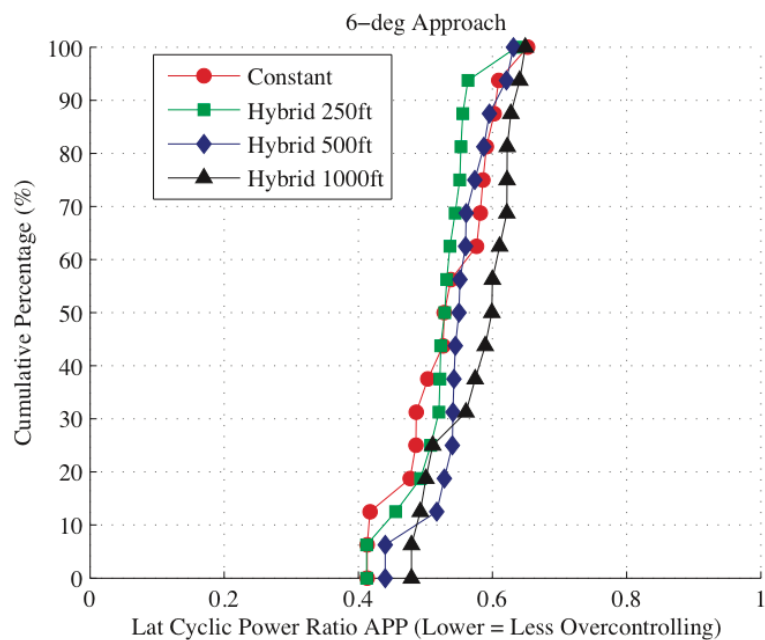
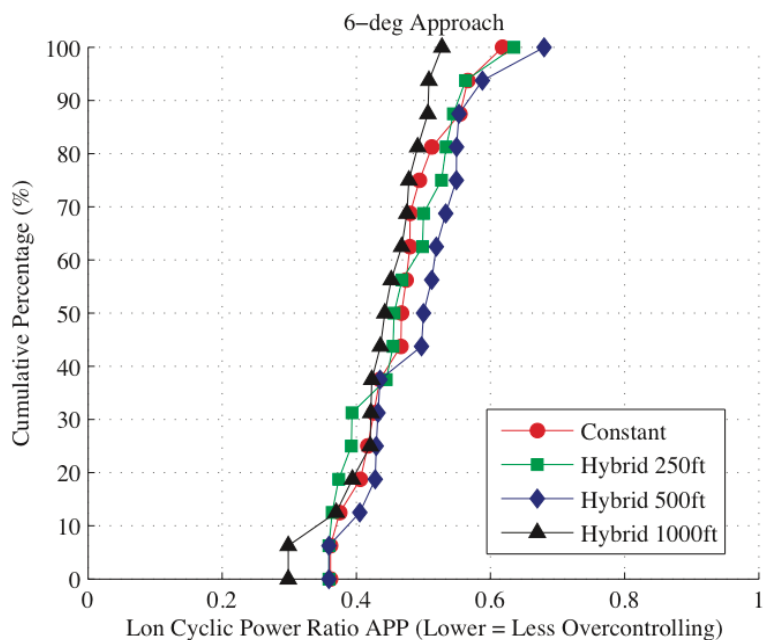Figure G29: Cumulative histogram of lateral cyclic power ratio, 6-degree approach.

General Linear Model: Collective Power versus Algorithm, Approach

```
Factor      Type   Levels  Values
Algorithm   fixed       4  1, 2, 3, 4
Approach    fixed       2  1, 2


Analysis of Variance for Collective Power Ratio APP, using Adjusted SS for
     Tests

Source              DF    Seq SS    Adj SS    Adj MS      F      P
Algorithm            3  0.003847  0.003847  0.001282   0.27  0.847
Approach             1  0.113181  0.113181  0.113181  23.86  0.000
Algorithm*Approach   3  0.010159  0.010159  0.003386   0.71  0.546
Error              120  0.569282  0.569282  0.004744
Total              127  0.696469


S = 0.0688768   R-Sq = 18.26%   R-Sq(adj) = 13.49%
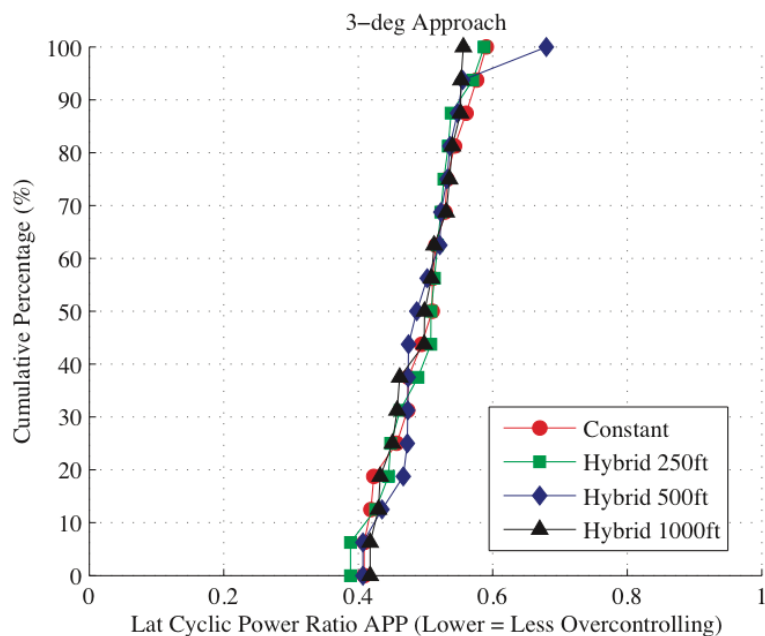```

Figure G30: GLM ANOVA analysis for collective power ratio.
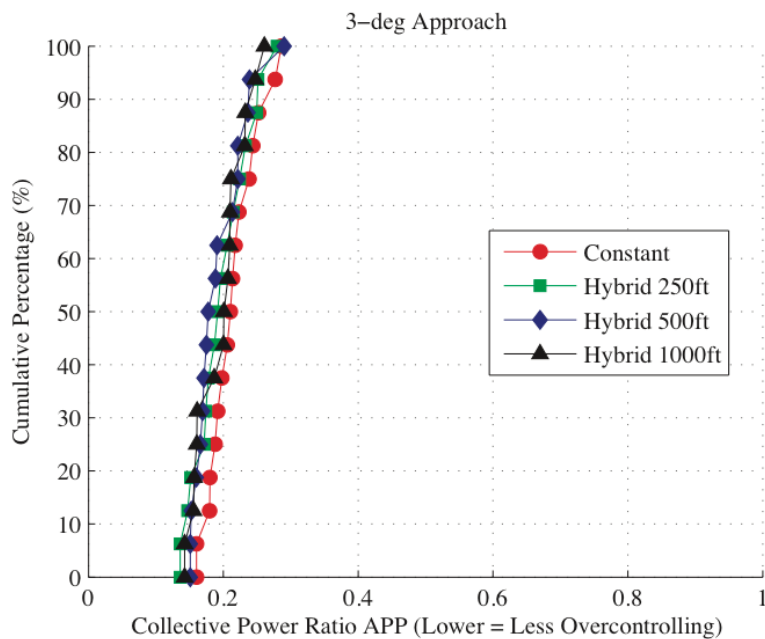


Figure G31: Cumulative histogram of collective power ratio, 3-degree approach.
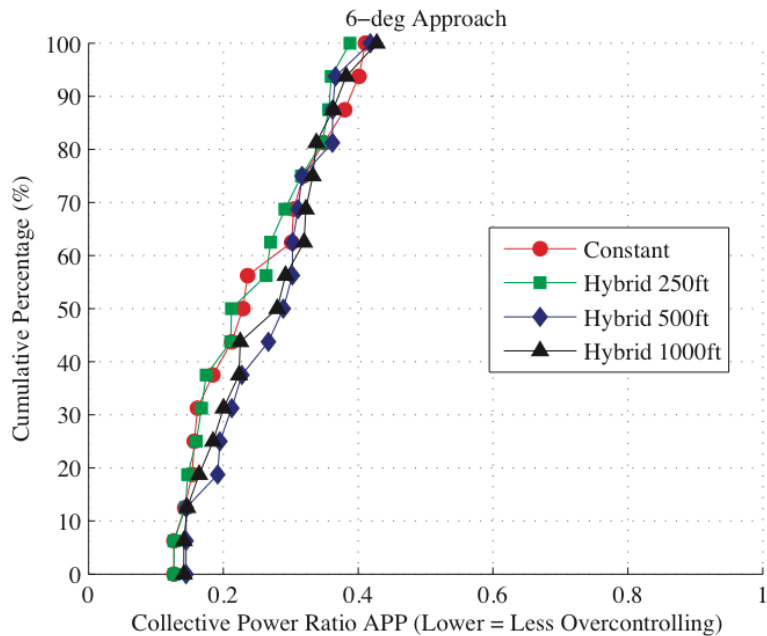
Figure G32: Cumulative histogram of collective power ratio, 6-degree approach.

## General Linear Model: TLX versus Algorithm, Approach

```
Factor      Type   Levels  Values
Algorithm   fixed       4  1, 2, 3, 4
Approach    fixed       2  1, 2


Analysis of Variance for TLX, using Adjusted SS for Tests

Source             DF    Seq SS   Adj SS   Adj MS     F      P
Algorithm           3    11.410   11.410    3.803   1.92  0.136
Approach            1     2.587    2.587    2.587   1.31  0.258
Algorithm*Approach  3     0.696    0.696    0.232   0.12  0.950
Error              56   110.708  110.708    1.977
Total              63   125.401


S = 1.40603   R-Sq = 11.72%   R-Sq(adj) = 0.68%
```

Figure G33: GLM ANOVA analysis for TLX workload score.
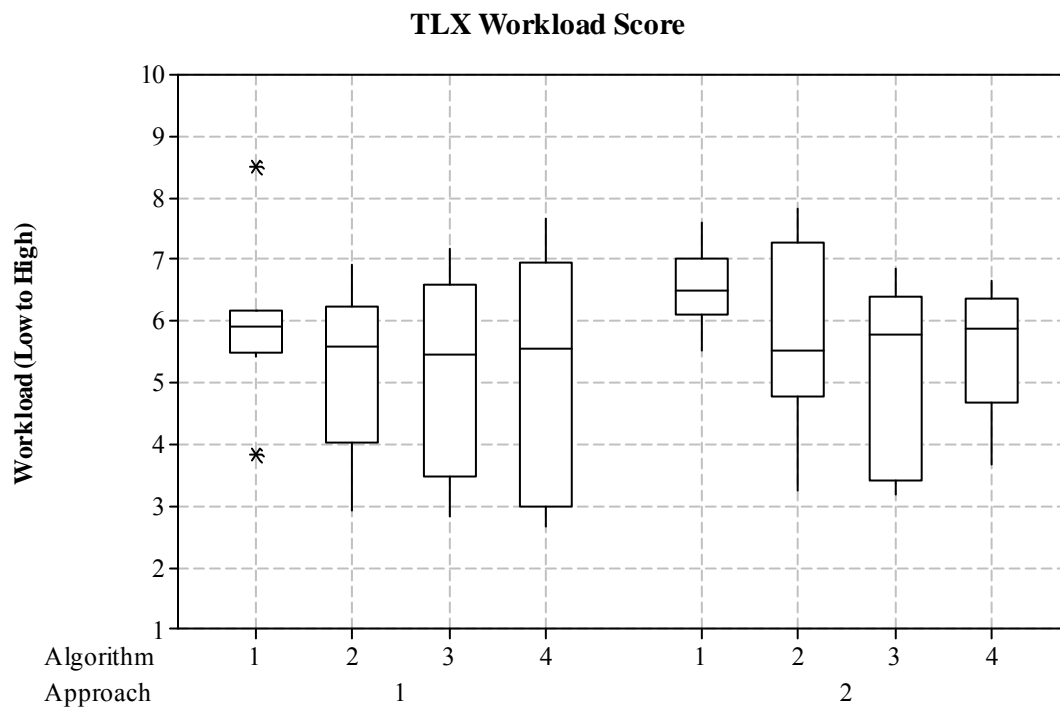
TLX Workload Score

Figure G34: Boxplot of NASA-TLX workload.

General Linear Model: Temporal versus Algorithm, Approach

```
Factor      Type    Levels  Values
Algorithm   fixed        4  1, 2, 3, 4
Approach    fixed        2  1, 2


Analysis of Variance for Temporal, using Adjusted SS for Tests

Source             DF   Seq SS   Adj SS   Adj MS     F      P
Algorithm           3   28.016   28.016   9.339   2.85  0.046
Approach            1    5.641    5.641   5.641   1.72  0.195
Algorithm*Approach  3    2.141    2.141   0.714   0.22  0.884
Error              56  183.688  183.688   3.280
Total              63  219.484


S = 1.81111   R-Sq = 16.31%   R-Sq(adj) = 5.85%
```

Figure G35: GLM ANOVA analysis for temporal demand (TLX).

Table G6: Algorithm pairwise comparison for temporal demand (TLX).

Tukey's Pairwise Comparison p-values				
	Constant	250ft Hybrid	500ft Hybrid	1000ft Hybrid
Constant	X			
250ft Hybrid	0.1118	X		
500ft Hybrid	0.1118	1.0000	X	
1000ft Hybrid	0.0649	0.9948	0.9948	X

TLX - Temporal Demand
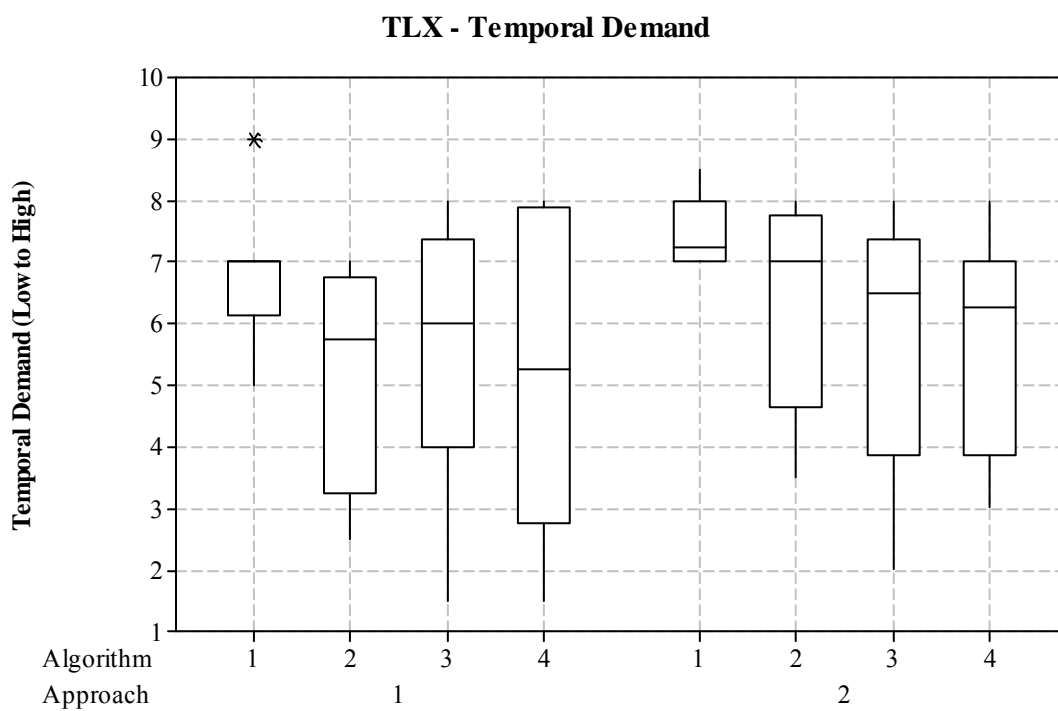
Figure G36: Boxplot of TLX temporal demand.

General Linear Model: Frustration versus Algorithm, Approach

```
Factor      Type   Levels  Values
Algorithm   fixed      4   1, 2, 3, 4
Approach    fixed      2   1, 2


Analysis of Variance for Frustration, using Adjusted SS for Tests

Source              DF   Seq SS   Adj SS   Adj MS     F      P
Algorithm            3   11.219   11.219    3.740   0.81  0.496
Approach             1    1.000    1.000    1.000   0.22  0.644
Algorithm*Approach   3    1.844    1.844    0.615   0.13  0.940
Error               56  259.937  259.937    4.642
Total               63  274.000


S = 2.15447   R-Sq = 5.13%   R-Sq(adj) = 0.00%
```

Figure G37: GLM ANOVA analysis for frustration (TLX).

Figure G38: Boxplot for frustration (TLX).

General Linear Model: Mental versus Algorithm, Approach

```
Factor      Type   Levels  Values
Algorithm   fixed       4  1, 2, 3, 4
Approach    fixed       2  1, 2


Analysis of Variance for Mental, using Adjusted SS for Tests

Source             DF    Seq SS    Adj SS   Adj MS      F      P
Algorithm           3     5.074     5.074    1.691   0.49  0.692
Approach            1     2.066     2.066    2.066   0.60  0.443
Algorithm*Approach  3     0.512     0.512    0.171   0.05  0.985
Error              56   194.156   194.156    3.467
Total              63   201.809


S = 1.86201   R-Sq = 3.79%   R-Sq(adj) = 0.00%
```

Figure G39: GLM ANOVA analysis for mental demand (TLX).

TLX - Mental Demand

Figure G40: Boxplot for mental demand (TLX).

General Linear Model: Performance versus Algorithm, Approach

```
Factor     Type    Levels  Values
Algorithm  fixed        4  1, 2, 3, 4
Approach   fixed        2  1, 2


Analysis of Variance for Performance, using Adjusted SS for Tests

Source             DF    Seq SS    Adj SS   Adj MS     F      P
Algorithm           3    14.641    14.641    4.880   1.27  0.293
Approach            1     1.891     1.891    1.891   0.49  0.486
Algorithm*Approach  3     1.766     1.766    0.589   0.15  0.927
Error              56   215.063   215.063    3.840
Total              63   233.359


S = 1.95969   R-Sq = 7.84%   R-Sq(adj) = 0.00%
```

Figure G41: GLM ANOVA analysis for performance (TLX).
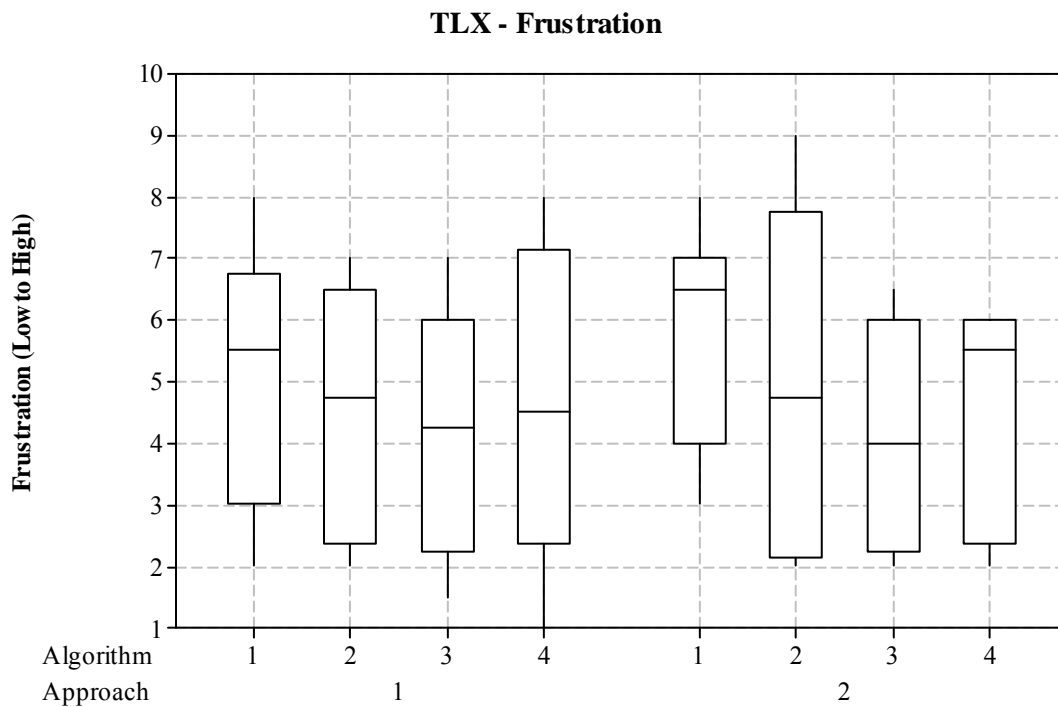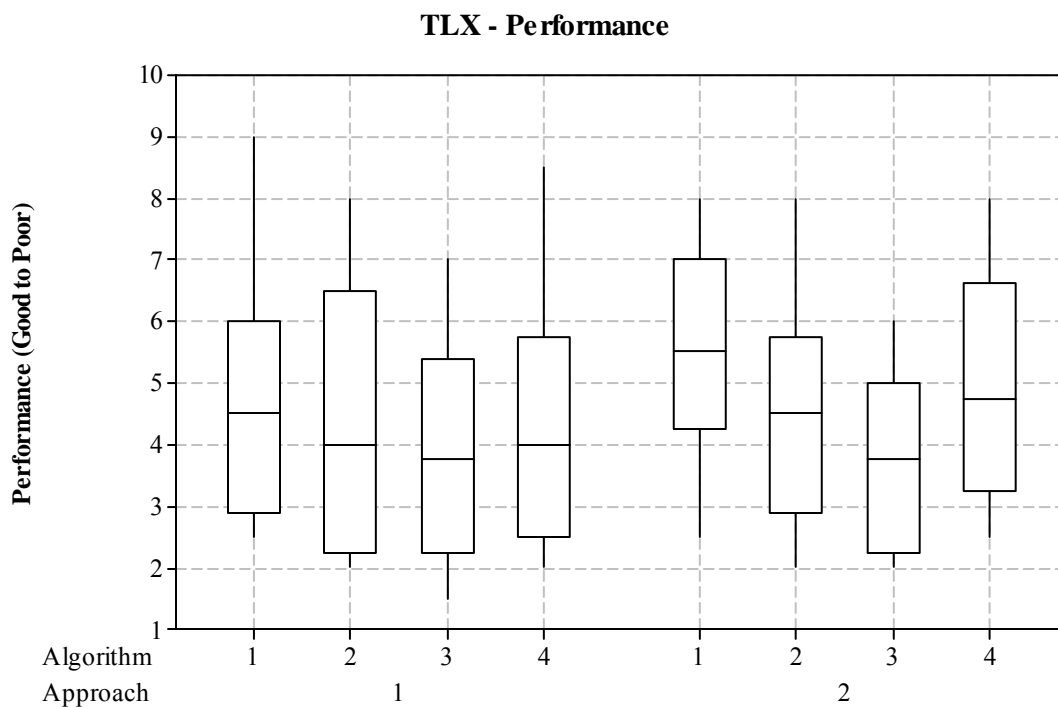
TLX - Performance

Figure G42: Boxplot for performance (TLX).

```
General Linear Model: Physical versus Algorithm, Approach

Factor      Type    Levels  Values
Algorithm   fixed       4   1, 2, 3, 4
Approach    fixed       2   1, 2


Analysis of Variance for Physical, using Adjusted SS for Tests

Source            DF    Seq SS    Adj SS   Adj MS     F      P
Algorithm          3     5.137     5.137    1.712   0.59  0.625
Approach           1     3.754     3.754    3.754   1.29  0.261
Algorithm*Approach 3     0.324     0.324    0.108   0.04  0.990
Error             56   163.094   163.094    2.912
Total             63   172.309


S = 1.70657   R-Sq = 5.35%   R-Sq(adj) = 0.00%
```

Figure G43: GLM ANOVA analysis for physical demand (TLX).
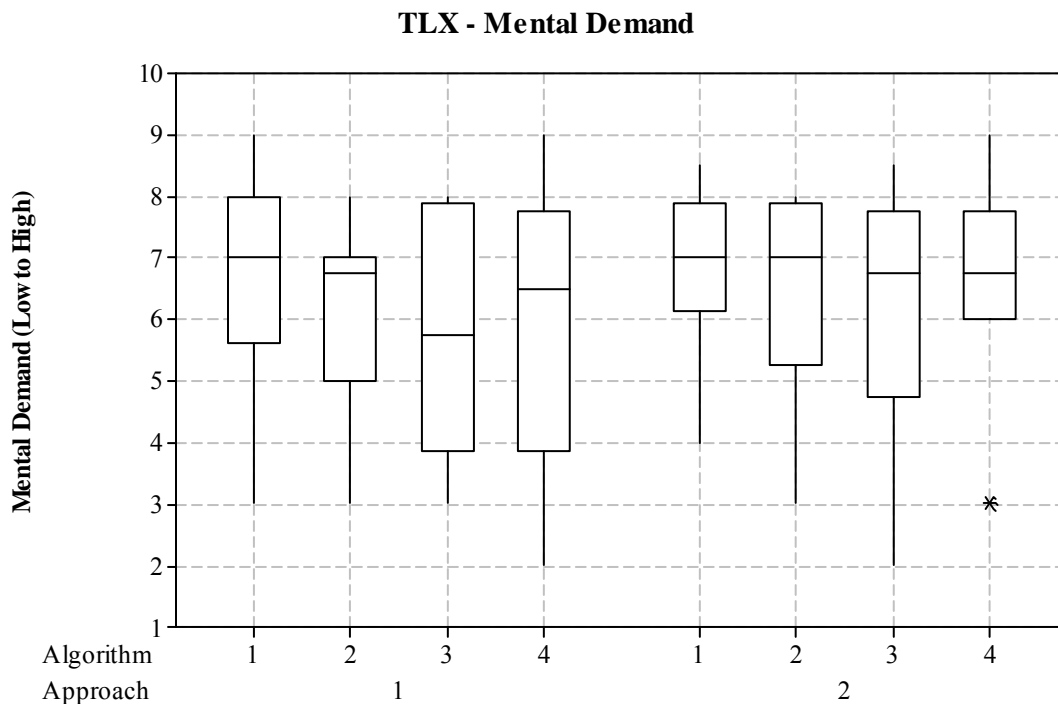
TLX - Physical Demand
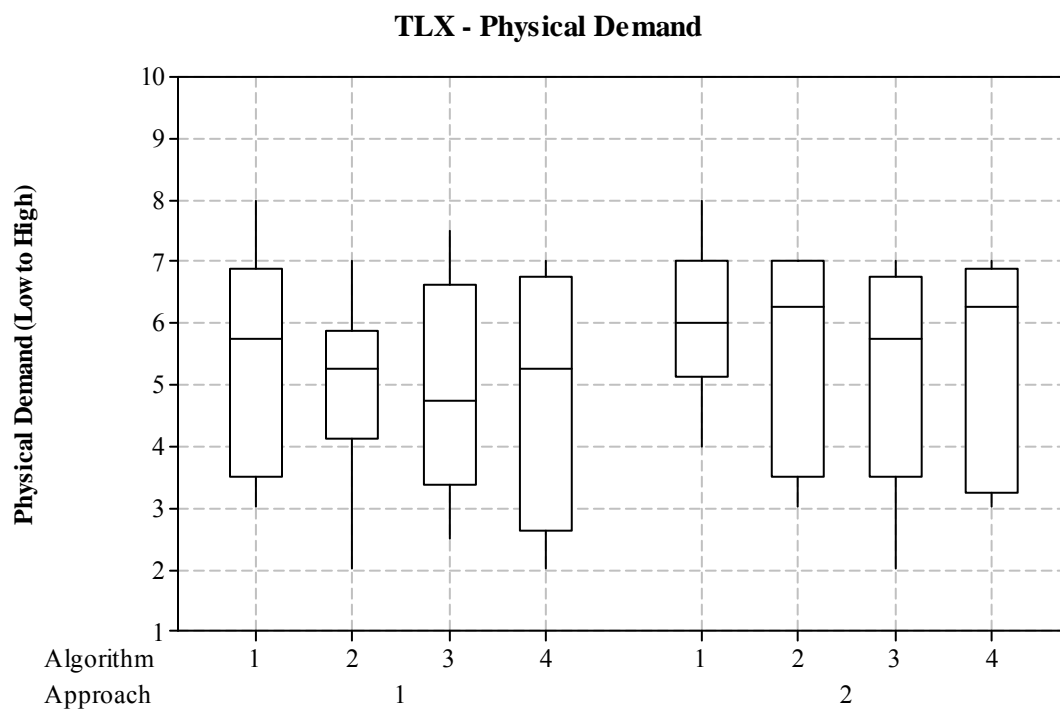
Figure G44: Boxplot for physical demand (TLX).

General Linear Model: Effort versus Algorithm, Approach

```
Factor      Type    Levels  Values
Algorithm   fixed        4  1, 2, 3, 4
Approach    fixed        2  1, 2


Analysis of Variance for Effort, using Adjusted SS for Tests

Source              DF    Seq SS    Adj SS   Adj MS     F      P
Algorithm            3    16.688    16.688    5.563   2.17   0.102
Approach             1     2.250     2.250    2.250   0.88   0.353
Algorithm*Approach   3     1.875     1.875    0.625   0.24   0.865
Error               56   143.625   143.625    2.565
Total               63   164.438


S = 1.60148   R-Sq = 12.66%   R-Sq(adj) = 1.74%
```
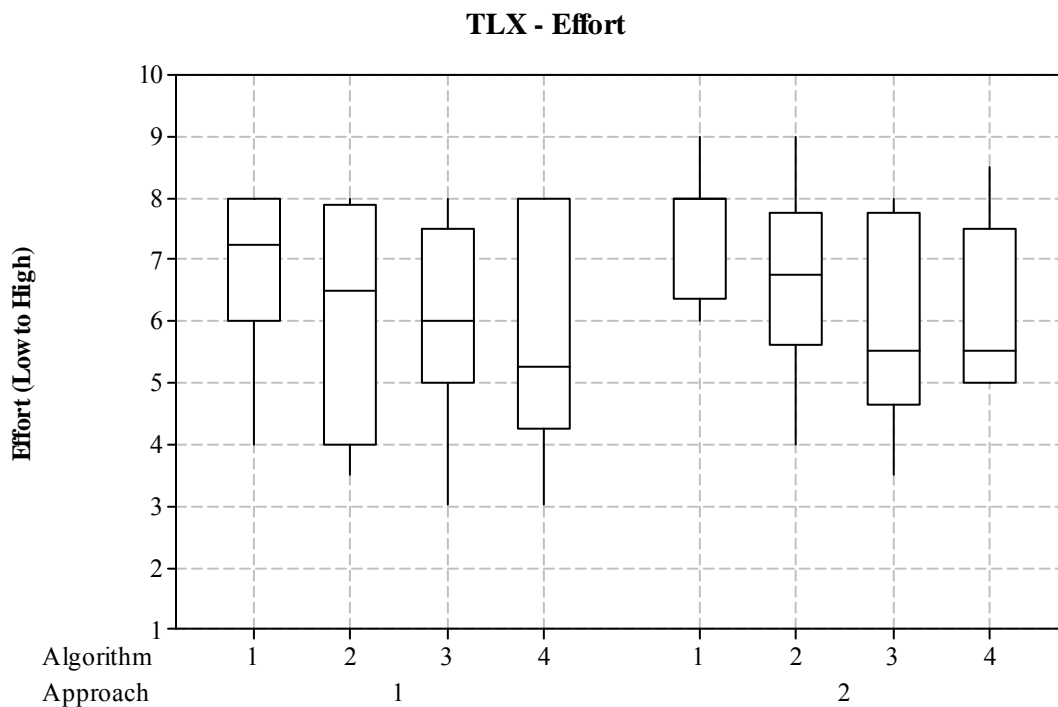
Figure G45: GLM ANOVA analysis for effort (TLX).

TLX - Effort

Figure G46: Boxplot for effort (TLX).

REFERENCES

[1] Colucci, F. *American Helicopter Society Vertiflite* **2007**, 53(1), 50-55.

[2] Sherer, Capt J. *Brownout.* http://www.afsc.af.mil/news/story.asp?id=123085802 (accessed November 2, 2009).

[3] Anderson, Maj L.; Doty, Maj P.; Griego, Maj M.; Timko, Maj K.; Hermann, B.; Colombi, J. Solutions Analysis for Helicopter Brownouts. Presented at the 9th Annual Systems Engineering Conference, San Diego, CA, October 22-26, 2006

[4] Couch, M.; Lindell, D. Study on Rotorcraft Survivability. US Department of Defense, Briefing, December 9, 2009.

[5] Colucci, F. *American Helicopter Society Vertiflite* **2009**, 55(2), 24-28.

[6] Wagtendonk, W.J. *Principles of Helicopter Flight,* 1st ed. revised; Aviation Supplies & Academics, Inc.: Newcastle, WA, 1996.

[7] United States Army. *Operator's Manual For E/UH-60A/L Helicopter*; TM 1-1520-237-10; Deparment of the Army: Washington DC, Oct 1996.

[8] Leishman, J.G. *Principles of Helicopter Aerodynamics*, 2nd ed.; Cambridge University Press: New York, 2006.

[9] Cowherd, C. *Sandblaster 2 Support of See-Through Technologies for Particulate Brownout*; final technical report to Defense Advanced Research Projects Agency (DOD) on Grant W31P4Q-07-C-0215; Midwest Research Institute: Kansas City, MO, 2007.

[10] Phillips, C.; Brown, R.E. Eulerian Simulation of the Fluid Dynamics of Helicopter Brownout. Presented at the American Helicopter Society 64th Annual Forum, Montreal, Canada, April 29-May 1, 2008.

[11] Phillips, C.; Brown, R.E. The effect of helicopter configuration on the fluid dynamics of brownout. Presented at the 34th European Rotorcraft Forum, Liverpool, England, September 16-19, 2008.

[12] Wadcock, A.J.; Ewing, L.A.; Solis, E.; Potsdam, M.; Rajagopalan, G. Rotorcraft Downwash Flow Field Study to Understand the Aerodynamics of Helicopter Brownout. Presented at the American Helicopter Society Southwest Region Technical Specialist's Meeting "Technologies for the Next Generation of Vertical Lift Aircraft", Dallas-Fort Worth, TX, Oct 15-17, 2008.

[13] Rabaja, C.K. The Use of Commercial Remote Sensing In Predicting Helicopter Brownout Conditions. M.S. Thesis, The Naval Postgraduate School, Monterey, CA, 2009.

[14]Key, D.L. Analysis of Army Helicopter Pilot Error Mishap Data and the Implications for Handling Qualities. Proceedings from the 25th European Rotorcraft Forum, Rome, Italy, September 14-16, 1999.

[15]Antunano, M.J.; *Spatial Disorientation: Visual Illusions;* AM-400-00/1; Federal Aviation Administration: Oklahoma City, OK.

[16]Antunano, M.J.; *Spatial Disorientation*; AM-400-03/1; Federal Aviation Administration: Oklahoma City, OK.

[17]Cheung, B. *Nonvisual Spatial Orientation Mechanisms*. In Spatial Disorientation in Aviation; Zarchan, P.: AIAA: Reston, VA, 2004; Vol. 203; pp. 37-94.

[18]Newman, D.G. *An overview of spatial disorientation as a factor in aviation accidents and incidents;* B2007/0063; Australian Transport Safety Bureau: Civic Square ACT, Australia, 2007.

[19]Matthews, R.J.S. Wg Cdr; Previc, F.; Bunting, A. USAF Spatial Disorientation Survey. Presented at the RTO HRM Symposium on "Spatial Disorientation in Military Vehicles: Causes, Consequences, and Cures", La Coruna, Spain, April 15-17, 2002, RTO-MP-086.

[20]Holmes, S.R.; Bunting, A.; Brown, D.L.; Hiatt, K.L.; Braithwaite, M.G.; Harrigan, M.J. *Aviation, Space, and Environmental Medicine* **2003**, 74(9), 957-965.

[21]Previc, F.H. *Visual Illusions in Flight*. In Spatial Disorientation in Aviation; Zarchan, P.: AIAA: Reston, VA, 2004; Vol. 203; pp. 283-321.

[22]Wickens, C.D.; Prevett, T.T. *Journal of Experimental Psychology* **1995**, 1(2), 110-135.

[23]Wickens, C.D. *Current Directions in Pyschological Science* **2002**, 11(4), 128-133.

[24]McCann, R.; Foyle, D. *AGARD Conference Proceedings* **1995**, 16(555),1-11.

[25]Sachs, G.; Dobler, K.; Theunissen, E. *AIAA Guidance, Navigation, and Control Conference and Exhibit*, Portland, OR, Aug, 1999; 574-582.

[26]Newman, D. A Review of Pathway-In-The-Sky Displays. Presented at the FAA Synthetic Vision Workshop, Seattle, Washington, February 15, 2006.

[27]Snow, M.P.; Reising, J.M.; Liggett, K.K. Barry, T.P. *Proceedings of the 10th International Symposium on Aviation Psychology*, Columbus, OH, May,1999; 1-7.

[28]Haskell, I.D.; Wickens, C.D. *The International Journal of Aviation Psychology* **1993**, 3(2), 87-109.

[29]Williams, K.W. *Human Factors* **2002**, 44(1),18-27.

[30]Keller, B.M.; Neiswander, G.M.; Schnell, T. *Rotorcraft Hover Symbology Study for Operation in Poor Visibility Conditions*; final report to Aeroflightdynamics Directorate on Grant NNA04CL16G; Operator Performance Laboratory, Iowa City, 2006.

[31]Turpin, T.S.; Dowell, S.R.; Szoboszlay, Z. *Comanche Helmet-Mounted Display Symbology Simulation*; NASA/CR-2006-212834, NASA: Ames Research Center, CA, 2006.

[32]Merrick, V.K.; Farris, G.G.; Vanags, A.A. *A Head Up Display for Application to V/STOL Aircraft Approach and Landing*; NASA TM 102216; NASA: Ames Research Center, CA, 1990.

[33]McNerney, M.W. Blackhawk Down. Presented at the University of Notre Dame, IN, February 2010.

[34]Szoboszlay, Z.P.; Turpin, T.S.; Albery, W.B.; Neiswander, G.M. Brown-Out Symbology Simulation (BOSS) on the NASA Ames Vertical Motion Simulator. Presented at the American Helicopter Society 64th Annual Forum, Montreal, Canada, April 29 - May 1, 2008.

[35]United States Army. *Operator's Manual For Helicopter, Attack, AH-64A Apache*; TM 1-1520-238-10; Deparment of the Army: Washington DC, Oct 1994.

[36]Harrington, W.; Braddom, S. LTC; Savage, J.; Szoboszlay, Z.; McKinley, A. 3D-LZ Brownout Landing Solution; Presented at the American Helicopter Society 66th Annual Forum, Phoenix, AZ, May, 2010.

[37]Haas, E.C. *Proceedings of the HFES 42nd Annual Meeting*, Chicago, IL; HFES: Santa Monica, 1998; 1117-1121.

[38]Schnell, T.; Keller, M.; Etherington, T. Multi-Sensory Methods to Aid Pilot Spatial Orientation Upset Recovery in Real Flight. Presented at the 25th Digital Avionics Systems Conference, Portland, OR, October 15, 2006.

[39]Albery, W. *Development of Multisensory Orientation Technology for Reducing Spatial Disorientation Mishaps*; AFRL-HE-WP-TR-2006-0024; Air Force Research Laboratory: Wright-Patterson AFB, OH, 2006.

[40]Jansen, C.; Wennemers, A.; Vos, W.; Groen, E. *Proceedings of the 6th International Conference, EuroHaptics 2008*, Madrid, Spain; Springer: Berlin/Heidelberg, 2008; 867-875.

[41]Leishman, J.G. *Rotorcraft Brownout: Advanced Understanding, Control, and Mitigation*; AFRL-SR-AR-TR-09-0124; Air Force Office of Scientific Research: Arlington, VA, 2008.

[42]Luttman, J.C. CAPT. *Dealing With Brownout: Environmental, Mechanical, and Training Solutions*; United States Marine Corps, Quantico, VA, February, 2005.

[43]Tingle, J.S.; Harrison, A.; Rushing, J.F. Evaluation of Expedient Methods for Mitigating Dust on Helipads; ERDC/GSL TR-04-XX; US Army Corps of Engineers, April, 2004.

[44]Lebacqz, J.V. A Ground-Simulation Investigation of Helicopter Decelerating Instrument Approaches; AIAA Paper 82-1346, Proceedings from the AIAA 9th Atmospheric Flight Mechanics Conference, San Diego, CA, August 9-11, 1982.

[45]Fletcher, J.W.; Lusardi, J.; Mansur, M.H.; Moralez, E., III; Robinson, D.E., LTC, et al. UH-60M Upgrade Fly-By-Wire Flight Control Risk Reduction using the RASCAL JUH-60A In-Flight Simulator. Presented at the American Helicopter Society 64th Annual Forum, Montreal, Canada, April 29-May1, 2008.

[46]Braithwaite, M.G. Controlling the Hazard of Spatial Disorientation in Rotary-Wing Operations by Enhanced Training. Presented at the TRO HFM Symposium on "Current Aeromedical Issues in Rotary Wing Operations", San Deigo, CA, October 19-21, 1998.

[47]Johnson, P.A.; Estrada, A.; Braithwaite, M.G.; Manning, J.C. Assessment of Simulated Spatial Disorientation Scenarios in Training U.S. Army Aviators. Presented at the TRO HFM Symposium on "Current Aeromedical Issues in Rotary Wing Operations", San Deigo, CA, October 19-21, 1998.

[48]Wachspress, D.A.; Whitehouse, G.R.; Keller, J.D.; Yu, K.; Gilmore, P.; Dorsett, M.; McClure, K. A High Fidelity Brownout Model for Real-Time Flight Simulations and Trainers. Presented at American Helicopter Society 65th Annual Forum, Grapevine, TX, May 27-29, 2009.

[49]Garren, J.F., Jr.; Kelly, J.R.; Sommer, R.W.; DiCarlo, D.J. *Flight Investigation of VTOL Control and Display Concept for Performing Decelrating Appraoches to an Instrument Hover;* NASA TN D-6108; NASA: Langley Research Center, VA, 1971.

[50]Padfield, G.; Lee, D.N.; Bradley, R. How Do Helicopter Pilots Know When to Stop, Turn or Pull Up? (Developing guidelines for vision aides). Presented at the American Helicopter Society 57th Annual Forum, Washington, DC, May 9-11, 2001.

[51]Moen, G.C.; DiCarlo, D.J.; Yenni, K.R. *A Parametric Analysis of Visual Approaches for Helicopters*; NASA TN D-8275; NASA: Langley Research Center, VA, 1976.

[52]Kelly, J.R.; Niessen, F.R.; Yenni, K.R.; Person, L.H, Jr. *Flight Investigation of a Vertical-Velocity Command System for VTOL Aircraft;* NASA TN D-8480, NASA: Langley Research Center, VA, 1977.

[53]Kelly, J.R.; Niessen, F.R.; Thibodeaux, J.J.; Yenni, K.R.; Garren, J.F., Jr. *Flight Investigation of Manual and Automatic VTOL Decelerating Instrument Approaches and Landings*; NASA TN D-7524; NASA: Langley Research Center, VA, 1974.

[54]United States Army. *Aircrew Training Manual: Utility Helicopter: HH-60 Series*; TC 1-237; Department of the Army: Washington DC, Feb 2005.

[55]McCauley, M.E. *Do Army Helicopters Training Simulators Need Motion Bases?*; TR 1176; United States Army Research Institute for the Behavioral and Social Sciences: Alrington, VA, 2006.

[56]Szoboszlay, Z.P.; Turpin, T.S.; McKinley, A.R. Symbology for Brown-Out Landings: The First Simulation for the 3D-LZ Program; Presented at the American Helicopter Society 65th Annual Forum, Grapevine, TX, May 27-29, 2009.

[57]Szoboszlay, Z.P; Jennings, S. *Subjective Results and Open Comments for the Loon Study 2008;* white paper to Canadian National Research Council; AFDD/NRC Technology Cooperation Panel (AER-TP2): Moffett Field, CA, 2008.

[58]McKinley, A.R.; Esken, B.; Harrington, W.; Szoboszlay, Z.P., Burns, B. *3D-LZ Simulation*; Briefing, Air Force Research Laboratory: Wright Patterson Air Force Base, OH, June, 2009.

[59]Harrington, W. United States Air Force Research Laboratory, Wright-Patterson Air Force Base, OH. Comparison of Approach Profiles; Technical memorandum, 2009.

[60]Harrington, W. United States Air Force Research Laboratory, Wright-Patterson Air Force Base, OH. BOSS Guidance Algorithms and Symbology; Technical memorandum, 2009.

[61]Phatak, A.V.; Peach, L.L.; Hess, R.A.; Ross, V.L.; Hall, G.W.; Gerdes, R.M. A piloted simulator investigation of helicopters precision decelerating approaches to hover to determine single-pilot IFR/SPIFR/requirements. AIAA Paper 79-1886; Presented at the Guidance and Control Conference, Boulder, CO, August 6-8, 1979.

[62]Lebacqz, J.V. A review of helicopter control-display requirements for decelerating instrument approach. AIAA Paper 79-1683; Presented at the Atmospheric Flight Mechanics Conference for Future Space Systems, Boulder, CO, Aug 6-8, 1979.

[63]Moen, G.C.; Yenni, K.R. *Simulation and Flight Studies of an Approach Profile Indicator for VTOL Aircraft*; NASA TN D-8051; NASA: Washington, DC, November, 1975.

[64]Niessen, F.R.; Kelly, J.R.; Garren, J.F., Jr.; Yenni, K.R.; Person, L.H. *The Effect of Variations In Controls And Displays On Helicopter Instrument Approach Capability*; NASA TN D-8385; NASA: Langley Research Center, VA, February, 1977.

[65]Heffley, R.K. A Model for Manual Decelerating Approaches to Hover. AFFDL-TR-70-3134; Presented at the 15th Annual Conference on Manual Control, November, 1979, pp. 545-554.

[66]Szoboszlay, Z.P.; Braddom, S., LTC; McKinley, R.A.; Harrington, W.; Savage, J. Landing an H-60 Helicopter in Brown-Out Conditions Using 3D-LZ Displays; Presented at the American Helicopter Society 65th Annual Forum, Pheonix, AZ, May 11-13, 2010.

[67]Ballin, M.G. *Validation of a Real-Time Engineering Simulation of the UH-60A Helicopter*; NASA TM-88360, NASA: Ames Research Center, CA, February, 1987.

[68]Box, G.E.P.; Hunter, J.S.; Hunter, W.G. *Statistics for Experimenters*, 2nd ed.; John Wiley & Sons, Inc.: Hoboken, NJ, 2005.

[69]Hart, S.G.; Staveland, L.E. *Development of NASA-TLX (Task Load Index): Results of Empirical and Theoretical Research*. In Human Mental Workload; Hancock, P.A.; Meshkati, N.; Elsevier Science Publishers: Amsterdam, The Netherlands, 1988; pp 139-178.

[70]Cooper, G.E.; Harper, R.P., Jr. *The Use of Pilot Rating in the Evaluation of Aircraft Handling Qualities*; NASA TN D-5153; NASA: Ames Research Center, CA, April, 1969.

[71]Howlett, J.J.*UH-60A Black Hawk Engineering Siumlation Program: Volume 1 - Mathematical Model*; NASA CR-166309, final report to NASA on Contract NAS2-10626; Sikorsky Aircraft: Stratford, 1981.

[72]Lee, J.D. The University of Iowa, Iowa City, IA. Fourier Analysis; Modeling Operator Performance course notes, 2009.

[73]Wickens, C.D.; Lee, J.D.; Liu, Y.; Gordon Becker, S.E. *An Introduction to Human Factors Engineering*, 2nd ed.; Pearson Education, Inc.: Upper Saddle River, NJ, 2004; pp 330-331.